ANALYSIS OF ASYMMETRIC DIVISION OF NEURAL STEM CELLS IN *DROSOPHILA*

CHEN KENG

(*M. Sc.* & *B. Sc.*, Shanghai Jiao Tong University)

A THESIS SUBMITTED

FOR THE DEGREE OF DOCTOR OF PHILOSOPHY

NUS GRADUATE SCHOOL FOR INTEGRATIVE SCIENCES AND ENGINEERING

NATIONAL UNIVERSITY OF SINGAPORE

2016

DECLARATION

I hereby declare that the thesis is my original work and it has been written by me in its entirety. I have duly acknowledged all the sources of information which have been used in the thesis.

This thesis has also not been submitted for any degree in any university previously.

Chen Keng

20 March 2016

ACKNOWLEDGEMENTS

I would like to express my utmost appreciation and grateful to my wonderful supervisor, Assoc Prof. Wang Hongyan. Hongyan is my co-supervisor for my phD studies, and her excellent guidance, valuable suggestions and unflagging encouragement had allow me to explore any possibility in my research work. Her exceptional talented insight and great enthusiasm in science is always a role model for young researchers. Without her kindness and patience to impart her skills and knowledge to me, my research work would not have been carried on.

Special thanks also go to my main-supervisor, Assoc Prof. Reshma Taneja for her guidance and support from my start of my phD candidature. Thanks to Prof. Hong Wanjin, for his kindness and helpful suggestions provided in the thesis advisory committee meetings. I owe my deepest gratitude to Dr. Yu Fengwei, Ms. Tang Quan and Ms. Zong Wenhui for providing several critical transgenic stocks that allow my research project to be carried on. Thanks to Prof. Sharyn Endow and Mr. Benny Zhanyuan Xing for their helps in the analysis of several fluorescent imaging data. My gratitude also goes to Assoc Prof. Chunlai Wu and Dr. Xiaolin Tian for carrying out the tandem affinity purification and mass spectrometry experiments. Also thanks to Prof. Cayetano Gonzalez and Dr. Fabrizio Rossi, who had carried out allography analysis of *arl2* and *msps* mutants. I am also grateful to be supported by NGS Scholarship, which had funded me for my studies. Also thanks a broader fly community for their generosity in providing useful stocks and reagents.

I would like to show my appreciation to all current and past members in Hongyan lab for providing me a motivating and stimulating environment. Special thanks to Dr. Koe Chwee Tat for the isolation and sequencing of the *msps*^{P18} mutant, and many tremendous helps in my research work. Thanks to Dr. Wang Cheng for the helps in analyzing the centrosome phenotypes in Arl2 over-activation mutants. Also thanks to Dr. Li Song, Ms. Zhang Yingjie, Ms. Yong Wei Lin, Ms. Tan Ye Sing, Mr. Huang Jiawen and Ms. Ly Phuong Thao for their assistance in various ways.

Lastly, I am also thankful to my parents and family for their unconditional love and support. I want to express my heartfelt gratitude to my wife, Huifang, and my daughter, Ziqi, who have always been the pillar of my strength throughout my life.

Chen Keng

20 March 2016

TABLE OF CONTENTS

SUMMARY

During the development of *Drosophila* central nervous system (CNS), the larval central brain neural stem cell (neuroblast) undergoes asymmetric cell division to balance self-renewal and differentiation. Failure of asymmetric division may result in un-controlled proliferation of neuroblasts, a phenotype resembling brain tumors. Although several centrosomal proteins have been identified as regulators of asymmetric division, how microtubules regulate asymmetric division of neuroblasts remains poorly understood. Here, I show that microtubule growth, which is dependent on ADP ribosylation factor-like 2 (Arl2) and Mini spindles (Msps), is important for the asymmetric division in neuroblasts. Loss of *Drosophila arl2* disrupted polarity protein localization and mitotic spindle orientation, causing overgrowth of neuroblasts in larval central brains. Arl2 is essential for microtubule formation, as loss of *arl2* resulted in depletion of interphase microtubule aster and mitotic spindle, whereas over-activation of Arl2 caused microtubule overgrowth and severe mitotic defects. In addition, Arl2 functions together with tubulin binding cofactors C, D and E, supporting its central role in regulating microtubule polymerization. Interestingly, Msps, a known microtubule-binding protein, is also required for neuroblast asymmetric division and homeostasis. Furthermore, Arl2 regulates microtubule growth and asymmetric division through localizing Msps to the centrosomes in neuroblasts. Therefore, Arl2 and Msps-dependent microtubule growth is a new paradigm regulating asymmetric division of neural stem cells.

LIST OF TABLES AND FIGURES

Chapter 3

LIST OF ABBREVIATIONS

aa	amino acid
ac/sc	Achaete-Scute
ALH	After larval hatching
Ana2	Anastral spindle 2
AP-2	Adaptor Protein complex 2
APC/C	Anaphase promoting complex/cyclosome
aPKC	atypical Protein kinase C
ARF	ADP Ribosylation Factor
Arl2	ADP Ribosylation Factor-Like 2
Ase	Asense
Asl	Asterless
AurA	Aurora-A
Baz	Bazooka
BDSC	Bloomington *Drosophila* Stock Center
bp	base pair
Brat	Brain tumor
Brm	Brahma
BSA	Bovine serum albumin
Btd	Buttonhead
Cas	Castor
CBD	Cargo-binding-domain
CD8	Cluster of differentiation 8
Cdc2	Cell division cycle 2
Cdc42	Cell division cycle 42
cDNA	Complementary DNA
Cep135	Centrosome protein 135kD
Cnb	Centrobin
Cnn	Centrosomin
Cno	Canoe
CNS	Central nervous system
Co-IP	Co-immunoprecipitation
COX7A	Cytochrome c oxidase subunit 7A

CRIB-PDZ	Cdc42/Rac interactive binding
Ctp	Cut-up
Cul1	Cullin1
cycE	CyclineE
D	Dichaete
D-TACC	*Drosophila* transforming acidic coiled coil
DGRC	*Drosophila* Genomics Resource Center
Dgrip	*Drosophila* ϒ ring protein
Dhc64C	Dynein heavy chain 64C
Dlg	Disc large
DNA	Deoxyribonucleic acid
Dpn	Deadpan
dsRBD	double strand ribonucleic acid (dsRNA)-binding-domain
dsRNA	double strand ribonucleic acid
DTT	Dithiothreitol
EB1	End-binding1
EDTA	Ethylenediaminetetraacetic acid
EdU	5-ethynyl-2'-deoxyuridine
EGTA	Ethylene glycol tetraacetic acid
Elav	Embryonic lethal abnormal vision
Erm	Earmuff
ESTs	Expressed-sequence tags
Ets	E26 transformation-specific
Ey	Eyeless
FBS	Fetal bovine serum
Flfl	Falafel
FLP	Flipase
FRT	FLP recombinase target
Gal	Galactose
GAP	GTPase activating protein
GDI	Guanine nucleotide-dissociation inhibitor
GDP	Guanosine diphosphate
GEF	Guanine nucleotide-exchange factor
GFP	Green flourescent protein

GMC	Ganglion mother cell
GoLoco	Gαi/o-Loco interaction
Grh	Grainy head
GTP	Guanosine triphosphate
Gαi	G protein α i subunit
Gβ13F	G protein β-subunit 13F
Ham	Hamlet
Hb	Hunchback
HDAC3	Histone deacetylase 3
hs	heat-shock
Ida	Imaginal discs arrested
INP	Intermediate neural progenitor
Insc	Inscuteable
Khc-73	Kinesin heavy chain-73
Klp10A	Kinesin-like protein 10A
Klu	Klumpfuss
Kr	Kruppel
Lgl	Lethal (2) giant larvae
Lis1	Lissencephaly-1
Loco	Locomotion defects
MAP	Microtubule-associated protein
MARCM	Mosaic analysis with a repressible cell marker
Mdlc	Midlife crisis
MGC	Mammalian Gene Collection
Mira	Miranda
mRNA	messenger RNA
Msps	Mini spindles
MTOC	Microtubule organizing center
Mud	Mushroom body defect
NB	Neuroblast
Nerfin-1	Nervous finger 1
NHL	NCL-1, HT2A and Lin-41
NuMA	Nuclear mitotic apparatus
PAGE	Polyacrylamide gel electrophoresis

Par	Partitioning defective
PB1	Phox and Bem 1
PBS	Phosphate Buffered Saline
PCM	Pericentriolar material
PCR	Polymerase Chain Reaction
Pdm	POU domain protein
PDZ	PSD-95, Dlg, and Zo-1
pH3	phospho-Histone 3
Pins	Partner of inscuteable
Plk4	Polo-like kinase 4
Plp	Pericentrin-like protein
pNR	precephalic neurogenic region
PntP1	Pointed-P1
PP2A	Protein phosphatase 2A
PP4	Protein phosphatase 4
Pros	Prospero
Prox1	Prospero homeobox 1
PTB	Phosphotyrosine-binding
PTPA	Phosphotyrosyl phosphatase activator
Ral	Ras-like protein A
Ras	Rat sarcoma
Rgl	Ral guanine nucleotide dissociation stimulator-like ortholog
RIPA	Radio-Immune Precipitation Assay
RNA	Ribonucleic acid
RNAi	RNA interference
RT-PCR	Reverse transcription-polymerase chain reaction
SAK	Sak kinase
Sas4	Spindle assembly abnormal 4
Sas6	Spindle assembly abnormal 6
SCF	Skp1-Cullin1-F-box
SDS	Sodium Dodecyl Sulphate
Ser	Serine
SFM	Serum free medium
SkpA	S-phase kinase-associated protein subunit A

Slimb	Supernumerary limbs
Spd2	Spindle defective 2
Spdo	Sanpodo
STAN	STil/ANa2
Stau	Staufen
Svp	Seven-up
SWI/SNF	SWItch/Sucrose Non-Fermentable
TBCs	Tubulin binding cofactors
Thr	Threonine
TOG	Tumor overexpressed gene
TPR	Tetratricopeptide
TRiC/CCT	TCP-1 Ring Complex/Cytosolic chaperonin
Tws	Twins
UAS	Upstream activition sequence
UTR	Untranslated region
VDRC	Vienna *Drosophila* Resource Center
VNC	Ventral nerve cord
vNR	ventral neurogenic region
Wdb	Widerborst
wor	Worniu
XMAP215	Xenopus Microtubule-associated protein 215
α-Ada	α-Adaptin
α-Tub	α-Tubulin
β-Tub	β-Tubulin
γ-Tub	γ-Tubulin
γ-TuRC	γ-Tubulin ring complex

CHAPTER 1: INTRODUCTION

1.1 *Drosophila melanogaster* as a useful model organism

Since it was first used more than a century ago for genetic studies, *Drosophila melanogaster*, or commonly known as the fruit fly, has emerged as one of the most effective model organisms in biological studies. *Drosophila* has several experimental advantages, including their relatively small size, rapid life cycle, and easy maintenance. In addition, a large number of mutant and transgenic stocks are available, which facilitate the genetic manipulations carried out in *Drosophila* (St Johnston, 2002). Moreover, the completed genome sequence of *Drosophila* released in 2000 also facilitates the use of *Drosophila* in studies of many related human diseases. Nowadays, *Drosophila* and its derived models such as *Drosophila* S2 cells, have been widely used in research related to disease modeling and clinical drug screening and discovery (Bilen and Bonini, 2005; Pandey and Nichols, 2011). Furthermore, *Drosophila*-based research is continuing to contribute to the understanding of mechanisms underlying development and disease progression (Bier, 2005).

1.2 *Drosophila* neuroblasts as a model system for stem cell biology

Stem cells are characterized by their ability to self-renew and their potency to differentiate into variant cell types for different functions (Knoblich, 2010). The *Drosophila* neural stem cell, or neuroblast, is the neural progenitor cell type that gives rise to the complex central nervous system (CNS) (Homem and Knoblich, 2012). Over the past two decades, remarkable mechanistic insights into CNS development have been discovered.

1.2.1 Neurogenesis in *Drosophila*

The *Drosophila* central nervous system (CNS) is subdivided into the brain and the ventral nerve cord (VNC). The brain arises from the procephalic neurogenic region (pNR) near the anterior of the embryo, while the VNC develops from a bilateral sheet of neuroectodermal cells in the ventral neurogenic region (vNR). Early genetic studies have revealed that neuroblasts are first specified during the embryonic stages 9 to 10 through a process called lateral inhibition (Artavanis-Tsakonas and Simpson, 1991). In each neural equivalence group in the ventral neurogenic region, one cell will express higher levels of Achaete-Scute (ac/sc) genes (also called proneural genes) than its surrounding cells and is selected as a 'presumptive neuroblast' (Garcia-Bellido and Santamaria, 1978; Martin-Bermudo et al., 1991; Skeath and Carroll, 1992; Villares and Cabrera, 1987) (Fig. 1B). These proneural genes activate Delta in the presumptive neuroblast, which creates a positive feedback loop between Delta-Notch pathway and the ac/sc genes, resulting in the suppression of proneural genes in the remaining cells in the equivalence group (Artavanis-Tsakonas and Simpson, 1991; Heitzler et al., 1996; Heitzler and Simpson, 1991). Hence, only one cell within the equivalence group acquires the neuroblast cell fate and delaminates from the neuroepithelium, while the remaining cells are shunted towards epidermal development (Skeath and Carroll, 1992).

Once delaminated, neuroblasts are able to self-renew and divide in an asymmetric fashion. In each round of asymmetric division, neuroblasts generate one self-renewing neuroblast and one smaller ganglion mother cell (GMC), which divides terminally to give rise to two neurons or glia (Li et al., 2014b). Neuroblasts proliferate to generate neurons and glia in two waves of neurogenesis time windows during embryonic and larval stages (Reichert,

2011; Skeath and Thor, 2003) (Fig. 1A). In the first neurogenic wave, neuroblasts divide perpendicularly to the neuroectoderm, with the side closer to epithelial defined as the apical while the opposite side defined as the basal (Kaltschmidt et al., 2000). Neuroblasts can divide up to 12 times, with cell size shrinking after each division, before entering the quiescent stage at the end of the embryonic stage (Fuse et al., 2003) (Fig. 1A, B).

Most neuroblasts in the abdominal regions undergo apoptosis after completing their neuronal lineages at the end of the embryonic stage (Peterson et al., 2002; White et al., 1994), while most neuroblasts in the tho-

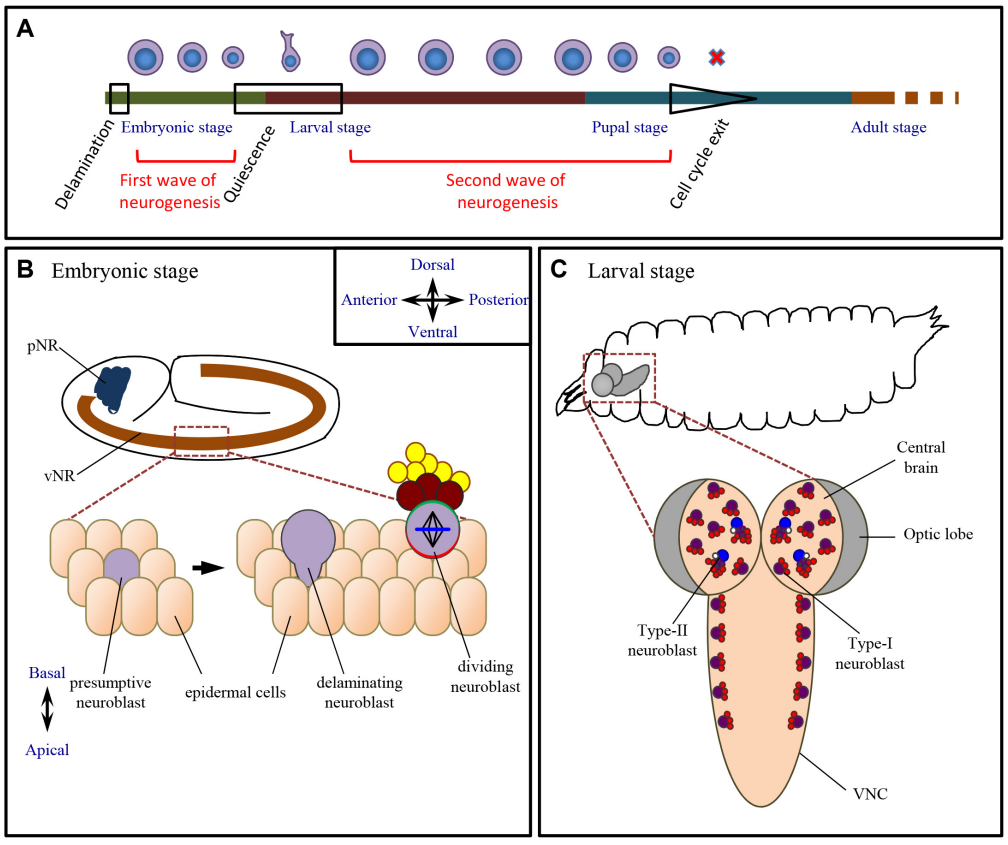

Figure 1. Neurogenesis in *Drosophila*.
(A) A schematic of the two waves of neurogenesis occurring during the development of *Drosophila* nervous system. The sizes and morphology of neuroblasts (magenta) are depicted throughout the timeline. (B) The major neurogenic regions during the embryonic stages. pNR (blue): procephalic neurogenic region; vNR (brown): ventral neurogenic region. (C) The larval brain region during the post-embryonic stages. The enlarged view shows a detailed larval brain. VNC: ventral nerve cord.

racic and cephalic regions exit from G1 and enter a G0-like quiescent stage (Homem and Knoblich, 2012). Quiescent neuroblasts have similar cell size compared to the surrounding neurons and exhibit cellular extensions (Chell and Brand, 2010). They also transiently express nuclear Prospero (Pros), a differentiation factor that is excluded from the nucleus in proliferating neuroblasts (Lai and Doe, 2014). During the late first instar larval stage, neuroblasts exit quiescence and are reactivated. They undergo an enlargement in cell size and re-entry into cell cycle, through the regulation of a fat-body-glia-neuroblast relay (Britton and Edgar, 1998; Chell and Brand, 2010; Sousa-Nunes et al., 2011; Truman and Bate, 1988). Upon reactivation, neuroblasts enter the second wave of neurogenesis, during which 90% of the neurons in the adult CNS are generated (Maurange et al., 2008) (Fig. 1A, C).

In the larval stage, neuroblasts continue to divide asymmetrically and after each round of division, the newly generated neuroblasts are able to re-grow to a similar cell size to the mother neuroblasts (Ito and Hotta, 1992). Hence, the larval neuroblasts can undergo 50-100 rounds of division and generate larger number of neural cells in the second wave of neurogenesis. Unlike embryonic neuroblasts, larval neuroblasts do not divide in a fixed orientation and their apico-basal axis is defined by the polarized proteins. The neuroblast proliferation is terminated during the pupal stage, either through a Pros-dependent cell-cycle exit, or programmed cell death via a Reaper/Hid/Grim-dependent manner (Maurange et al., 2008).

1.2.2 Neuroblast lineage progression in the larval central brain

Neuroblasts are able to generate progenies that are committed to the differentiation pathway, and the larval central brain neuroblasts have been used extensively to study how neuroblast lineage progression is regulated.

Based on differences in progeny types and gene expression, there are at least two types of neuroblasts in the larval central brain (Li et al., 2014b). Type I neuroblasts, which make up majority of the neuroblast population in the central brain, express the nuclear transcriptional factors Deadpan (Dpn) and Asense (Ase), and cytoplasmic or basal cortical Pros. Type I neuroblasts divide asymmetrically and generate one GMC in each division. In contrast, type II neuroblasts, which still express nuclear Dpn, are negative for Ase or Pros (Bello et al., 2008; Boone and Doe, 2008; Bowman et al., 2008). There are 8 type II neuroblasts in each brain hemisphere, and instead of generating GMCs directly, they divide asymmetrically to generate Intermediate Neural Progenitors (INPs). The newly born INPs, which do not

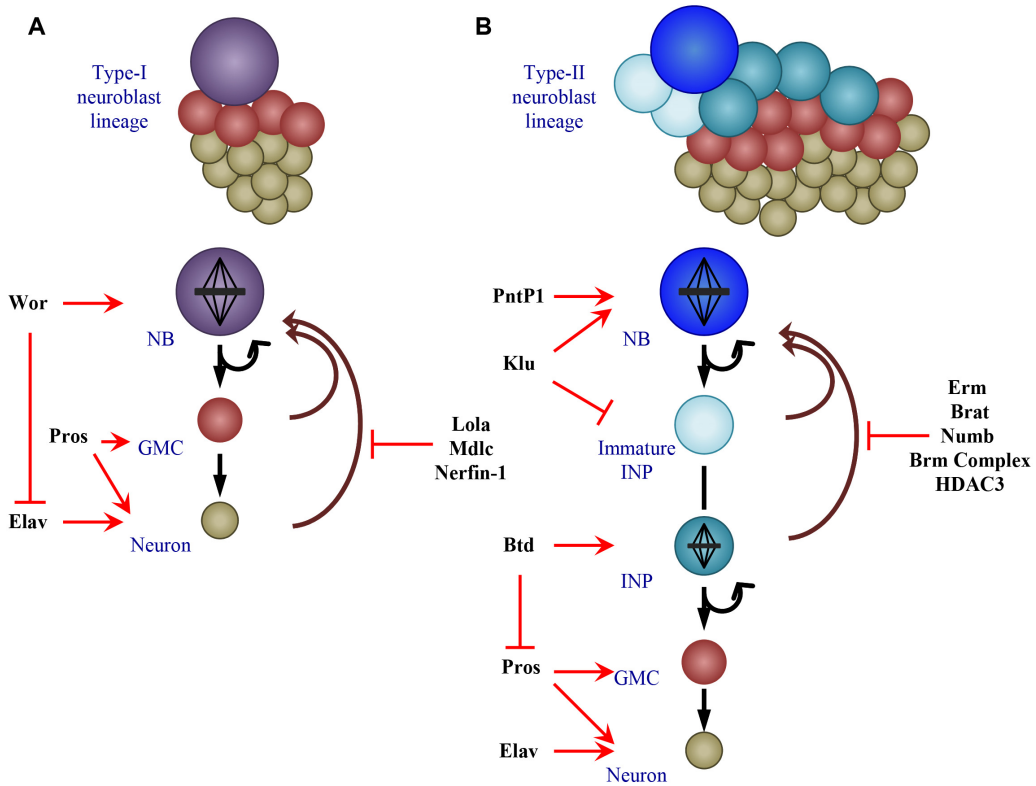

Figure 2. Type I and type II neuroblast lineages in the larval central brain.
Type-I (A) and type-II (B) neuroblast lineages with major regulators mediating the cell fate identities and preventing the de-differentiation pathway are shown. NB: neuroblast; GMC: ganglion mother cell; INP: intermediate neural progenitor.

express Dpn, Ase or Pros, are non-proliferative and are in an immature state. After maturation, the INPs gain the expression of nuclear Ase and Dpn together with cytoplasmic Pros, and they can undergo limited rounds of asymmetric division to self-renewal and give rise to GMCs (Xiao et al., 2012). Hence, type II neuroblast lineages contain larger populations than type I neuroblast lineages (Bello et al., 2008; Boone and Doe, 2008; Bowman et al., 2008) (Fig. 2).

Several regulators responsible for neuroblast lineage progression have been discovered. The RNA binding protein Elav (embryonic lethal abnormal visual system), and transcriptional factors Pros, are two important regulators promoting differentiating cell fates in post-mitotic neurons in both types of neuroblast lineages (Choksi et al., 2006; Koushika et al., 1996; Koushika et al., 2000; Lisbin et al., 2001; Robinow and White, 1988). The snail family protein, Worniu, maintains the neuroblast self-renewal by antagonizing Elav-induced premature differentiation (Lai et al., 2012). Transcriptional factors like Lola, Midlife crisis (Mdlc) and Nerfin-1 are required in neurons to maintain Pros levels and inhibit neuronal de-differentiation (Carney et al., 2013; Froldi et al., 2015; Southall et al., 2014) (Fig. 2A).

Due to the presence of INPs and the similarities to mammalian neurogenesis (Merkle and Alvarez-Buylla, 2006), type II neuroblast lineages have emerged as an excellent model to study the fundamental mechanisms controlling cell fate specification and limited self-renewal capacities in neuroblast progenies. Point-P1 (PntP1), which encodes an Ets transcriptional factor, is responsible for the type II neuroblast lineage identities and generation of INPs, at least partially through inhibiting Ase expression in type II neuroblasts (Zhu et al., 2011). A zinc-finger transcriptional factor, Klumpfuss (Klu), functions to maintain type II neuroblast identities and

prevents the immature differentiation of type II neuroblasts (Berger et al., 2012; Xiao et al., 2012). Cell fate determinants Brain tumor (Brat) and Numb are required to ensure the maturation of immature INPs and their commitments to the INP fate (Bowman et al., 2008). The self-renewal capacity in INPs is limited by another zinc-finger transcriptional factor, Earmuff (Erm), which prevents the de-differentiation of INPs back into the neuroblast state (Janssens et al., 2014; Weng et al., 2010). In contrast, Buttonhead (Btd), a Sp8 transcriptional factor, is required to suppress Pros expression in immature INPs to prevent the premature differentiation of INPs (Xie et al., 2014) (Fig. 2B).

Recently, the roles of several essential epigenetic regulators in type II neuroblast lineage progression have also been identified. The *Drosophila* SWI/SNF Brahma (Brm) remodeling complex was initially identified as regulator of neuroblast self-renewal from a genome-wide RNAi screen (Neumuller et al., 2011). Subsequent studies demonstrated that multiple components of the Brm complex function cooperatively with histone deacetylase 3 (HDAC3) and Erm to suppress de-differentiation of INPs back to neuroblasts in type II neuroblast lineages (Koe et al., 2014) (Fig. 2B). Another transcriptional factor, Hamlet (Ham), is directly induced by the signature subunit of the Brm complex, Osa (Eroglu et al., 2014). Ham functions to limit the proliferation of INPs and to regulate temporal patterning in progenitors (Eroglu et al., 2014). The epigenetic regulation remains of great interest for the studies of neuroblast lineage progression.

1.2.3 Specification of temporal identities in neuroblasts and their progenies

In the developing central nervous system, the same neural progenitor is able to generate various neuronal cell types over time. In *Drosophila*, this is mediated by the 'neuroblast clock', which is a temporal cascade of transcriptional factors expressed in neuroblasts (Homem and Knoblich, 2012). During the first wave of neurogenesis in the embryonic stage, neuroblasts sequentially express Hunchback (Hb), Kruppel (Kr), POU domain protein 1/2 (Pdm1/Pdm2), Castor (Cas) and Grainy head (Grh) (Brody and Odenwald, 2000; Isshiki et al., 2001; Kambadur et al., 1998; Pearson and Doe, 2003; Yang et al., 1993). The temporal transcription factor series progress to the second wave of neurogenesis. During the quiescence stage, the VNC thoracic neuroblasts are able to maintain Cas expression. Upon exit from quiescence, neuroblasts resume the temporal series for the second wave of neurogenesis in the larval stage (Maurange et al., 2008). The transcription factors expressed in neuroblasts are inherited by the daughter GMCs when they are born, and these transcription factors in turn specify the temporal cell fates in neurons (Pearson and Doe, 2003). Hence, early born neurons expressing early transcription factors are often found at the deeper layer of the neuroblast lineage, while later born neurons expressing later transcription factors are located on more superficial layers (Grosskortenhaus et al., 2005).

Several fundamental features of the 'neuroblast clock' have been identified. Evidence has shown that the temporal pattern is established in the neural progenitors rather than in the mature post-mitotic neurons (Pearson and Doe, 2003). Moreover, a network of feedback and feed-forward loops between the transcription factors is responsible for their temporal changes in

a cell intrinsic manner (Kambadur et al., 1998; Pearson and Doe, 2003). However, it remains unclear what is the molecular mechanism that determines the switch between different transcription factors. It has been suggested that the early transition between Hb to Kr is cell cycle-dependent and requires the transient expression of an orphan nuclear receptor, Seven-up (Svp) (Grosskortenhaus et al., 2005; Isshiki et al., 2001; Kanai et al., 2005; Mettler et al., 2006). The efficient expression of Svp requires successive cytokinesis, and blockage of cell divisions disrupts the Hb to Kr transition in neuroblasts (Grosskortenhaus et al., 2005; Mettler et al., 2006). By contrast, the subsequent transitions from Kr to Pdm to Cas occur in a cell cycle-independent manner, suggesting an unknown neuroblast-intrinsic timer is also present to regulate the neuroblast temporal cascade during CNS development (Grosskortenhaus et al. 2005).

The neural diversity in the adult brain central complex is expanded by two combinatorial temporal patterning axes presented in the type-II neuroblast lineages (Bayraktar and Doe, 2013). The intermediate neural progenitors (INPs) within the type-II neuroblast lineages sequentially express transcription factors Dichaete (D), Grainy head (Grh) and Eyeless (Ey), forming a temporal patterning axis which is distinct from the 'neuroblast clock'. Moreover, the parental type-II neuroblasts also temporally express D and Cas in early stage, and Svp in later stage. The INP temporal axis acts together with the temporal axis in their parental neuroblasts to generate distinct neural subtypes, thereby expanding the neural diversity in the adult CNS (Bayraktar and Doe, 2013).

1.3 Intrinsic regulation of neuroblast asymmetric cell division

Stem cells can divide either symmetrically or asymmetrically. They can give rise to two daughter cells with the same identity, generating either two stem cells or two daughter cells with committed cell fates. Alternatively, stem cells can divide asymmetrically to generate two daughter cells with distinct cell fates in one round of division. Both symmetric and asymmetric divisions are utilized by different types of stem cells to tightly regulate the balance between proliferation and differentiation.

Drosophila neuroblasts divide asymmetrically to balance self-renewal and differentiation concomitantly. In each division, one neuroblast divides unequally to generate two daughter cells different in cell size and identity. The bigger daughter cell inherits the self-renewal ability and becomes a new neuroblast, whereas the smaller daughter cell becomes a ganglion mother cell (GMC) that is committed to differentiation pathway (Fig. 3A). The intrinsic regulations of cell polarity, mitotic spindle orientation and asymmetric segregation of cell fate determinants are tightly controlled in neuroblasts. Failure in asymmetric division can disrupt the balance of self-renewal and differentiation, resulting in neuroblast over-proliferation or aberrant differentiation (Li et al., 2014b). In the sections below, some basic features of neuroblast asymmetric division are reviewed.

1.3.1 Establishment of cell polarity

To ensure the asymmetric cell division, the first step is to set up the cell polarity. The neuroblast polarity is established during the late interphase before entering mitosis and is mediated mainly by a group of proteins that are localized at the apical cell cortex. These proteins are termed as the Par complex, including atypical protein kinase C (aPKC), Par6 and Par3/Bazooka

(Baz) (Petronczki and Knoblich, 2001; Rolls et al., 2003; Schober et al., 1999; Wodarz et al., 2000; Wodarz et al., 1999) (Fig. 3B). The Par complex and their homologues in other organisms are known to play essential roles in almost all known cell polarity events (Suzuki and Ohno, 2006).

Baz protein, which contains multiple protein-interacting PDZ domains, is responsible for the coordination of cell polarity axis and positioning of daughter cells after division (Kuchinke et al., 1998). Localized at the apical

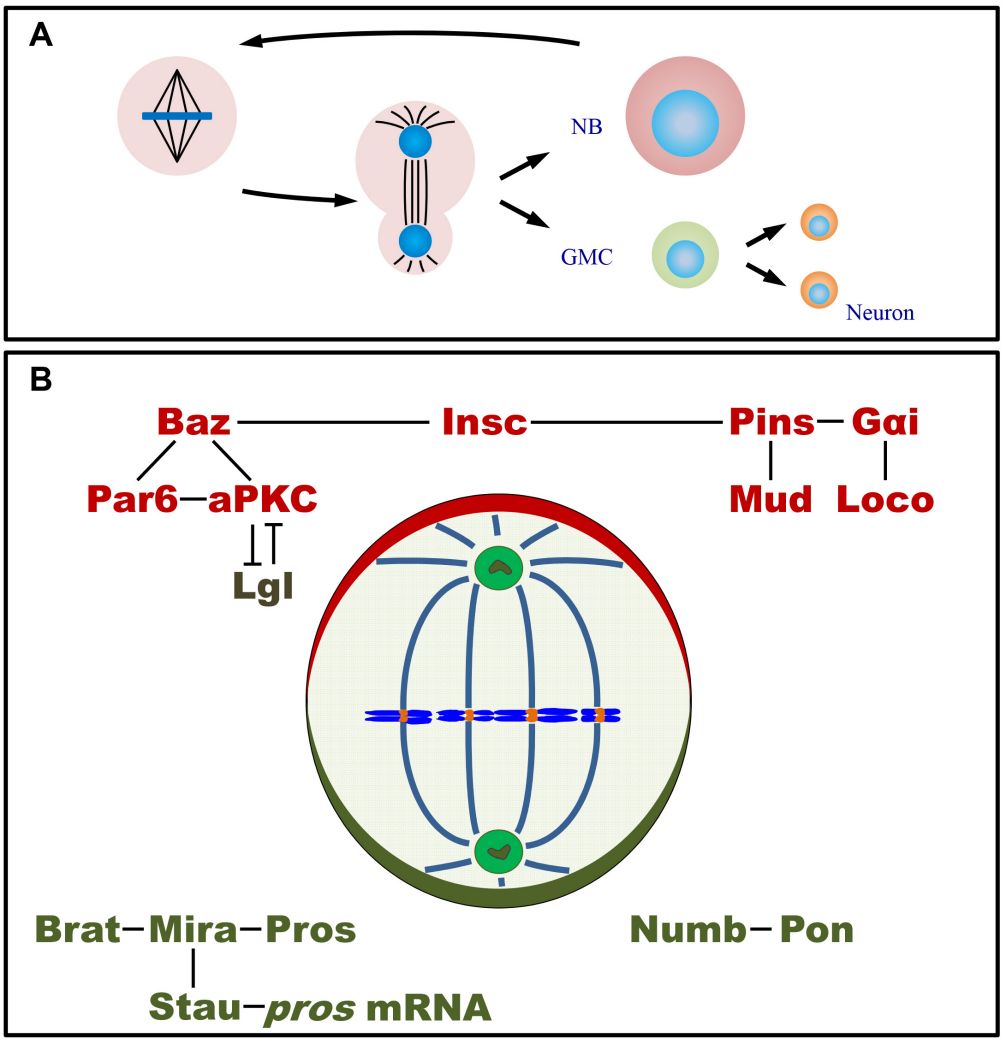

Figure 3. The *Drosophila* neuroblast undergoes asymmetric division.
(A) During asymmetric division, the neuroblast (NB) gives rise to one self-renewing neuroblast and one ganglion mother cell (GMC), which divide terminally to generate two neurons. (B) Asymmetric protein localization in the metaphase neuroblast.

cortical cytoplasm in neuroblasts, Baz is required for the recruitment of Par6 and aPKC to the apical cortex (Petronczki and Knoblich, 2001; Wodarz et al., 2000). Par6 directly binds to Baz. The asymmetric localization of Baz and Par6 is interdependent on each other, and they function co-operatively to establish the cell polarity (Petronczki and Knoblich, 2001). Par6 can also bind to aPKC through the PB1 domain and repress aPKC activity (Atwood et al., 2007; Noda et al., 2003; Wirtz-Peitz et al., 2008). In the neuroblast, aPKC is responsible to mediate the basal localization and correct segregation of cell fate determinants (Atwood and Prehoda, 2009; Smith et al., 2007).

Many factors regulating the activity of the Par complex have been identified. aPKC can function as a proliferative factor, and the levels of aPKC in neuroblasts need to be tightly controlled (Lee et al., 2006b). A zinc-finger transcriptional factor, Zif, is able to directly repress aPKC transcription and prevent the over-elevation of aPKC levels in neuroblasts (Chang et al., 2010). In addition, Zif is also required to prevent mis-localization of aPKC to the entire cell cortex. Interestingly, aPKC is able to phosphorylate and exclude Zif from the nucleus, hence forming a reciprocal repression loop with Zif (Chang et al., 2010). The Rho GTPase Cdc42 is co-localized with the Par complex at the apical cortex in neuroblasts. Acting downstream of Baz, Cdc42 is required for the apical localization of Par6-aPKC and the establishment of cell polarity in neuroblasts (Atwood et al., 2007). Cdc42 binds to the CRIB-PDZ domain of Par6, which in turn activates aPKC by relieving Par6 inhibition (Atwood et al., 2007; Hutterer et al., 2004). The Par complex is also regulated by the heterotrimeric G protein: the β subunit of G protein complex in *Drosophila*, Gβ13F, functions upstream of Baz/Par6/aPKC for their apical localization (Schaefer et al., 2001; Yu et al., 2003). The apically localized Partner of Inscuteable (Pins) and Locomotion defect (Loco) bind to GDP-Gαi through

their GoLoco domains, and act as receptor-independent G protein activators to release and activate Gβ13F (Schaefer et al., 2001; Yu et al., 2003).

In addition, the activity of the Par complex is also controlled by a series of cell cycle regulators. For instance, Aurora-A (AurA) kinase phosphorylates Par6 and triggers the exchange of Lethal (2) giant larvae (Lgl) for Baz, thus activates the Par complex (Wirtz-Peitz et al., 2008). The activity of the Par complex is also modulated by Protein Phosphatase 2A (PP2A) (Chabu and Doe, 2009; Krahn et al., 2009; Ogawa et al., 2009). Through controlling the phosphorylation states of Baz and Par6, PP2A plays essential roles in directing the cell polarity in neuroblasts (Krahn et al., 2009; Ogawa et al., 2009). Recently it is also reported that the SCF^{Slimb} E3 ubiquitin ligase complex composed of Cullin 1 (Cul1), SkpA, Roc1a and the F-box protein Supernumerary limb (Slimb), plays important roles to regulate aPKC localization, in part through the cell proliferation factor Akt (Li et al., 2014a).

Serving as the effector of the Par complex, aPKC is able to govern basal localization of Miranda (Mira) and Numb through direct phosphorylation (Atwood and Prehoda, 2009; Smith et al., 2007). In addition, aPKC also directs the basal Mira localization through interplays with the famous tumor suppressor Lgl. Lgl directly inhibits the kinase activity of aPKC and prevents Mira phosophorylation by aPKC, thus allowing Mira to be retained at the basal cortex (Atwood and Prehoda, 2009). Reversely, aPKC phosphorylates and releases Lgl from its association with membranes and actin cytoskeleton (Betschinger et al., 2003). The phosphorylation of Lgl to an auto-inhibition form thus induces the ‘repressive cascade’ to prevent the apical localization of cell fate determinants (Betschinger et al., 2005; Betschinger et al., 2003).

Furthermore, Baz also interacts with an adaptor protein Inscuteable (Insc), which is linked to the Pins/Gαi complex to mediate spindle orientation

(Schober et al., 1999; Wodarz et al., 1999; Yu et al., 2000) (Fig. 3B). Hence, the establishment of cell polarity is critical for both spindle orientation and segregation of cell fate determinants into the future ganglion mother cell (GMC), which are the other two important features of the asymmetric cell division.

1.3.2 Mitotic spindle orientation

During neuroblast asymmetric division, the mitotic spindle is aligned along the apico-basal axis. This is essential to direct the position of cleavage furrow upon cytokinesis, which is important for the exclusive segregation of asymmetric proteins into different daughter cells (Li et al., 2014b). The proper

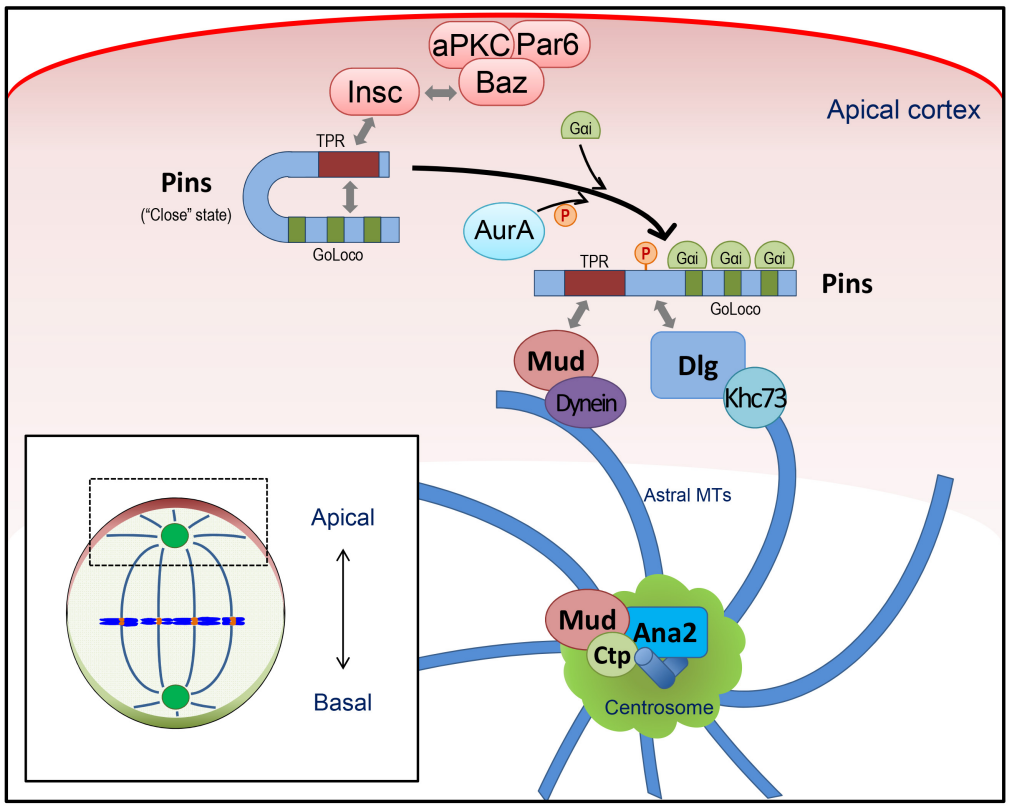

Figure 4. The molecular machinery controlling spindle orientation in neuroblasts.
The apically localized Pins is activated through the binding of Gαi and the phosphorylation by AurA, and acts through Pins/Dlg/Khc73 pathway and Pins/Mud/Dynein pathway to direct the spindle alignment. At the centrosome, the Ana2/Ctp/Mud complex is responsible for the proper spindle orientation.

spindle orientation is mediated mainly by the apically localized complex consists of the heterotrimeric G protein α subunit i (Gαi), Partner of Inscuteable (Pins), Locomotion defect (Loco) and Mushroom body defects (Mud), together with the centrosome, which serves as the major microtubule organizing center (MTOC) (Fig. 3B and Fig. 4).

Insc is the first identified regulator to orient neuroblast division in *Drosophila* (Kraut et al., 1996). Inherited from the neuroepithelium upon neuroblast delamination, Insc is localized at the apical cortex and acts as an adaptor protein linking the Pins/Gαi complex to the Par complex (Wodarz et al., 1999; Yu et al., 2000). The apical localization of Insc is dependent on Baz, which binds to the central region of Insc directly (Schober et al., 1999; Tio et al., 1999; Wodarz et al., 1999). On the other hand, Insc is required for the stability of Baz, presumably by preventing Baz from undergoing proteolytic degradation in neuroblasts (Wodarz et al., 1999).

Pins is identified as a protein binding to the central asymmetric localized domain of Insc (Yu et al., 2000). Pins contains seven Tetratricopeptide (TPR) motifs at the N-terminal and three GoLoco domains near the C-terminal (Schaefer et al., 2000; Yu et al., 2000). Localized at the apical cortex, Pins is required for Insc localization and spindle orientation in dividing neuroblasts (Schaefer et al., 2000; Yu et al., 2000). Pins forms a complex with the apically localized Gαi, and the polarized localization of Pins and Gαi is dependent on each other (Schaefer et al., 2001; Schaefer et al., 2000; Yu et al., 2000). Loss of *Gαi* displays similar phenotype as loss of *pins*, indicating that Pins and Gαi function in the same pathway (Cai et al., 2003; Yu et al., 2003). Interestingly, overexpression of wild-type Gαi, but not GTP-bound Gαi, displays defects in spindle orientation in neuroblasts (Schaefer et al., 2001; Yu et al., 2003). This spindle mis-orientation phenotype upon overexpression of Gαi is presumably

caused by the inhibition of Gβ13F, which is upstream of both the Par complex and the Pins/Gαi complex (Schaefer et al., 2001). The two GoLoco domain proteins, Pins and Loco, act synergistically as guanine nucleotide dissociation inhibitors (GDIs) for Gαi to release free Gβ13F in neuroblasts (Yu et al., 2003; Yu et al., 2005). In addition, the *Drosophila* Ric8 acts as a receptor-independent guanine nucleotide exchange factor (GEF) for Gαi, which maintains the Gβ13F levels and facilitates the asymmetric localization of Gαi in neuroblasts (Wang et al., 2005).

In addition to the apical Par/Insc pathway, the cortical polarity of Pins/Gαi can be induced by a signaling network consisting of astral microtubules (MTs), the kinesin heavy chain Khc-73, and the tumor suppressor Discs large (Dlg) (Siegrist and Doe, 2005). Khc-73 is a motor protein that binds to the plus-end of microtubules (Li et al., 1997a). Khc-73 forms a complex with the membrane-localized Dlg, while Dlg is able to bind to the linker domain of Pins to induce the Pins/Gαi cortical polarity independent of the Par/Insc pathway (Siegrist and Doe, 2005). Hence, the astral microtubules/Khc-73/Dlg pathway and the cortical Pins/Gαi/Dlg proteins form bidirectional signaling pathways between the mitotic spindle and the apical cortex (Siegrist and Doe, 2005) (Fig. 4).

The downstream effector for Pins/Gαi in regulating spindle orientation is the NuMA-related protein Mud (Bowman et al., 2006; Izumi et al., 2006; Siller et al., 2006). Pins directly binds to Mud through its N-terminal TPR motifs, and is required to target Mud to the apical cortex in neuroblasts (Bowman et al., 2006; Izumi et al., 2006; Siller et al., 2006). Biochemical data showed that Pins protein can form a ‘closed’ state, through intracellular interaction between its N-terminal TPR motifs and C-term GoLoco domains (Nipper et al., 2007). The binding of Gαi to the GoLoco domains activates Pins from this

auto-inhibition state and allows the TPR motifs to recruit Mud to the apical cortex, hence aligns mitotic spindles along the apico-basal polarity in neuroblasts (Nipper et al., 2007) (Fig. 4). Another signaling pathway consisting of the Ras-like small GTPase Rap1, guanine exchange factor Rgl and its effector Ral, is also important for the spindle orientation (Carmena et al., 2011). The Rap1-Rgl-Ral pathway signals through the apically localized PDZ protein Canoe (Cno), which forms a complex with Pins and is required for the cortical localization of Mud in neuroblasts (Carmena et al., 2011; Speicher et al., 2008).

Besides the apical protein complex, the centrosome also plays crucial roles for the correct alignment of mitotic spindles in neuroblasts. Spindle orientation is disrupted upon loss of several centrosome-associated proteins (Gonzalez, 2007). For example, the centriolar protein Anastral spindle 2 (Ana2), which is implicated in the centriole duplication and centrosome formation, plays essential roles in the alignment of mitotic spindles along the apico-basal polarity in larval central brain neuroblasts (Stevens et al., 2010; Wang et al., 2011). Ana2 forms a complex with a cytoplasmic dynein light chain Cut up (Ctp), and together they localize Mud to the spindle poles/centrosomes and maintain the Pins-Mud interaction at the apical cortex (Wang et al., 2011) (Fig. 4).

1.3.3 Asymmetric localization and segregation of cell fate determinants

Several proteins are localized at the basal cortex during the metaphase of the cell division, and they are segregated into the future ganglion mother cells to initiate the differentiation pathway (Fig. 3B). These proteins include Prospero (Pros), Brain tumor (Brat) and Numb, which are well known cell fate determinants, and their adapting proteins, Miranda (Mira), Staufen (Stau) and

Partner of Numb (Pon) (Bello et al., 2006; Betschinger et al., 2006; Broadus et al., 1998; Knoblich et al., 1995; Lee et al., 2006c; Lu et al., 1998; Matsuzaki et al., 1998; Spana and Doe, 1995).

Mira functions as a scaffold protein that directs the basal localization of Pros, Brat, Stau and *pros* RNA (Betschinger et al., 2006; Ikeshima-Kataoka et al., 1997; Lee et al., 2006c; Schuldt et al., 1998; Shen et al., 1997). It is asymmetrically localized at the basal cortex and is segregated to the GMC upon division (Ikeshima-Kataoka et al., 1997; Shen et al., 1997). The cortical association of Mira is regulated by a conserved Phosphotyrosyl Phosphatase Activator (PTPA), together with the Protein Phosphatase 4 (PP4) complex. The PTPA/PP4 complex facilitates the de-phosphorylation of Mira at the threonine 591 residue and allows it to be localized to the cell cortex (Zhang et al., 2016). The Par complex component aPKC is required to restrict the basal localization of Mira. aPKC is able to directly phosphorylate several threonine

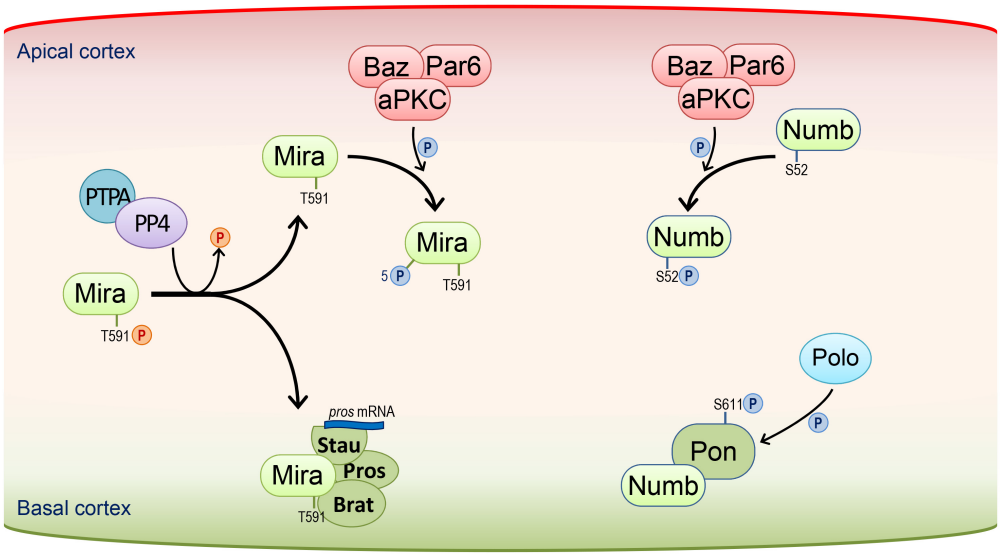

Figure 5. The molecular machinery for basal localization of cell fate determinants in neuroblasts.
Mira is first targeted to the cell cortex through de-phosphorylation by the PTPA/PP4 complex, and is subsequently restricted to the basal cortex mediated by apical aPKC. The basal localization of Numb and Pon is also directed through the phosphorylation by aPKC and Polo.

and serine residues located at the N-terminal 1-290aa region of Mira, resulting in displacement of Mira from the apical cortex (Atwood and Prehoda, 2009). On the other hand, aPKC phosphorylates Lgl and initiates the 'repressible cascade' to mediate the basal localization of Mira (Betschinger et al., 2003). Hence, the basal cortical localization of Mira is established by a two-step process: upon nuclear envelop breakdown, the PTPA/PP4 complex directs Mira to the cell cortex, followed by the apical aPKC-mediated basal restriction (Zhang et al., 2016) (Fig. 5).

Analysis of different Mira functional domains revealed that the N-terminal 1-290 aa region is required for its basal cortical localization, the central 446-727 aa domain is responsible for its 'cargo binding' of Pros, Brat, Stau as well as *pros* mRNA, whereas the C-terminal 727-830 aa domain is necessary for its timely degradation and the release of cargos upon cytokinesis (Fuerstenberg et al., 1998; Jia et al., 2015; Lee et al., 2006c). The central cargo-binding-domain (CBD) of Mira (514-595 aa) can form an elongated parallel coiled-coil dimer, and the dimerization of the Mira CBD is essential for the asymmetric localization of Pros, Brat and Stau in neuroblasts (Jia et al. 2015). Mira undergoes degradation upon division, allowing its cargos to be released from the membrane to initiate the differentiation pathway in GMCs (Ikeshima-Kataoka et al., 1997; Lee et al., 2006c).

The cell fate determinant Pros is a homeodomain-containing protein belonging to the Prox1 (Prospero homeobox 1) family (Doe et al., 1991; Knoblich et al., 1995; Vaessin et al., 1991). Pros is a differentiation factor, as loss of *pros* results in aberrant expression of cell-cycle genes and change of GMC cell fates, whereas ectopic expression of Pros causes premature termination of cell division (Bello et al., 2006; Li and Vaessin, 2000). Synthesized in most neuroblasts, Pros is localized to the basal cell cortex

during mitosis, and is asymmetrically segregated into the GMC daughter cells (Bowman et al., 2008; Hirata et al., 1995; Knoblich et al., 1995). The central 825-943 aa region of Pros, which interacts with the adaptor protein Mira, is responsible for its asymmetric localization in neuroblasts (Hirata et al., 1995; Shen et al., 1997). Pros is released from the cell cortex and translocated into the nucleus in GMCs, functioning as a transcription factor to suppress cell cycle genes and activate differentiation genes. Hence, Pros acts as a binary switch between self-renewal and differentiation (Choksi et al., 2006).

Stau is a dsRNA-binding protein, which mediates mRNA transportation in different systems (Heraud-Farlow and Kiebler, 2014; St Johnston et al., 1991). Through the dsRNA-binding-domains (dsRBDs), Stau binds to the 3' UTR of *pros* mRNA and directs its localization in dividing neuroblasts (Broadus et al., 1998; Li et al., 1997b). Stau and *pros* mRNA are co-localized with Insc at the apical cortex during interphase (Li et al., 1997b; Schuldt et al., 1998). The dsRBD5 of Stau interacts with the cargo-binding-domain (CBD) of Mira, and during prophase, Stau and *pros* mRNA are recruited by to the basal cell cortex (Jia et al., 2015; Schuldt et al., 1998). This allows the segregation of *pros* mRNA to the GMCs, in which *pros* mRNA and Pros protein act redundantly to specify GMC cell fates (Broadus et al., 1998). Since *pros* gene is not transcribed in GMCs, the asymmetric segregation of Stau and *pros* mRNA may play important roles to maintain the Pros protein levels and to ensure the differentiation in GMCs (Broadus et al., 1998).

Another cell fate determinant recruited by Mira is Brat, which is a posttranscriptional regulator belonging to a family of conserved tumor suppressors (Arama et al., 2000). In larval central brain neuroblasts, Brat is asymmetrically distributed to the basal cortex and is partitioned to the smaller daughter cell, and loss of *brat* generates a massive overgrowth of type II

neuroblast-like cells that are negative for Ase or Pros (Bello et al., 2006; Betschinger et al., 2006; Bowman et al., 2006; Lee et al., 2006c). The N-terminus of Brat contains two B-boxes and a coiled-coil motif, while the C-terminus contains an evolutionarily conserved NHL (NCL-1, HT2A and LIN-41) domain, which is involved in the regulation of mRNA translation (Arama et al., 2000; Sonoda and Wharton, 2001). Brat acts as a posttranscriptional regulator of dMyc, presumably through the NHL domain, and controls ribosome biogenesis and protein translation to prevent de-differentiation of immature INPs (Betschinger et al., 2006). Moreover, a recent study has revealed that the N-terminus B-boxes of Brat are required for the specification of INP fates by downregulation of β-catenin/Armadillo activity in immature INPs (Komori et al., 2014).

The other basally localized complex consists of the Notch inhibitor Numb and its adaptor Pon. The Phosphotyrosine-binding (PTB) domain protein Numb belongs to a conserved family controlling cell fate decisions in variant systems (Dho et al., 1998; Verdi et al., 1996). In the *Drosophila* central nervous system (CNS), Numb functions upstream and antagonizes the Notch pathway to specify sibling neuron fates (Skeath and Doe, 1998). In neuroblasts, Numb is directly phosphorylated by aPKC at Ser52 and Ser304, and is targeted to the basal cell cortex (Smith et al., 2007; Wirtz-Peitz et al., 2008) (Fig. 5). Loss of *numb* generates supernumerary neuroblasts, suggesting that Numb functions as a tumor suppressor (Bowman et al., 2008; Lee et al., 2006a; Wang et al., 2006). Through interaction with the endocytic AP-2 complex subunit, α-Adaptin (α-Ada), Numb is required to promote the endocytosis of the Notch signaling enhancer Sanpodo (Spdo), thus down-regulates Notch pathway in the differentiating daughter cells (Song and Lu, 2012). Phosphorylation at conserved sites at the PTB domain by Polo kinase

inhibits the tumor suppressor activity of Numb, and PP2A acts antagonistic to Polo to maintain Numb activity (Ouyang et al., 2011).

Identified as a binding partner to the PTB domain of Numb, Pon is also localized at the basal cell cortex in neuroblasts (Lu et al., 1998). Pon is a part of the cellular machinery relaying the cortical polarity cues to localize Numb to the basal cortex, as loss of *pon* causes a delay in the formation of Numb crescents (Lu et al., 1998). The dynamics of the asymmetric localization of Pon has been revealed: Pon protein is first recruited from the cytosol to the cell cortex at early stage of mitosis, which is dependent on its C-terminal region. The cortically recruited Pon protein is later restricted to the basal side, and this procedure requires actomyosin and Insc (Lu et al., 1999). Moreover, the serine 611 residue of Pon is phosphorylated by the cell cycle regulator Polo for the proper Numb localization, suggesting that the regulation of Pon is critical for neuroblast asymmetric division (Wang et al., 2007).

1.4 Defective asymmetric division in neuroblasts: a model of tumorigenesis

Tumorigenesis is a process when normal cells are transformed into cancer cells and gaining the capacity to undergo uncontrolled proliferation, generating a malignant tissue mass. *Drosophila* larval brain neuroblast has emerged as a useful model to recapitulate the progression of tumorigenesis (Knoblich, 2010). In normal brains, self-renewal and differentiation in neuroblasts are tightly controlled through asymmetric division, so that correct number of stem cells and proper amount of progenies are generated. Mis-regulation of neuroblast asymmetric division can cause shift of the balance, resulting in disruption of neuroblast homeostasis. Growing evidence has shown that failure in neuroblast asymmetric division often results in un-

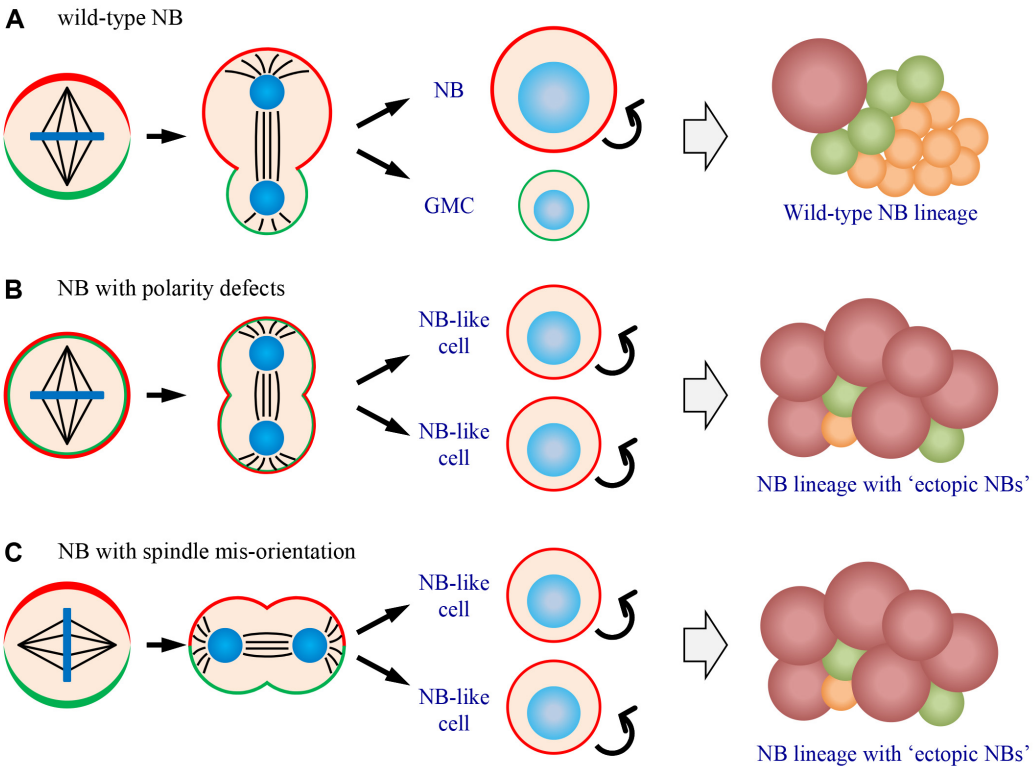

Figure 6. Defects in asymmetric division can result in formation of ectopic neuroblasts.
A wild-type neuroblast (A) segregates asymmetric proteins exclusively to two daughter cells to balance self-renewal and differentiation, whereas neuroblasts with cell polarity defects (B) or spindle mis-orientation (C) can mis-segregate determinants to both daughter cells, generating two neuroblast-like cells in one division. NB: neuroblast; GMC: ganglion mother cell.

controlled proliferation of neuroblasts in the central brain (Li et al., 2014b). Moreover, the neuroblast overgrowth in the central brain is often accompanied with enlarged brain sizes and increase of proliferating cells positive for cyclin E (cycE), phospho- Histone 3 (pH3) and dMyc (Wang et al., 2009a; Wang et al., 2007; Wang et al., 2006), which resembles the phenotype of brain tumor.

One explanation for tumor formation caused by defective asymmetric division is that determinants are not properly segregated upon cytokinesis, resulting in inheritance of self-renewal capacity in both daughter cells. As

introduced in section 1.3.1, the apically localized Par complex is responsible for the establishment of the cell polarity. The core effector in the Par complex, aPKC, functions as a proliferative factor in neuroblasts (Lee et al., 2006b). When aPKC was forced localized to the entire cell cortex by overexpression of a membrane-bound aPKC (aPKC-CAAX) in neuroblasts, both daughter cells acquired stem cell identities, causing over-proliferation of neuroblasts in the brain (Lee et al., 2006b). In mutants such as *lgl*, *aurA*, *polo*, *mts* and *cul1* that alter the asymmetric localization of aPKC, brain tumor phenotype is also observed, suggesting the correlation between cell polarity defects and tumorigenesis (Lee et al., 2006a; Wang et al., 2009a; Wang et al., 2007; Wang et al., 2006) (Fig. 6B). In addition, mitotic spindle mis-orientation can also cause mis-segregation of asymmetric proteins, generating overgrowth of neuroblast in the larval brains. In *mud* or *ana2* mutants, mitotic spindles are often randomly orientated while cell polarity remains normal in metaphase neuroblasts. However, upon cell division, asymmetric proteins are mis-segregated to both daughter cells due to improper alignments of mitotic spindles (Bowman et al., 2006; Izumi et al., 2006; Siller et al., 2006; Wang et al., 2011), suggesting the importance of proper spindle orientation for the maintenance of neuroblast homeostasis (Fig. 6C).

The association of defective asymmetric divisions with tumorigenesis is further supported by a transplantation assay (Caussinus and Gonzalez, 2005; Wang et al., 2011; Wang et al., 2006). When the brain tissue from mutants displaying defective asymmetric divisions (for example from *lgl*, *pins*, *ana2* mutants) was transplanted into the abdomen of wild-type hosts, the allograft tissue underwent massive overgrowth, exhibited many hallmarks of malignant tumor and was able to kill the host within several weeks (Caussinus and

Gonzalez, 2005). These results further support that disruptions in asymmetric division can lead to formation of malignant tumor.

1.5 Major regulators of neuroblast asymmetric division

Over the previous two decades, numerous proteins have been identified as important regulators in neuroblast asymmetric divisions. In this section, previous results regarding the two major groups of regulators controlling neuroblast asymmetric division are reviewed.

1.5.1 Cell cycle regulators

The cortical polarity shows a cell cycle dependent manner, and a series of cell cycle regulator are identified as critical regulators of the neuroblast asymmetric division (Li et al., 2014b). Cdc2, which is known to promote G2 to M phase transition, is the first identified factor linking cell cycle regulation and neuroblast asymmetric division machineries (Nurse, 1990; Tio et al., 2001). Attenuation of *cdc2* function results in defective cortical polarity in mitotic neuroblasts, suggesting that cell cycle regulators could play essential roles in controlling asymmetric division (Tio et al., 2001).

Cell cycle-related kinase, Aurora-A (AurA), is required for neuroblast asymmetric division and suppression of neuroblast overgrowth (Lee et al., 2006a; Wang et al., 2006). AurA regulates cortical localization of aPKC and Numb, as well as the mitotic spindle orientation. Evidence showed that the Notch signal inhibitor Numb is the major downstream target for AurA to regulate neuroblast self-renewal (Wang et al., 2006), and the detailed signaling cascade of this process has been discovered. AurA directly phosphorylates Par6 and initiates the release of aPKC from an inhibition state. The activated aPKC phosphorylates and release Lgl, allowing the

recruitment of Baz into the Baz/Par6/aPKC complex. Consequently, aPKC is able to phosphorylate and mediate the basal localization of Numb in neuroblasts (Wirtz-Peitz et al., 2008). Besides, AurA regulates the spindle orientation, presumably through mediating the asymmetric localization of Mud (Lee et al., 2006c; Wang et al., 2006). AurA phosphorylates Pins at the serine 436 residue in the LINKER domain, and functions upstream of the $Pins^{LINKER}$-Dlg-Khc-73 and $Pins^{TPR}$-Mud-Dynein/Dynactin pathway to govern the proper orientation of mitotic spindles (Johnston et al., 2009).

Another cell-cycle-related kinase, Polo, is also identified as an important regulator of neuroblast asymmetric division and self-renewal. Loss of *polo* results in defective asymmetric localization of aPKC, Pon and Numb, as well as spindle mis-orientation. As a consequence, *polo* mutant brains display neuroblast overgrowth (Wang et al., 2007). Polo phosphorylates Pon at serine 611 residue in the C-terminal localization domain, and phosphorylation of Pon-S611 is required for the cortical polarity of Pon and Numb in metaphase neuroblasts. Evidence revealed that Numb functions downstream of Polo to regulate neuroblast self-renewal (Wang et al., 2007). However, how Polo kinase regulates the localization of aPKC and spindle orientation still remains unknown. Interestingly, Polo kinase can also phosphorylate Numb at the conserved PTB domain, causing attenuation of Numb activity. Over-activation of Polo generates ectopic type II neuroblasts, presumably via boosting endogenous phosphor-Numb levels (Ouyang et al., 2011). Together, these data highlight the link between cell cycle kinases and the control of asymmetric division in neuroblasts.

The asymmetric machinery is also regulated by protein phosphatases. For example, the roles of Protein Phosphatase 2A (PP2A) complex in regulating neuroblast cell polarity have been revealed in several studies. The

Drosophila PP2A complex is composed of a catalytic C-subunit Microtubule star (Mts), a scaffolding A-subunit PP2A-29B, and a variable regulatory B-subunit responsible for substrate specificity, such as Twins (Tws), Widerborst (Wdb), B56-1 and PR-72 (Janssens and Goris, 2001). Disruption of PP2A functions results in defects in cell polarity and spindle orientation (Chabu and Doe, 2009; Krahn et al., 2009; Ogawa et al., 2009; Ouyang et al., 2011; Wang et al., 2009a). Moreover, PP2A also functions as a brain tumor suppressor to inhibit neuroblast self-renewal in the larval brain (Chabu and Doe, 2009; Ouyang et al., 2011; Wang et al., 2009a). Variant evidence has indicated the roles of PP2A in regulating the activity of the apical Par complex (Chabu and Doe, 2009; Krahn et al., 2009; Ogawa et al., 2009). Different components of the Par complex are found associated with Mts, PP2A-29B and the B-subunit Tws. PP2A is able to mediate the de-phosphorylation of Par6 or Baz, which in turn contributes to the establishment of cell polarity and division orientation (Chabu and Doe, 2009; Krahn et al., 2009; Ogawa et al., 2009). In addition, PP2A complex regulates neuroblast self-renewal through a Polo/Numb pathway, in which PP2A is required to maintain Polo levels to control Numb localization and activity (Wang et al., 2009a). Interestingly, PP2A can also control Numb activity directly through de-phosphorylation of several conserved sites in the PTB domain, thus preventing the formation of ectopic neuroblasts in type II neuroblast lineages (Ouyang et al., 2011).

Besides the PP2A complex, the conserved Protein Phosphatase 4 (PP4) complex is also required for neuroblast asymmetric division. The PP4 complex functions as a heterotrimeric complex consisting of one catalytic subunit PP4C, and two regulatory subunits PP4R2 and PP4R3/Falafel (Flfl) (Gingras et al., 2005). When PP4 function is compromised, Mira and its cargo proteins are mis-localized to the cytoplasm, whereas apically localized

proteins and the basally localized Pon-Numb complex are not affected (Sousa-Nunes et al., 2009). In interphase and prophase neuroblasts, the regulatory subunit of PP4 complex, Flfl, is localized predominantly in the nucleus and is required to exclude nuclear Pros and Mira. After nuclear envelop breakdown, Flfl is cytoplasmic, and is responsible to target Mira to the cell cortex (Sousa-Nunes et al., 2009). PP4 complex directs Mira to the cell cortex through de-phosphorylation on the threonine 591 residue, and this event is coordinated by Phosphotyrosyl Phosphatase Activator (PTPA) and is prerequisite for the aPKC-mediated Mira basal cortical localization (Zhang et al., 2016).

A few groups of ubiquitin ligase responsible for protein degradation are also identified as regulators of asymmetric division. The Anaphase-Promoting-Complex/Cyclosome (APC/C), which belongs to the cell cycle machinery coordinating the transition from metaphase to anaphase, is an E3 ubiquitin ligase responsible for targeting cell cycle proteins to the degradation pathway (Holloway et al., 1993). Loss of *imaginal discs arrested* (*ida*), a subunit of the APC/C multi-protein complex, results in mis-localization and accumulation of Mira at pericentrosomal regions. Evidence showed that APC/C is required for the ubiquitylation of Mira via its C-terminal domain, and this event is required for the asymmetric localization of Mira and its cargo proteins (Slack et al., 2007). The SCF^{Slimb} E3 ligase complex is recently identified as essential regulators for neuroblast homeostasis in the larval brains. Loss of *cul1*, *skpA*, *roc1A* or *slimb* results in defective cortical polarity of aPKC and Numb, which causes overgrowth of neuroblasts (Li et al., 2014a). The cell growth and proliferation factor Akt is ubiquitinated by Slimb, and hyperactivation of Akt phenocopies loss of *cul1*, suggesting that the

SCF^{Slimb} complex functions upstream of Akt to regulate cortical polarity and inhibit ectopic neuroblast formation (Li et al., 2014a).

1.5.2 Centrosome and microtubule-associated proteins

Neuroblast asymmetric division is also regulated by a series of centrosomal proteins and microtubule-associated proteins. Evidence has shown that loss of centrosome function can lead to failure of mitotic spindle alignment (Li et al., 2014b). A centrosome consists of one pair of centrioles surrounding by an amorphous matrix of pericentriolar material (PCM). The centriolar proteins Asterless (Asl), Spindle assembly abnormal 4 (Sas-4) and Anastral spindle (Ana2), which are essential regulators of centriole duplication and assembly, are required for the proper spindle orientation in dividing neuroblasts (Basto et al., 2006; Dzhindzhev et al., 2010; Giansanti et al., 2001; Wang et al., 2011). In addition, a number of important PCM components including Centrosomin (Cnn), AurA and Polo, are crucial regulators of spindle orientation (Lee et al., 2006a; Megraw et al., 1999; Wang et al., 2007; Wang et al., 2006).

As discussed in the above sections, defective spindle orientation can often result in mis-segregation of asymmetric proteins into different daughter cells, leading to formation of ectopic neuroblasts in the larval brain (Fig. 6C). Neuroblast overgrowth is found in mutant brains of *cnn*, *ana2* and *mud*, which display mis-alignment of mitotic spindles (Bowman et al., 2006; Cabernard and Doe, 2009; Wang et al., 2011). The underlying mechanism of how centrosomal proteins regulating spindle orientation can be exemplified by the studies carried out in *ana2* mutants (Wang et al., 2011). The centriolar protein Ana2 is able to interact with a cytoplasmic dynein light chain protein Cut up (Ctp), and together they are required for the centrosomal localization of Mud.

Through mediating the centrosomal Mud localization and the apical Pins-Mud interaction, Ana2 and Ctp play critical roles in orienting the mitotic spindles along the apico-basal axis (Wang et al., 2011).

Defective in aPKC and Numb localization is also observed in loss of centrosomal proteins AurA and Polo (Lee et al., 2006a; Wang et al., 2007; Wang et al., 2006). However, the cortical polarity defect in loss of *aurA* or *polo* may not be attributed to their function in centrosomes. Notably, loss of *ana2*, which depletes the centrosome, causes severe spindle mis-orientation without altering the cell polarity, suggesting that the centrosome is not required for cortical polarity during neuroblast asymmetric division (Wang et al., 2011).

The centrosome is the major microtubule-organizing center. Loss of centrosome often accompanies with devoid of astral microtubules, while the assembly of mitotic spindle can still be initiated from chromosomes (Compton, 2000; Giansanti et al., 2001). Several studies have revealed the roles of astral microtubules and microtubule-associated proteins in the regulation of spindle orientation in neuroblasts. One such regulator is the plus-end direct motor protein, Kinesin heavy chain 73 (Khc-73). Khc-73 functions downstream of the $Pins^{LINKER}$/Dlg complex to mediate the spindle orientation (Johnston et al., 2009). In addition, Khc-73 participates in the astral microtubules/Khc-73/Dlg pathway to induce Pins/Gαi cortical polarity (Siegrist and Doe, 2005). Another example is the dynein complex, a minus end-directed motor complex consisting of two heavy chains, two intermediate chains and several light chains (Roberts et al., 2013). The function of the dynein complex in transportation of cargo proteins is assisted by the dynactin complex and its cofactor Lissencephaly-1 (Lis1). Studies using live imaging in larval brain neuroblasts revealed that astral microtubule and Lis1/dynactin are required to

mediate spindle-cortex forces, which in turn contribute to the mitotic spindle alignment with the cortical polarity axis (Siller and Doe, 2008). The dynein/dynactin is also involved in the $Pins^{TPR}$/Mud/Dynein pathway to direct spindle orientation in an induced polarized S2 cell system (Johnston et al., 2009). Consistently, loss of the dynein light chain *cut up (ctp)* and the heavy chain *dhc64C* results in random orientation of mitotic spindles in larval brain neuroblasts (Wang et al., 2011).

1.6 The roles of centrosomes during cell division

The centrosome is an essential organelle functioning as the microtubule organizer in most dividing cells. Each centrosome contains a pair of centrioles located at its core, and a matrix of pericentriolar material (PCM) which can contain up to hundreds of different proteins surrounding the centrioles. The *Drosophila* and its derived models have been used extensively to understand the structures and functions of the centrosome during cell division (Conduit et al., 2015; Fu et al., 2015). Nowadays, the mechanisms underlying centrosome assembly and how it functions to organize microtubule in dividing cells have been elucidated. Particularly, the mother and daughter centrosomes in *Drosophila* neural stem cells behave unequally. In the section below, the characteristics of centrosome cycle and the regulation of the centrosome asymmetry in *Drosophila* neuroblasts are reviewed.

1.6.1 Centrosomes serve as the major microtubule organizing centers (MTOCs)

The behaviors of centrosomes are tightly regulated in dividing cells, which ensures the centrosome cycle is in concert with the cell-division cycle. The centriole duplication starts from G1/S phase, when the procentriole is

assembled perpendicular to its 'mother' centriole. Each procentriole elongates until it reaches a similar size with its 'mother' throughout the G2 phase. Before mitosis, the fibrous tether linking the two centriole pairs is broken, and the two centriole pairs separate and move towards the opposite sites of the cells in preparation for spindle assembly. Accompanied with the centrosome separation/disjunction is the centrosome maturation, when the amount of PCM proteins recruited dramatically expands. Many of these PCM proteins are required for the nucleation of microtubules, and they contribute to the assembly of a robust mitotic spindle (Conduit et al., 2015; Fu et al., 2015) (Fig. 7).

The core pathway for centriole duplication has been revealed in several systems. In *Drosophila*, a group of highly conserved centriolar proteins including Asl, Plk4 (SAK), Sas6, Ana2 and Sas4, are required for the *de novo*

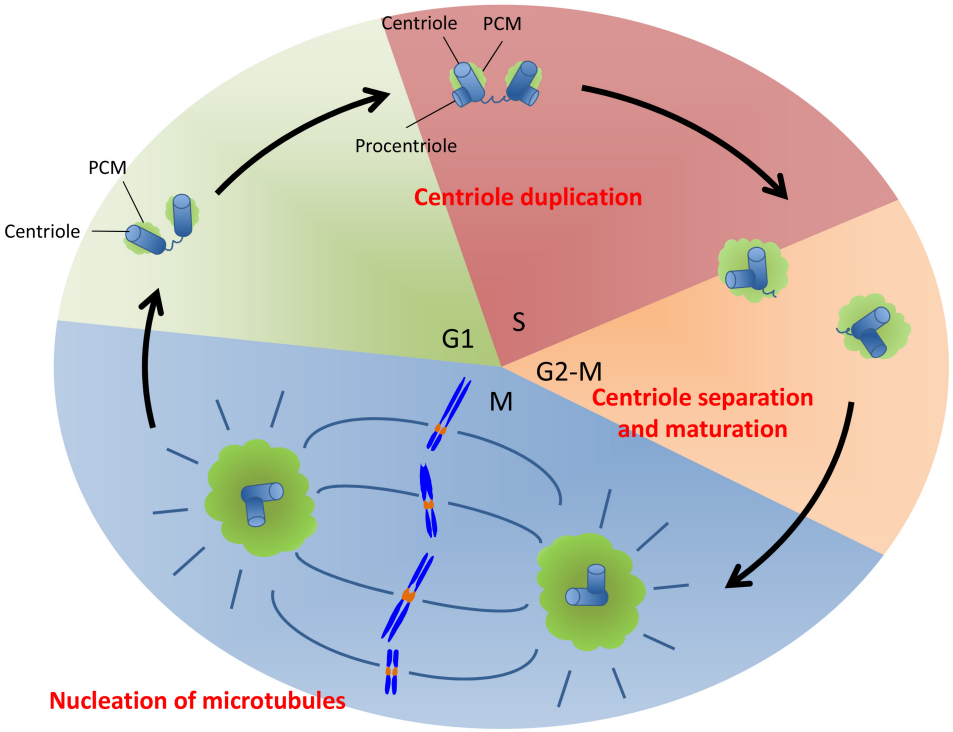

Figure 7. The duplication cycle of centrosomes in dividing cells.
The centrosome undergoes centriole duplication, separation and maturation processes to function as microtubule organizing center (MTOC), and the centrosome duplication cycle occurs in concert with the cell-division cycle.

assembly of the centriole. It is believed that the basic structure of the centriole is conserved among most eukaryotic cells, with a symmetric 'cartwheel-like' structure in the inner core surrounding by the microtubule wall (Conduit et al., 2015). Several key components of the *Drosophila* centriole structures have been revealed by the 3-dimentional structured illumination microscopy (3D-SIM): the Sas6 and Ana2 are localized at the innermost part of the centriole (Dzhindzhev et al., 2014), while Sas4 is co-localized with the microtubule wall (Fu and Glover, 2012). Consistently, evidence showed that Sas6 and Ana2 are both required to work cooperatively to trigger centriole assembly (Dzhindzhev et al., 2014; Rodrigues-Martins et al., 2007a; Stevens et al., 2010).

One key component regulating the *de novo* assembly pathway is the kinase Plk4 (SAK). Overexpression of Plk4 in unfertilized eggs is sufficient to drive *de novo* centriole formation (Rodrigues-Martins et al., 2007b). Plk4 phosphorylates Ana2 at its conserved STAN domain, and this event is essential for the Sas6 recruitment and procentriole formation (Dzhindzhev et al., 2014). Moreover, the recruitment of Plk4 to the centrosome is dependent on Asl, which interacts with the Polo-box domains of Plk4 and function upstream of the *de novo* pathway (Dzhindzhev et al., 2010). The levels and activities of Plk4 are tightly controlled by a series of cell cycle regulators. For example, Plk4 is auto-phosphorylated and is targeted by the SCF^{Slimb} ubiquitin ligase complex for degradation, thus ensuring that only one pair of centrosomes are present in one cell-division cycle (Cunha-Ferreira et al., 2009). In contrast, the $PP2A^{Tws}$ complex is required to counteract Plk4 auto-phosphorylation, thus stabilizing Plk4 for the centriole duplication (Brownlee et al., 2011).

Once the cartwheel structure is assembled, the procentriole starts to elongate, with centriolar microtubules added on the microtubule wall. Another centriolar protein, CP110, which localized at the distal end of the centriole, is able to act as a physical barrier to prevent over-elongation of the centriole (Fu and Glover, 2012). CP110 cooperates with the kinesin-13 protein Klp10A to control centriole microtubule length (Delgehyr et al., 2012). However, it remains unknown whether factors controlling microtubule growth is required for centriole elongation and assembly process.

During G2/M phase, the two centriole pairs lose their connection and start to move apart from each other. The mechanisms underlying centrosome disjunction have been revealed in human cell culture models. It has been shown that an Mst2-Nek2A pathway is responsible to phosphorylate the proximal end-localized C-Nap1 and Rootletin to promote centrosome disjunction at G2/M transition (Bahe et al., 2005; Fry et al., 1998a; Fry et al., 1998b; Helps et al., 2000; Mardin et al., 2010), and the Polo-like kinase (Plk1) functions upstream of the Mst2-Nek2A pathway in human cells (Mardin et al., 2010). Consistently, inhibition of *Drosophila* Plk1 (Polo) displays defective centriole separation (Riparbelli et al., 2014). In addition, centrosome separation is also regulated by several microtubule associated proteins. In *Drosophila* neuroblasts, centrosome separation requires Ensconsin/MAP7 and its binding partner Kinesin-1 (Gallaud et al., 2014), indicating that microtubule may play some functions in the regulation of centrosome disjunction.

The centrosome begins to recruit a much larger amount of PCM proteins before mitosis, a process named ‘centrosome maturation’. The centriolar protein Asl is a critical regulator for PCM recruitment (Conduit et al., 2010; Varmark et al., 2007). Another key regulator is Sas4, which localizes at the

microtubule wall of the centriole, serves as a bridge linking the centriole with PCM (Dzhindzhev et al., 2010). In addition, the Sas4-mediated PCM assembly is interfered by the binding with tubulin (Gopalakrishnan et al., 2012), suggesting a potential role of tubulin in regulating PCM recruitment, which may be independent of the *de novo* centriole pathway. Interestingly, only three PCM proteins, Polo, Cnn and Spd2, are identified as essential components required for PCM expansion during mitosis (Dobbelaere et al., 2008). Recently, several studies indicated the presence of a scaffold-like structure, which serves as a platform for PCM assembly. Two PCM proteins, Cnn and Spd2, exhibit unique dynamic behaviors when they are recruited to the centrosome. They are always first incorporated into the vicinity of the centriole, and then spread outward to the PCM (Conduit et al., 2010; Conduit et al., 2014b). Through this way, Cnn and Spd2 assemble into scaffold-like structures to allow the recruitment of most other PCM proteins (Conduit et al., 2010; Conduit et al., 2014b). Polo kinase is able to phosphorylate several conserved Ser/Thr residues in the PReM domain of Cnn. This specific phosphorylation in the mitotic centrosome triggers the multimerization of Cnn molecules, which is essential for the formation of Cnn-scaffolds (Conduit et al., 2014a).

Many of the PCM proteins recruited upon centrosome maturation are essential for the microtubule-organizing activity (Fu et al., 2015). Evidence showed that microtubules are nucleated primarily from the γ-tubulin ring complex (γ-TuRC), a complex of PCM proteins consisting of γ-tubulin, Dgrip84, Dgrip91, Dgp71WD, Dgrip75, Dgrip128 and Dgrip163 (Verollet et al., 2006). The efficient assembly of bipolar spindles also requires the microtubule-stabilizing protein Mini spindles (Msps), which belongs to the XMAP215/TOG family, and its binding partner *Drosophila* transforming acidic

coiled-coil protein (D-TACC) (Cullen et al., 1999; Lee et al., 2001). D-TACC and Msps are recruited to the centrosomes and coordinating with γ-TuRC to regulate microtubule assembly from centrosomes. The recruitment of D-TACC and Msps to the centrosome is dependent on the mitotic kinase Aur-A, which phosphorylates D-TACC at Ser863 and activates D-TACC-Msps complex to promote microtubule assembly at centrosomes (Barros et al., 2005). It has been proposed that the centrosome localization of D-TACC-Msps complexes stabilize microtubules in two ways: they are directly loaded onto the microtubule plus-ends since microtubules are once nucleated, or they may stabilize the minus-ends of microtubules after released from the nucleation sites (Barros et al., 2005).

1.6.2 Unequal centrosomes in *Drosophila* neuroblasts

Increasing evidence has revealed that the two centrosomes can behave differently in many asymmetrically dividing stem cell types, and the centro-

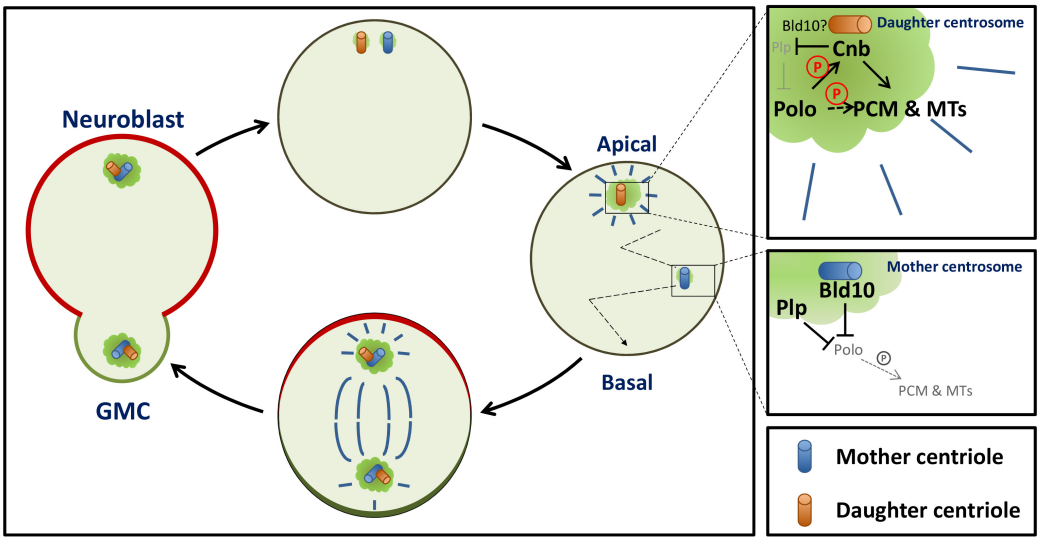

Figure 8. Unequal centrosomes in *Drosophila* neuroblast.
In dividing neuroblast, the mother centrosome is inherited by the GMC daughter, while the daughter centrosome is inherited by the NB daughter. Factors controlling the behaviors of mother and daughter centrosomes are shown in enlarged views. NB: neuroblast; GMC: ganglion mother cell.

some asymmetry is important for the cell fate decision (Wang et al., 2009b; Yamashita et al., 2007). In *Drosophila* neuroblasts, the two centrosomes split early in the cell cycle, and display significant structural and functional differences (Rebollo et al., 2007; Rusan and Peifer, 2007). The daughter centrosome, which is anchored near the apical cortex, retains certain amounts of PCM and organizes the microtubule aster, whereas the mother centrosome loses PCM and MTOC activity, and migrates extensively during interphase. Shortly before mitosis, the mother centrosome settles down near the basal cortex, where it starts to recruit PCM and organizes the second mitotic aster (Conduit and Raff, 2010; Januschke et al., 2011; Rebollo et al., 2007; Rusan and Peifer, 2007). Upon asymmetric division, the mother centrosome is segregated to the GMC, while the daughter centrosome is inherited by the newly born neuroblast (Januschke et al., 2011) (Fig. 8).

The centrosome asymmetry is an essential element driving the spindle orientation in neuroblasts. The apical cortex localized Pins is required for the maintenance of the microtubule-organizing activity of the daughter centrosome, which in turn provides a 'memory' for the division orientation in neuroblasts (Januschke and Gonzalez, 2010; Rebollo et al., 2007). In addition, several centrosomal proteins are also identified as important regulators of the centrosome asymmetry in neuroblasts. The *Drosophila* Centrobin (Cnb), which specifically localizes at the daughter centrosome, is necessary for the recruitment of PCM and the organization of interphase microtubule asters (Januschke et al., 2011; Januschke et al., 2013). Cnb is phosphorylated and regulated by Polo kinase, suggesting that Polo is also required for the maintenance of the centrosome asymmetry during interphase (Januschke et al., 2013). In contrast, the *Drosophila* Pericentrin-like protein (Plp) is enriched at the mother centrosome, where it blocks the recruitment of

Polo and in turn restricts the microtubule-organizing activity of the mother centrosome (Lerit and Rusan, 2013). The centriolar protein Bld10 (the *Drosophila* ortholog of Cep135), is also required for the downregulation of PCM recruitment and microtubule-organizing activity in the mother centrosome. Bld10 prevents PCM recruitment through shedding of Polo kinase from the mother centrosome. However, it remains unclear how Bld10 regulates the Polo localization specifically at one centrosome (Singh et al., 2014) (Fig. 8).

1.7 Roles of Tubulin Binding Co-factors and ADP Ribosylation Factor-Like 2 (Arl2) in microtubule growth

Microtubules are cytoskeletal filaments that play critical functions for diverse cellular processes, such as cell division, intracellular protein trafficking and cell motility (Akhmanova and Steinmetz, 2008). These highly dynamic polymers are primarily composed of stable αβ-tubulin heterodimers, which assemble longitudinally in a polarized head-to-tail fashion into protofilaments, while thirteen protofilaments associate laterally to form a hollow tube (Alushin et al., 2014). Each αβ-tubulin heterodimer contains two GTP-binding sites: a non-exchangeable N-site in α-tubulin buried inside the intra-dimer interface, and an active exchangeable E-site in β-tubulin that is exposed on the surface of an un-polymerized dimer (Alushin et al., 2014). The binding and hydrolysis of GTP at the E-site is critical for the dynamic instability, when microtubules exhibit stochastic switching between microtubule growth and shrinkage (Alushin et al., 2014; Brouhard and Rice, 2014) (Fig. 9).

Microtubule dynamics are essentially regulated by a group of proteins namely microtubule-associated proteins (MAPs) (Akhmanova and Steinmetz, 2008). MAPs are able to stabilize or destabilize microtubules through direct

targeting of soluble tubulins, the microtubule lattice or microtubule ends. For example, microtubule growth is mediated by a conserved Dis1/XMAP215 family of microtubule-associated proteins. XMAP215 and its homologs (such as human TOGp and *Drosophila* Msps) contain several tumour-overexpressed gene (TOG) domains at their N-terminal, and the TOG domain is responsible for the binding to tubulin (Brouhard et al., 2008). XMAP215 promotes microtubule growth by targeting microtubule plus-end, acting as a processive polymerase to catalyze the addition of tubulin dimers (Brouhard et al., 2008). Consistently, defective microtubule growth such as shorter or disorganized mitotic spindles is often observed upon disruption of gene products of the XMAP215 family (Cullen et al., 1999; Gergely et al., 2003; Kemphues et al., 1986), supporting the importance of this conserved family in regulating microtubule dynamics.

Intracellular microtubule dynamics are also critically dependent on the cytoplasmic soluble αβ-tubulin pools. Genetic and biochemical studies have revealed a stepwise *de novo* assembly pathway for the dimerization of αβ-tubulin in the cytoplasm (Lewis et al., 1997; Lundin et al., 2010; Tian et al., 1996). The translated α- and β-tubulin monomers are properly folded in the type II cytosolic chaperonin (TRiC/CCT) before binding to a group of tubulin binding cofactors (TBCs) to trigger the biogenesis of αβ-tubulin heterodimers (Lewis et al., 1997; Lundin et al., 2010). The family of TBCs contains five highly conserved members, namely TBCA, TBCB, TBCC, TBCD and TBCE (Lewis et al., 1997). The α-tubulin is first bound to TBCB and then handed off to TBCE, whereas β-tubulin is first bound to TBCA before being delivered to TBCD. The two parallel pathways then converge, when TBCC triggers the association of the complexes, forming a ‘super-complex’ consisting of TBCC,

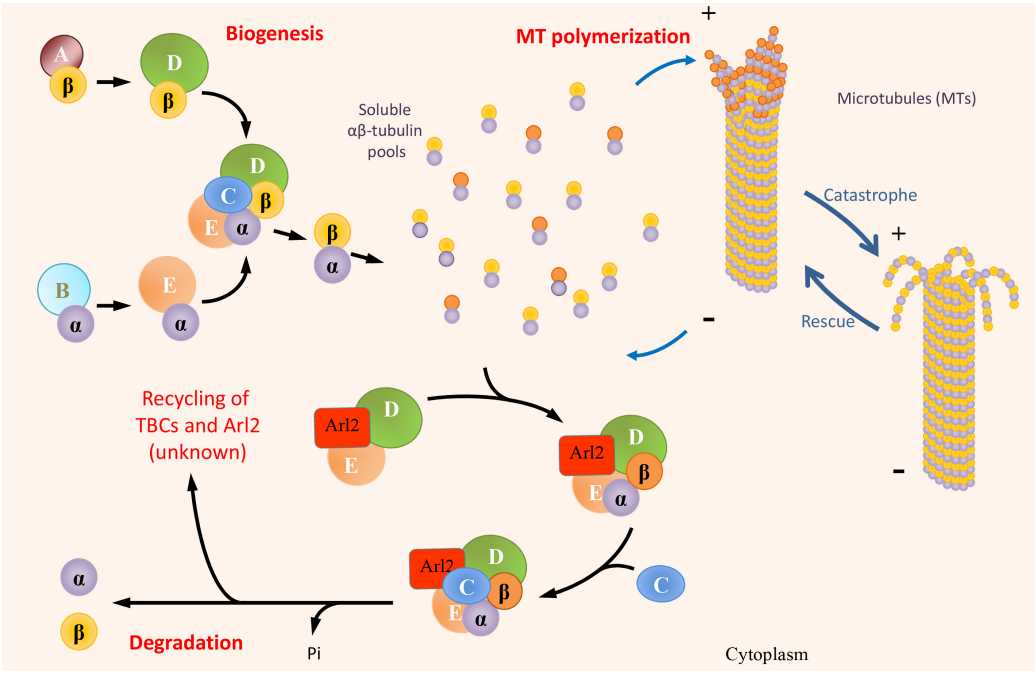

Figure 9. Essential regulators for tubulin biogenesis/maintenance and dynamic instability of microtubules.
The microtubule dynamics depend on the soluble tubulin pool in the cytoplasm, which is regulated by a group of tubulin binding co-factors (TBCs) and Arl2. The β-tubulin subunit can be in GTP-bound (orange) or GDP-bound (yellow) form.

TBCD, TBCE together with α- and β-tubulin. The entering of TBCC also results in the release of αβ-tubulin heterodimer, which is competent for GTP exchange and polymerization into microtubules (Lewis et al., 1997; Lundin et al., 2010; Tian et al., 1996) (Fig. 9).

In the cytoplasm, the vast pool of soluble αβ-tubulin units is tightly maintained, but the mechanisms for the maintenance and degradation of soluble αβ-tubulin heterodimers remain poorly understood. Biochemical and genetic results suggested that overexpressed TBCD or TBCE destroys the tubulin heterodimers and microtubules in cultured cells; while a small GTPase named Arl2 (ADP Ribosylation Factor-Like 2) specifically inhibits the destruction effect by TBCD (Bhamidipati et al., 2000; Tian et al., 1997). Moreover, the yeast homolog of TBCC functions as a GAP for Arl2, and they are proposed to be operating in parallel with the pathway for the *de novo*

tubulin assembly (Mori and Toda, 2013). Consistent with these early results, a recent study revealed that the yeast Arl2, TBCD and TBCE form a stable cage-like complex (TBC-DEG). This complex serves as a platform to allow the binding of soluble αβ-tubulin heterodimer, followed by the binding of TBCC to trigger the hydrolysis of Arl2 and release the energy needed to alter the conformation of αβ-tubulin (Nithianantham et al., 2015). This novel paradigm may function as a pathway to regulate the maintenance and degradation of the soluble tubulin pool in the cytoplasm (Nithianantham et al., 2015) (Fig. 9).

Despite a series of biochemical studies have been carried out on the TBCs and Arl2, we still rarely understand the *in vivo* functions of these regulators in controlling the assembly and maintenance of soluble αβ-tubulin. Particularly, in *Drosophila*, loss of TBCB, TBCD or TBCE results in loss of microtubules in various systems, causing defective neuronal morphologies or impaired cell polarity in oocyte (Baffet et al., 2012; Jin et al., 2009; Okumura et al., 2015). However, the roles of TBCs and Arl2 in neural stem cells remain unknown. In this thesis, some functional studies of Arl2 and TBCs in *Drosophila* neuroblast are provided, and a new paradigm of Arl2- and Msps-dependent microtubule growth mediating asymmetric division is proposed.

CHAPTER 2: MATERIALS AND METHODS

2.1 Fly Genetics

2.1.1 Fly stocks used in this study and growth conditions

Generally the genetic crosses were grown at 25°C, except that flies for overexpression and RNAi knockdown were raised at 29°C. Fly strains used in this study are listed in Table 1:

Table 1. Fly stocks used in this study

Genotype	Stock name (short form)	Source	Reference
ase-Gal4 (II)		T. Lee	(Hoch and Jackle, 1998)
w; UAS-Dcr2, wor-Gal4, ase-Gal80/CyO (II); UAS-mCD8-GFP/TM3, Ser (III)	Type-II neuroblast driver	J. Knoblich	(Neumuller et al., 2011)
pUbiquitous-GFP-α-Tubulin84B (X)	*pUbq-GFP-α-Tub*	C. Gonzalez	(Rebollo et al., 2007)
UASp-EB1-GFP (III)		C. Gonzalez	(Rebollo et al., 2007)
$msps^{P}$/TM3 (III)		H. Ohkura	(Cullen et al., 1999)
ctp^{exc6}/FM6C (X)		W. Chia	(Dick et al., 1996)
mud^{1}/FM6C (X)		F. Matsuzaki	(Izumi et al., 2006)
P{GAL4}MZ1407 (II)	*insc-Gal4*	J. Urban	(Luo et al., 1994)
elav-Gal4, hsFLP, UAS-nLacZ, UAS-CD8-GFP (X); FRT2A tub-Gal80/TM6 (III)	FRT2A (3L) MARCM driver	W. Chia	(Lee and Luo, 1999)
elav-Gal4, hsFLP, UAS-nLacZ, UAS-CD8-GFP (X); FRT82B tub-Gal80/TM6B, Tb^{1} (III)	FRT82B (3R) MARCM driver	W. Chia	(Lee and Luo, 1999)
w^{1118}; P{UAS-Dcr2.D}10 (III)	*UAS-Dcr2*	B. Dickson	
UAS-$Arl2^{T30N}$ (III)		F. Yu	
y^{1} w^{*}; P{tubP-GAL4}LL7/TM3, Sb^{1}, Ser^{1} (III)	*tub-Gal4*	BDSC #5138	
y^{1} w^{*}; P{UAS-mCD8-GFP.L}LL5 (III)	*UAS-CD8-GFP*	BDSC #5137	

y^1 w^*; Pin^{Yt}/CyO (II); P{UAS-mCD8::GFP.L}LL6 (III)		BDSC #5130	
w^{1118}; P{XP}$COX7A^{d04921}$/TM6B, Tb^1 (III)		BDSC #19210	
w^{1118}; P{PTT-GA}$Jupiter^{G00147}$ (III)	*G147-GFP*	BDSC #6836	(Morin et al., 2001)
w^{1118}; Df(3R)Exel6148, P{XP-U}Exel6148/TM6B, Tb^1 (III)	Arl2 Df	BDSC #7627	
w^{1118}; P{UAS-mito-HA-GFP.AP}3, e^1 (III)	*UAS-Mito-GFP*	BDSC #8443	
w^*; $dhc^{64C4-19}$, P{FRT(w^{hs})}2A/TM6B, Tb^1 (III)		BDSC #23863	
P{neoFRT}82B, ry^{506} (III)	*FRT82B*	BDSC #2035	
w; P{FRT(w^{hs})}2A (III)*	*FRT2A*	BDSC #1997	
$mts^{XE-2258}$/CyO, P{ry[+t7.2]=sevRas1.V12}FK1 (II)		BDSC #5684	
w^{1118}; P(GD12240}v44334/TM3 (III)	Arl2 RNAi (*GD44334*)	VDRC	
P{KK110627}VIE-260B (III)	Arl2 RNAi (*KK110627*)	VDRC	
w^{1118}; P{GD11498}v21982/TM3 (III)	Msps RNAi (*GD21982*)	VDRC	
w^{1118}; P{GD147478}v29359 (II)	TBCC RNAi (*GD29359*)	VDRC	
y^1 w^{67c23}; P{GSV6}GS17851/TM3, Sb^1, Ser^1 (III)	*$arl2^{GS17851}$/TM3, Sb^1 (III)*	DGRC #200665	
UAS-Venus-Ctp (II)		H. Wang lab	(Wang et al., 2011)
UAS-Venus-Ctp (III)		H. Wang lab	(Wang et al., 2011)
UAS-Venus-Ctp^{CAAX} (II)		H. Wang lab	(Wang et al., 2011)
$mts^{XE-2258}$/CyOGB (II)		H. Wang lab	
insc-Gal4 (II); UAS-Dcr2 (III)		H. Wang lab	
UAS-β-Tub-Venus/CyO (II)		H. Wang lab	
insc-Gal4, UAS-Venus-Ctp (II)		H. Wang lab	
mud^1/FM7, GB (X)		H. Wang lab	
P{neoFRT}82B, $msps^{P18}$/TM6B, Tb^1 (III)		H. Wang lab	
UAS-Msps-FL (III)		H. Wang lab	
UAS-$Arl2^{WT}$/CyOGB (II)		this study	
UAS-$Arl2^{WT}$-Venus (II)		this study	

UAS-Arl2^{Q70L}/TM6B, Tb^{1} (III)		this study	
UAS-mArl2 (II)		this study	
P{KK110627}VIE-260B (II); P(UAS-Dcr-2.D}10 (III)	*KK110627/CyOGB (II); UAS-Dcr2 (III)*	this study	
insc-Gal4 (II); UAS-Arl2^{T30N} (III)		this study	
insc-Gal4, UAS-Arl2^{WT}-Venus (II)		this study	
arl2$^{\Delta156}$/TM6B, Tb^{1} (III)		this study	
arl2$^{\Delta309}$/TM6B, Tb^{1} (III)		this study	
P{neoFRT}82B, arl2$^{\Delta156}$/TM6B, Tb^{1} (III)		this study	
P{neoFRT}82B, arl2$^{\Delta309}$/TM6B, Tb^{1} (III)		this study	
P{neoFRT}82B, P(GSV6}GS17851/ TM3, Sb^{1}, Ser^{1} (III)		this study	
insc-Gal4 (II); P{neoFRT}82B, arl2$^{\Delta156}$/TM6B, Tb^{1} (III)		this study	
P{neoFRT}82B, tubP-Gal4, arl2$^{\Delta309}$/TM6B, Tb^{1} (III)		this study	
UAS-Arl2^{WT}/CyOGB (II); P{neoFRT}82B, arl2$^{\Delta156}$/TM6B, Tb^{1} (III)		this study	
UAS-Arl2^{WT}/CyOGB (II); P{neoFRT}82B, arl2$^{\Delta309}$/TM6B, Tb^{1} (III)		this study	
UAS-Arl2^{WT}/CyOGB (II); P{neoFRT}82B, P(GSV6}GS17851/ TM3, Sb^{1}, Ser^{1} (III)		this study	
UAS-Arl2^{WT}/CyOGB (II); P{neoFRT}82B, tubP-Gal4, arl2$^{\Delta309}$/TM6B, Tb^{1} (III)		this study	
UAS-mArl2 (II); P{neoFRT}82B, arl2$^{\Delta156}$/TM6B, Tb^{1} (III)		this study	
UAS-Venus-Ctp, P{neoFRT}82B, arl2$^{\Delta156}$/TM6B, Tb^{1} (III)		this study	
UAS-TBCD (III)		this study	
msps^{P}/TM6B, Tb^{1} (III)		this study	
insc-Gal4 (II); P{neoFRT}82B, msps^{P18}/TM6B, Tb^{1} (III)		this study	
UAS-Msps-FL, P{neoFRT}82B, msps^{P18}/TM6B, Tb^{1} (III)		this study	
UAS-Arl2^{T30N}, P{neoFRT}82B, msps^{P18}/TM6B, Tb^{1} (III)		this study	
UAS-COX7A (II)		this study	
UAS-COX7A (II); P{neoFRT}82B, arl2$^{\Delta309}$/TM6B, Tb^{1} (III)		this study	

ctp^{exc6}/FM7, GB (X)		this study	
insc-Gal4 (II); UAS-mCD8-GFP (III)		this study	
ase-Gal4 (II); UAS-mCD8-GFP (III)		this study	
insc-Gal4, UAS-Venus-Ctp^{CAAX} (II)		this study	

2.1.2 Generation of transgenic flies

UAS-Arl2^{T30N}, *UAS-Arl2^{WT}*, *UAS-Arl2^{WT}-Venus*, *UAS-Arl2^{Q70L}*, *UAS-TBCD*, *UAS-Msps-FL* and *UAS-COX7A* transgenic lines were generated by standard P-element mediated transformation performed by BestGene Inc. The procedures of generating DNA constructs for transgenic flies are described in 2.2 Molecular Biology.

2.1.3 RNA interference screen to identify novel regulators of neuroblast asymmetric division

An un-biased RNA interference (RNAi) screen was carried out in order to identify novel regulators involved in neuroblast asymmetric division and homeostasis. The RNAi transgenic collection was from Vienna *Drosophila* Resource Center (VDRC). Generally, individual transgenic lines carrying inducible UAS-RNAi were crossed to a neuroblast-specific driver, *insc-Gal4*. The progenies were allowed to grow at 29°C until they reached the late 3rd-instar larval stage and were proceeded for immunohistochemistry (described in 2.5 Immunohistochemistry and microscopy). For the initial screen, larval brains were stained for Miranda, which was able to efficiently label neuroblasts in the brains. Subsequently potential positive lines were further analyzed with staining for Deadpan and other neuroblast markers. Several regulators of neuroblast asymmetric division have been identified using similar RNAi screen strategies (Wang et al. 2011; Li et al. 2014; Koe et al.

2014). In this thesis, a previous poorly characterized gene in *Drosophila*, *arl2*, has been identified as a regulator of neuroblast asymmetric division and self-renewal.

2.1.4 Imprecise excision of P-element to generate *arl2*-null mutants

To generate *arl2* mutants, a lethal P element, *P{XP}COX7A^{d04921}*, was used to induce imprecise excision in the presence of a transposase source. Briefly, over 200 female flies of *P{XP}COX7A^{d04921}/TM6B, Tb^{1}* were crossed with 100 male flies of *Δ2-3, Sb^{1}/TM3, Ser^{1}*. More than 400 individual male progeny of *P{XP}COX7A^{d04921}/Δ2-3, Sb^{1}* with mosaic eye phenotype were collected, and crossed with female balancer flies *TM3, Sb^{1}/TM6B, Tb^{1}*. From each individual cross, one white eye male fly was collected and crossed with female balancer flies *Ly, hs-hid/TM6B, Tb^{1}* to obtain stable stocks after the heat-shock. These individual *w* revertant lines were then subjected to complementation tests with deficiency (Df) line *Df(3R)Exel6148/TM6B, Tb^{1}*. More than 15 *w* revertant lines failed to complement with Df lines were obtained, and deleted regions in each line were mapped by standard DNA sequencing. The oligos used for the sequencing are listed in Table 2, and the genomic regions recognized by the oligos are depicted in Fig. 10.

Table 2. Oligos used for the mapping of *arl2* deleted regions

Oligos name	Sequence	Genome location and direction
Arl2-PE-F1	GTA GAG CAC GTT GTC CAC GA	3R: 8,340,604, Forward
Arl2-PE-F2	TGA CAG CTG ACA ACT GGA GA	3R: 8,341,005, Forward
Arl2-PE-R1	CAG TGT GGG TGA GAT GGT GT	3R: 8,341,381, Reverse
Arl2-PE-R2	CGC CCT AGA CGA AGG ATT TA	3R: 8,341,976, Reverse
Arl2-PE-R3	ATT TCC TGG GCA AAC AAG TG	3R: 8,342,463, Reverse
Arl2-PE-R4	CCG TCA GAG AAA TCC GAG AG	3R: 8,343,034, Reverse
Arl2-PE-R5	CAA TTG GTA TTT GCA TTC GTG	3R: 8,344,218, Reverse

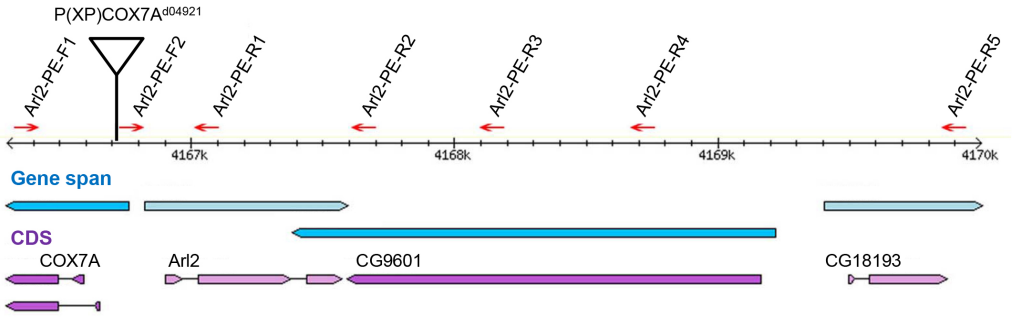

Figure 10. A schematic diagram of *P{XP}COX7A*^{d04921} location in genome, and primers used for mapping (modified from FlyBase website).
The red arrows show the locations and directions of the primers. CDS: coding sequence.

In this study, two *arl2* null alleles (*arl2*$^{\Delta 156}$ and *arl2*$^{\Delta 309}$) generated from P-element excision were used. The entire coding region of *arl2* (555bp) is deleted in *arl2*$^{\Delta 156}$, while most of the *arl2* N-terminal coding region (339bp) is deleted in *arl2*$^{\Delta 309}$ (Fig. 13D). Although the C-terminus of *CG9601* is deleted in *arl2*$^{\Delta 156}$, the phenotype observed in *arl2*$^{\Delta 156}$ may not be contributed by loss of *CG9601*, as similar phenotype is also observed in *arl2*$^{\Delta 309}$. *arl2*$^{\Delta 156}$ and *arl2*$^{\Delta 309}$ are both putative *cox7A* loss-of-function alleles, as they also delete the 5'UTR of *COX7A*. Indeed, the lethality of homozygous *arl2*$^{\Delta 156}$ and *arl2*$^{\Delta 309}$ was overcome only when both Arl2 and COX7A transgenes were introduced. This suggested that mutation in *arl2* or *cox7A* is sufficient to cause the lethality. However, the phenotype seen in *arl2*$^{\Delta 156}$ and *arl2*$^{\Delta 309}$ neuroblast MARCM clones could be largely rescued by overexpression of Arl2^{WT}, but not by COX7A (unpublished data). Hence, it can be concluded that the phenotype in *arl2* mutants described in this study was solely attributed to loss of *arl2*.

2.1.5 Generation of neuroblast MARCM clones

Mosaic analysis with a repressible cell marker (MARCM) clones were generated as described previously (Lee and Luo, 1999). Mutants (*arl2*$^{\Delta 156}$, *arl2*$^{\Delta 309}$, *msps*^{P18} and *dhc64C*$^{4-19}$) carrying FRT (FLP recombinase recombination target) on the same chromosome arm were crossed to the corresponding MARCM drivers. In each vial/bottle, more than 45/150 flies were used (male: female = 1:2). The clones were generated by heat-shocking the larvae at 37°C for 2 hours twice at 24 h ALH and 48 h ALH. Larvae were further aged at 25°C for 2-3 days before processed for immunohistochemistry. The MARCM clones were recognized by the expression of Green Fluorescent Protein (GFP)-fused membrane protein, Cluster of Differentiation 8 (CD8-GFP). The MARCM drivers used in this study are listed in Table 1.

2.2 Molecular Biology

2.2.1 DNA templates used and Polymerase Chain Reaction (PCR)

The Expressed-sequence tags (ESTs) containing full-length coding sequences of *arl2* (FI08808), *msps* (LP04448), *TBCC/CG31961* (LD34582), *TBCD/CG7261* (LD16031), *TBCE/CG7861* (FI05242), *mts* (LD26077), *α-Tubulin84B* (AT25469), *β-Tubulin56D* (GH12877) and *COX7A-RA* (GM26747) were obtained from *Drosophila* Genomics Resource Center (DGRC). Mouse *arl2* cDNA (Clone ID: 5709669) was obtained from Mammalian Gene Collection (MGC). To amplify DNA fragments for cloning, Expand High Fidelity PCR reaction kit (Roche) was used. PCR products were analyzed on DNA gels. Oligos used for PCR are listed in Table 3.

Table 3. Oligo sequences used for PCR

Oligos name	Sequence	Plasmids generated
pENTR-Arl2-F	CAC CAT GGG CTT CCT CAC AGT A	pENTR-Arl2 (with or without stop codon)
pENTR-Arl2-R1 (with stop codon)	TTA ATC CAA AGT GAA TAT ACG	pENTR-Arl2 (with stop codon)
pENTR-Arl2-R2 (without stop codon)	ATC CAA AGT GAA TAT ACG CTT AG	pENTR-Arl2 (without stop codon)
pUAST-Msps-FL-F	AGG GAA TTG GGA ATT ATG GCC GAG GAC ACA GAG	pUAST-Msps-FL (with stop codon), using infusion cloning.
pUAST-Msps-FL-R (with stop codon)	CCC TCG AGC GCG GCC TTA TTG GGC ATG ATT CTC TTT CTT G	pUAST-Msps-FL (with stop codon), using infusion cloning.
pENTR-TBCC-F	CAC CAT GGA AGG CGA CGC GGA A	pENTR-TBCC (with stop codon)
pENTR-TBCC-R (with stop codon)	CTA AAT GAT GGA TAT GTC CTT GAC AT	pENTR-TBCC (with stop codon)
pENTR-TBCD-F	CAC CAT GTC GAA TTC TGT GGA A	pENTR-TBCD (with stop codon)
pENTR-TBCD-R (with stop codon)	TCA TTT ATC AGC ACT CGC	pENTR-TBCD (with stop codon)
pUAST-TBCD-F	AGG GAA TTG GGA ATT ATG TCG AAT TCT GTG GAA	pUAST-TBCD (with stop codon), using infusion cloning.
pUAST-TBCD-R (with stop codon)	CCC TCG AGC GCG GCC TCA TTT ATC AGC ACT CGC	pUAST-TBCD (with stop codon), using infusion cloning.
pENTR-TBCE-F	CAC CAT GGT GGG AAT TAT CGA TGA G	pENTR-TBCE (with stop codon)
pENTR-TBCE-R (with stop codon)	CTA TTG AAC CAA AAC TGT ATC ATG C	pENTR-TBCE (with stop codon)
pUAST-mArl2-F	AGG GAA TTG GGA ATT ATG GGG CTT CTG ACC ATT CT	pUAST-mArl2 (with stop codon), using infusion cloning.
pUAST-mArl2-R (with stop codon)	CCC TCG AGC GCG GCC TCA GTC GGC AGT AAA GAC ACG	pUAST-mArl2 (with stop codon), using infusion cloning.
Arl2-T30N-N-R1	GCG CTT CAG GAT TGT ATT CTT GCC GGC ATT ATC	For generation of Arl2-T30N mutant fragment
Arl2-T30N-C-F1	GAT AAT GCC GGC AAG AAT ACA ATC CTG AAG CGC	For generation of Arl2-T30N mutant fragment
Arl2-Q70L-N-R1	GGA TCG CAG AGA CTT CAG GCC ACC GAC ATC CCA	For generation of Arl2-Q70L mutant fragment
Arl2-Q70L-C-F1	TGG GAT GTC GGT GGC CTG AAG TCT CTG CGA TCC	For generation of Arl2-Q70L mutant fragment
XhoI-fragment-(+)	CAC CGG AGG AGG AGG ACT CGA GGG ATG ACG TTA AGC TAG	For generation of pAMW-XhoI through gateway cloning

XhoI-fragment-(-)	CTA GCT TAA CGT CAT CCC TCG AGT CCT CCT CCT CCG GTG	For generation of pAMW-XhoI through gateway cloning
pAMW-αTub84B-F	AGG AGG AGG ACT CGA GAT GCG TGA ATG TAT CTC TAT CCA	pAMW-αTub84B (with stop codon), using infusion cloning
pAMW-αTub84B-R (with stop codon)	AAC GTC ATC CCT CGA GTT AGT ACT CCT CAG CGC CC	pAMW-αTub84B (with stop codon), using infusion cloning
pAMW-βTub56D-F	AGG AGG AGG ACT CGA GAT GAG GGA AAT CGT TCA CAT C	pAMW-βTub56D (with stop codon), using infusion cloning
pAMW-βTub56D-R (with stop codon)	AAC GTC ATC CCT CGA GTT AGT TCT CGT CGA CCT CAG	pAMW-βTub56D (with stop codon), using infusion cloning

2.2.2 Gel electrophoresis and gel extraction of DNA

To purify DNA products after PCR, the PCR samples were mixed with 6X loading dye (Promega) and were loaded onto 0.6%-1.0% agarose gels. The DNA fragments were separated after running on the gels for 1 hour with 80-100 voltages, and gel extraction was performed using QIAquick Gel Extraction Kit (QIAGEN). 20 µl of ddH_2O was used to elute the PCR fragments from the column, and DNA concentration was measured using NanoDrop 2000c Spetrophotometers (Thermo Scientific).

2.2.3 Cloning strategies

All clonings were performed using the Gateway® Cloning system or In-Fusion® HD Cloning system.

2.2.3.1 Gateway Cloning

pENTR™ Directional TOPO® Cloning Kit (Invitrogen) and Gateway LR Clonase II Enzyme Mix (Invitrogen) were used in this study, to generate most of plasmids that were used for transgenic flies and expression in S2 cells. Briefly, blunt-end PCR products (started with CACC) were first directionally

cloned into pENTR^{TM}/D-TOPO® vector according to the manufacturer's protocols. Correct entry constructs containing target DNA fragments were selected on LB plates (described in 2.2.5) supplemented 50 µg/ml Kanamycin. Destination plasmids were generated, by performing LR recombination reactions between entry plasmids and Gateway destination vectors. In this study, pTW (pUAST) and pTWV (pUAST-C'Venus) vectors were used to generate *in vivo* transgenic constructs of pTW-Arl2^{WT}, pTW-Arl2^{Q70L} and pTWV-Arl2^{WT}. In addition, pAFW (pActin5C-N'Flag), pAHW (pActin5C-N'HA), pAMW (pActin5C-N'Myc) and pAWV (pActin5C-C'Venus) vectors were used to generate S2 cell expressing constructs of pAFW-TBCD, pAFW-TBCE, pAHW-TBCC, pAHW-TBCE, pAHW-Mts, pAWV-Arl2^{WT}, pAWV-Arl2^{T30N} and pAWV-Arl2^{Q70L}.

2.2.3.2 In-fusion Cloning

In-Fusion® HD Cloning Kit (Clontech) was also used to generate DNA constructs for transgenic flies and S2 cell expressing constructs. Briefly, DNA vectors were digested with required restriction enzymes (37°C for 2 hours) and were purified using QIAquick Gel Extraction Kit (QIAGEN). The PCR products, which contain 15 base-pair (bp) overhanging sequences that are corresponding to the DNA vectors at both ends, were incubated with the linearized DNA vectors at 50°C for 15 min according to the protocols. The reactions were then transformed into *E. Coli* cells (described in 2.2.5) and positive colonies were selected on LB plates containing 50 µg/ml Carbenicilin. In this study, the full-length coding regions of *msps*, *TBCD*, *COX7A (isoform RA)* and mouse *Arl2* (*mArl2*) were cloned into *EcoRI* and *NotI* sites of pUAST vector. To generate S2 cells expressing construct of N-terminus Myc-tagged α-Tub84B and β-Tub56D, a modified pAMW vector with an *XhoI* recognition

site introduced was first generated according to the protocols of pENTR Directional TOPO Cloning Kit (Invitrogen). The full-length coding regions of *α-Tub84B* and *β-Tub56D* were cloned into the *XhoI* site of this pAMW (*XhoI*-modified) vector.

2.2.4 Site-directed mutagenesis

To generate DNA fragments with single mutation (Arl2^{T30N} or Arl2^{Q70L}), a two-step PCR was carried out using primers containing mutated nucleotides. The strategy for generation of Arl2^{Q70L} DNA fragment for Gateway Cloning is in Fig. 11. In the first step, two pairs of primers were used to amplify the N-term and the C-term of the Arl2 CDS by PCR. The primers pENTR-Arl2-F and Arl2-Q70L-N-R1 were used to amplify Arl2^{Q70L}-N (PCR#1A), while Arl2-Q70L-C-F1

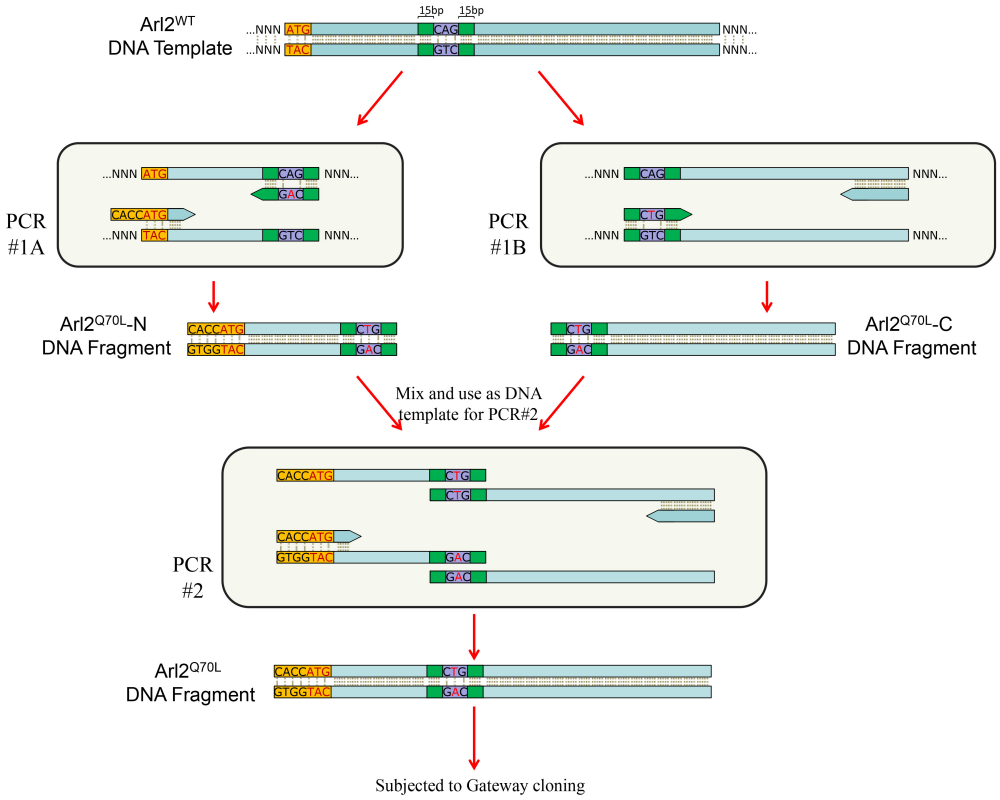

Figure 11. A schematic diagram of procedure to generate site-directed mutagenesis of Arl2^{Q70L}.
The mutated nucleotides are shown in red. Similar procedure was designed for Arl2^{T30N}.

and pENTR-Arl2-R1 (or R2) were used to amplify Arl2^{Q70L}-C (PCR#1B) (oligos sequences in Table 3). The reverse primer for N-term fragment and the forward primer for C-term fragment both contain mutated nucleotide(s). The PCR products from the initial step contained the mutated regions overlapped, and in the second step they were mixed and used as template DNA to amplify the full-length Arl2^{Q70L} (PCR#2). Similar procedure was designed to generate full-length Arl2^{T30N} fragment. The final PCR products were then used to generate pENTR-Arl2^{T30N} and pENTR-Arl2^{Q70L} according to the protocols for Gateway cloning.

2.2.5 Transformation of *E. coli* cells

The *E. Coli* strain used for most of cloning procedure was XL-1 Blue *(recA1 endA1 gyrA96 thi-1 hsdR17 supE44 relA1 lac [F´ proAB lacIqZΔM15 Tn10 (Tetr)*]). The *E. Coli* cells were cultured at 37°C in LB broth (1% bacto-tryptone, 0.5% bacto-yeast extract and 1% NaCl), or maintained on LB agar plates (LB containing 1.5% bacto-agar). When *E. Coli* cells containing plasmids were cultured, the LB broth or LB agar plates were supplemented with 50 μg/ml of Carbenicilin or 50ug/ml of Kanamycin for antibiotic selection.

For the heat-shock transformation, *E. Coli* competent cells taken out from -80°C were thawed on ice for 10 min, and about 10 ng of plasmid DNA, or 2-6 μl of reaction mix of Gateway® cloning or In-Fusion® cloning was added into the cells. After incubation on ice for another 15-30 min, the cells were heat-shocked for 45 sec at 42°C, and immediately cooled down on ice for 2 min. 0.9 ml of plain LB broth was then added to the cells for recovery. After incubation at 37°C in a shaker (250 rpm) for 30-60 min, the cells were spin down (at 2000 rpm, 1 min) and resuspended using 100 μl of plain LB, and were plated on a LB agar plate containing corresponding antibiotics.

2.2.6 Plasmid DNA preparation

For plasmid DNA minipreps, 3-4 ml of bacterial culture was incubated at 37°C in a shaker (250 rpm) overnight, and lysis and purification of plasmid DNA was carried out using QIAGEN Miniprep Kit (QIAGEN) according to the manufacturer's instructions. For large scale plasmid DNA preparation, 50 ml (for midipreps) or 200 ml (for maxipreps) of bacterial cultures were used according to the protocols of QIAGEN Plasmid Midi (Maxi) Kit with QIAGEN-tip 500 resin columns.

2.2.7 Isolation of total genomic DNA from 3rd instar larvae or adult flies

30-50 larvae or adult flies were collected in eppendorf tubes and homogenized in 400 µl of Buffer A (100mM Tris-HCl, pH7.5, 100mM EDTA, 100mM NaCl and 0.5% SDS), supplemented with 200 µg/ml Proteinase K (Promega). The homogenate was incubated at 56°C for 30 min, followed by 5 min heating at 95°C to denature the remaining Proteinase K. RNA was precipitated by adding 800 µl of LiCl/KAc solution (prepared by mixing 1 part 5M KAc and 2.5 parts 6M LiCl), followed by centrifuged at maximum speed at room temperature for 15 min. The supernatant was transferred to a fresh eppendorf tube and centrifuge was repeated one time to remove the debris thoroughly. The genomic DNA was then precipitated by adding 600 µl of isopropanol and centrifuged (max speed, 15 min, room temperature), followed by washing using 70% ethanol and spin down at room temperature at max speed for 2 min. The DNA pellet was air dried before resuspension in 150 µl of sterile water. The concentration and quality of genome DNA samples were assessed by NanoDrop 2000c Spetrophotometers (Thermo Scientific) and gel electrophoresis.

2.2.8 Reverse Transcription (RT)-PCR

2.2.8.1 Preparation of *Drosophila* embryos and different tissue samples for RNA isolation

Wild-type *Drosophila* embryos were collected on agar plates with normal fly food and a piece of yeast paste. 300 *yw* flies (about 220 female flies, aged 2-3 days) were caged and allowed to lay eggs on the agar plate within a two-hour window. The embryos were then washed from the agar plate and collected into an assembled filtration apparatus. After washing, the embryos were then dechorionated with 50% freshly prepared bleach for 2 min, and immediately washed with adequate amount of water. The dechorionated embryos were then collected into a clean eppendorf tube and processed for isolation of total RNA (see 2.2.8.2). Third-instar larval brains (from 30-50 larvae), third-instar larval intestine (from 30 larvae) or adult fly heads (from 30 adult flies) were dissected in cold PBS and immediately subjected for RNA isolation (see 2.2.8.2).

2.2.8.2 Isolation of total RNA

Total RNA was isolated using TRI reagent (Sigma-Aldrich) according to the manufacturer's instructions. Briefly, *Drosophila* embryos or different tissues samples (described in 2.2.8.1) were homogenized in 1 ml TRI reagent in an eppendorf tube at room temperature for 10 min. 100 µl of bromochloropropane was then added and the mixture was vortex vigorously. After incubation at room temperature for 10 min, the mixture was then centrifuged at 4 °C for 15 min (max speed). The aqueous phase (upper phase) containing RNA was transferred to a fresh eppendorf tube. 400 µl of isopropanol was added to the mixture, and the samples were incubated at room temperature for 5 min then centrifuged at max speed at 4 °C for 15 min.

The RNA pellet was then washed using 75% ethanol (fresh) and air dried, before resuspension in 50 µl of diethyl pyrocarbonate (DEPC)-treated water. The RNA concentration was measured by NanoDrop 2000c Spetrophotometers (Thermo Scientific), and the samples were aliquot and stored in -80 °C until ready to use.

2.2.8.3 First strand cDNA synthesis

Using total RNA as template, first strand cDNA was synthesized using ProtoScript® II First Strand cDNA Synthesis Kit (NEB) according the manufacturer's protocols. In general, 1 µg of total RNA was used as template for 20 µl reaction. The reaction was incubated at 42 °C for 1 hour, followed by 5 min's incubation at 85 °C for heat-inactivation. The cDNA concentration (ssDNA) was measured using NanoDrop 2000c Spetrophotometers (Thermo Scientific).

2.2.8.4 PCR after Reverse Transcription (RT)

The cDNA sample was used as template to perform RT-PCR. Target regions to be amplified were 250-500 bp in length, and PCR products were analyzed on DNA gels. The PCR primer pairs used for RT-PCR were listed in Table 4.

Table 4. Primer sequences used for RT-PCR

Oligos name	Sequence
Arl2-RT2-F	ATG GGC TTC CTC ACA GTA TTA AAA A
Arl2-RT2-R	CTC TTT AAT TTC GTT GGA TGA GAG G
Actin5C-F	CAG ATC ATG TTC GAG ACC TTC A
Actin5C-R	TCA TGA TGG AGT TGT AGG TGG T

2.3 S2 cell culture and plasmid transfection

Drosophila S2 cells were cultured in Express Five® SFM (Life technologies) supplemented with 2mM glutamine (Life technologies) in at 25°C. They were maintained in flasks, and the medium was changed every 2 to 3 days. For transient expression of different proteins for co-immunoprecipitation (Co-IP) experiments, plasmids were transfected using Effectene Transfection Reagent (QIAGEN) according to the instructions. S2 cells were seeded in 6-well plates at a density of $1X10^6$ to $2X10^6$ cells per well, and transfection was carried out 12-18 hours after seeding. In each well, totally 200-400 ng of plasmid DNA was transfected (based on the expression levels of proteins). Co-IP experiments were performed 48 hours after transfection.

2.4 Biochemistry

2.4.1 PAGE and Western blotting

Polyacrylamide gel electrophoresis (PAGE) and western blotting were performed according to standard procedures. Antibodies used for were listed in Table 5.

Table 5. Antibodies used for western blotting

Antibody Name	Host Species	Dilution Ratio	Source	Reference
anti-Msps	Rabbit	1:2000	J Raff	Lee et al 2001
anti-Actin (C4)	Mouse	1:5000	MP Biomedicals (691001)	
anti-α-Tubulin	Mouse	1:10000	Sigma (T6199)	
anti-β-Tubulin	Mouse	1:50	DSHB (E7)	
anti-GFP	Mouse	1:5000	Covance (MMS-118P)	
anti-FLAG (M2)-Peroxidase (HRP)		1:5000	Sigma (A8592)	
anti-Myc (9E10)	Mouse	1:1000	AbCam (ab32)	
anti-HA (3F10)	Rat	1:2000	Roche (11867423001)	

2.4.2 Extraction of protein samples from third instar larval brains

To extract protein samples for western blotting, 50 to 80 third instar larval brains were homogenized in 200 µl RIPA buffer (50mM Tris-HCl, pH7.5, 150mM NaCl, 1mM EDTA, 1% TritonX-100, 0.5% sodium deoxycholate, 0.1% SDS). The samples were then supplemented with 67 µl of 4X loading dye and boiled at 95°C for 5 min, before stored at -20°C or subjected to western blotting immediately.

2.4.3 Co-immunoprecipitation in S2 cells

Briefly, S2 cells expressing different proteins were harvested at 48 hours after transfection, and were homogenized in Co-IP buffer (25mM Tris-HCl, pH8.0, 27.5mM NaCl, 20mM KCl, 25mM sucrose, 10mM EDTA, 10mM EGTA, 1mM DTT, 10%(v/v) glycerol and 0.5% Nonidet P40) supplemented with Complete Protease Inhibitor (Roche) for 30mins at 4°C. For each Co-IP reaction, 2 to 3 wells of S2 cells were used, and 500 µl of lysis buffer was used for the initial lysis procedure. After saving 50 µl for input samples, the cell lysate was then pre-cleared with 25 µl of Protein A/G beads (Pierce) for 30mins, before incubating with antibodies overnight at 4°C. Proteins binding to the antibodies were then pulled down by incubating with 50 µl of Protein A/G beads for 2 hours, followed by washing once with Co-IP buffer and three times with PBS. After the last washing, the proteins bound to beads were added with 35 µl of 2X loading dye and 10 µl of 4X loading dye before boiling at 95°C for 5 min. The samples were then subjected to Western blotting for analysis.

2.5 Immunohistochemistry and microscopy

2.5.1 Antibodies used for immunostaining

The primary antibodies used were listed in Table 6. The corresponding secondary antibodies used were conjugated to Alexa-Fluor-488, Alexa-Fluor-555, Alexa-Fluor-405 and Alexa-Fluor-638 (Molecular Probes).

Table 6. Primary antibodies used for immunostaining

Antibody Name	Host Species	Dilution Ratio	Source	Reference
anti-Dpn	Guinea pig	1:1000	J Skeath	Bier et al 1992
anti-Ase	Rabbit	1:5000	YN Jan	Brand et al 1993
anti-CycE	Mouse	1:10	H Richardson	Richardson et al 1995
anti-Insc	Rabbit	1:1000	W Chia	Kraut et al 1996
anti-Mira	Mouse	1:40	F Matsuzaki	Ohshiro et al 2000
anti-Baz	Guinea pig	1:500	A Wodarz	Wodarz et al 1999
anti-Numb	Guinea pig	1:5000	J Skeath	Uemura et al 1989
anti-CNN	Rabbit	1:500	E Schejter	Vaizel-Ohayon and Schejter 1999
anti-Asl	Guinea pig	1:12000	G Rogers	Klebba et al 2013
anti-AurA	Rabbit	1:100	J Raff	Giet et al 2002
anti-Polo	Mouse	1:10	C Sunkel	Llamazares et al 1991
anti-DTACC	Rabbit	1:100	J Raff	Gergely et al 2000
anti-Msps	Rabbit	1:100	J Raff	Lee et al 2001
anti-CD8	Rat	1:100	Invitrogen (MCD0800)	
anti-GFP	Rabbit	1:1000	Molecular Probes (A-11122)	
anti-pH3	Rabbit	1:1000	Sigma (H0412)	
anti-pH3	Rat	1:1000	Sigma (H9908)	
anti-PKCζ C-20	Rabbit	1:200	Santa Cruz (sc-216)	
anti- α-Tubulin	Mouse	1:200	Sigma (T6199)	
anti- γ-Tubulin	Mouse	1:100	Sigma (T5326)	
anti- β-Tubulin	Mouse	1:50	DSHB (E7)	

2.5.2 Fixation and immunostaining of 3rd instar larval brains

Third instar larval brains were used for immunohistochemistry as described previously (Wang et al., 2006). Briefly, 10-15 larval brains were dissected in PBS and were immediately fixed with 1 ml of 4% formaldehyde in PBS for 15 min. For more efficient labeling of asymmetric proteins, microtubule proteins and centrosome proteins, the brain samples can be fixed for 22 min with 4% EM-grade formaldehyde. After washing with PBS supplemented with 0.3% TritonX-100 (PBT) for three times (10 min each), the fixed brains were blocked with 3% BSA in PBT for one hour before incubated with primary antibodies overnight at 4°C. Following three washes for 15 min each, larval brains were incubated with secondary antibodies (Invitrogen) diluted in PBT for 90 minutes at room temperature. Following by additional washing twice using PBT, DNA was labeled by incubating with ToPro-3 (Invitrogen) for 30 min. The brain samples were then mounted with Vectashield (Vector Laboratories). The confocal images were acquired on a Zeiss 710 LSM confocal microscopy system (Axio Observer Z1) in 21°C, using a Plan-APOCHROMAT 40X/1.3 NA oil DIC objective. The images were captured with an AxioCam HR camera with 1.5X to 6X of digital zoom through the control of ZEN software. The exported images were then processed with Adobe Photoshop CS5.1 for minor adjustments of brightness and contrast.

2.5.3 Quantification of neuroblast number and spindle orientation

The quantification of neuroblast number of third instar larval central brains was performed on 96 h ALH at 25°C, or 72 to 84 h ALH at 29°C. 4 to 8 hours embryo collections were obtained in a bottle with about 100 flies (synchronization). The larvae hatched 24 hours after the synchronization, and wandering larvae were collected and dissected at the desired time points. The

brain samples were stained with anti-Dpn antibody. The neuroblast number was counted based on Dpn labeling under the microscope. Central brain neuroblasts were located at the medial-superficial part of the brain, and they were distinguished from intermediate neural progenitors (INPs) based on the larger cell size and stronger immune-fluorescent signals of anti-Dpn. To quantify mitotic spindle orientation, confocal images of metaphase neuroblasts labeled for α-tubulin and Insc were used. The Insc crescent indicated the apical side of the neuroblast, and the apico-basal axis was inferred by a line perpendicular to the Insc crescent. And the spindle axis was inferred by the α-tubulin labeled mitotic spindles. The angles between these two axes were measured and quantified.

2.5.4 EdU labeling

EdU labeling was carried out using Click-iT EdU Alexa Fluor® 555 Imaging Kit (Invitrogen) according to the manufacturer's instructions. 10-15 third instar larval brains were dissected in PBS and incubated with 1 ml of 10μM EdU (5-ethynyl-2'deoxyuridine) on a nutator for 45 minutes at room temperature. The brains were then fixed with 1 ml of 4% formaldehyde in PBS for 15 minutes and blocked in 3% BSA for 1 hour. After incubating with Click-iT reaction cocktail according to the manufacturer's protocols, the brains were mounted and imaged using LSM 710 confocal microscope.

2.5.5 Microtubule regrowth assay

Microtubule regrowth assays were performed essentially as described previously (Gallaud et al., 2014). 10-15 third instar larval brains were dissected in Shield and Sang M3 insect medium (Sigma) supplemented with 10% FBS, and immediately transferred to an eppendorf tube with 50-100 μl of

medium. Microtubules were depolymerized by incubating the brain samples on ice for 30 minutes. The brains were allowed to recover at 25°C for various durations to allow microtubule regrowth, following by fixation in 1ml of 10% formaldehyde in Testis Buffer (183mM KCl, 47mM NaCl, 10mM Tris-HCl, 1mM EDTA, pH 6.8) supplemented with 0.01% TritonX-100. The fixed brains were washed once in PBS and twice in 0.1% TritonX-100 in PBS (each 10 min), followed by standard immunohistochemistry as described in 2.5.2.

2.5.6 Live-cell imaging

To record live-cell divisions, 3 to 5 third instar larval brains expressing a microtubule-binding protein, G147-GFP (Morin et al., 2001), were dissected in Shield and Sang M3 insect medium (Sigma) supplemented with 10% FBS (dissecting medium), and loaded into a Lab-Tek^{TM} chambered coverglass (Thermo Scientific) filled with dissecting medium supplemented with 2.5% methyl cellulose (Sigma), together with fat bodies isolated from about 10 wild-type third instar larvae. The time-lapse images were recorded in a Zeiss LSM 710 confocal microscope, with 20 sec intervals, and videos were exported and processed with Adobe Photoshop CS 5.1 and Image J.

2.5.7 MitoTracker stain

To label mitochondria in live neuroblasts, third instar larval brains expressing Arl2^{WT}-Venus or Mito-GFP were gently squashed in 10µl of Shield and Sang M3 insect medium (Sigma) containing 10% FBS and 200nM MitoTracker® Red FM (Invitrogen), and were incubated for 30min before imaged using Zeiss LSM710 confocal microscope.

CHAPTER 3: ARL2- AND MSPS-DEPENDENT MICROTUBULE GROWTH GOVERNS ASYMMETRIC DIVISIONS

3.1 Introduction

From the RNA interference (RNAi) screen, a previously poorly studied gene in *Drosophila* genome, *ADP ribosylation factor like 2* (*arl2*), was identified as a novel gene that prevents neuroblast overgrowth in the larval central brain (Chen K. and Wang H., unpublished data). *arl2* encodes a conserved small GTPase belonging to the Ras superfamily that cycles between GTP-bound and GDP-bound forms (Burd et al., 2004). Genetic evidence was provided showing that Arl2 functions upstream of *Drosophila* Transforming acidic coiled coil (D-TACC) and Mini spindles (Msps), to control microtubule growth and asymmetric division. Arl2 physically associates with tubulin binding cofactors C (TBCC), D (TBCD) and E (TBCE). Moreover, Arl2 functions together with TBCD to regulate D-TACC and Msps localization, and neuroblast self-renewal. Therefore, a new paradigm of Arl2 and Msps governing neuroblast asymmetric division through regulating microtubule growth is proposed in this thesis.

3.2 Results

3.2.1 ADP Ribosylation Factor-Like 2 (Arl2) inhibits neuroblast overgrowth in *Drosophila* larval brains

ADP ribosylation factor like 2 (Arl2) was identified as a neuroblast self-renewal regulator from a genome-wide RNAi screen (Chen K. and Wang H., unpublished data). Using a neuroblast specific driver, *insc*-Gal4, knockdown of *arl2* with two different RNAi lines, GD44334 and KK110627, both resulted

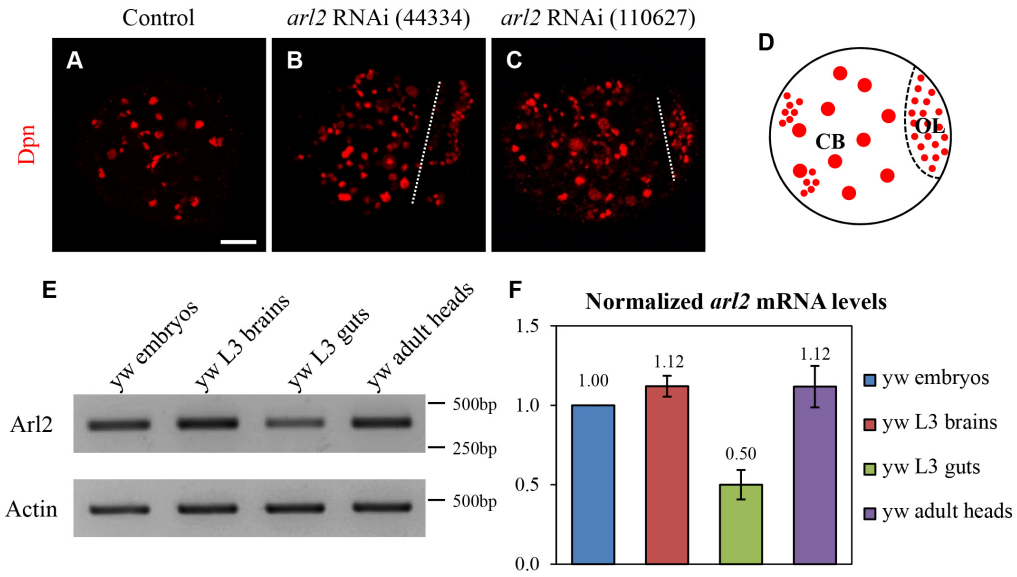

Figure 12. Knockdown of *arl2* by RNAi results in neuroblast overgrowth in larval central brains.
(A-C) Control (A), *arl2* RNAi (44334GD) (B) and *arl2* RNAi (110627KK) (C) larval brains labeled for Dpn. Central brain is to the left of the white dotted line. (D) A schematic diagram for the dorsal view of the larval brain. Dpn (red) labels neuroblasts and INPs. CB: central brain. OL: optic lobe. (E) mRNA levels of *arl2* and *actin5C* from wild-type embryos (lane 1), 3rd-instar larval brains (lane 2), 3rd-instar larval guts (lane 3) and adult fly head (lane 4) analyzed using RT-PCR. (F) The quantification of *arl2* mRNA levels normalized against the loading control (*actin5C*). Scale bar: 20 μm

in supernumerary neuroblasts in the larval central brains (Fig. 12A-C). *arl2* is highly expressed in the central nervous system during development. *arl2* mRNA could be detected in wild-type embryos, and similar levels of *arl2* mRNA were detected in 3rd-instar larval brains (1.12±0.07 folds) and adult fly heads (1.12±0.13 folds), while relatively lower levels were detected from 3rd-instar larval guts (0.50±0.09 folds) (Fig. 12E, F).

We generated an Arl2^{T30N} transgene (substitution of threonine 30 by asparagine), a dominant-negative form of *arl2* that mimicks the constitutive GDP-bound Arl2 (Bhamidipati et al., 2000). Overexpression of Arl2^{T30N} under *insc*-Gal4 driver caused neuroblast overgrowth in the central brains. There are about 100 neuroblasts in each wild-type larval central brain (Fig. 13A, C; 100±6 neuroblasts/brain hemisphere, n=31). In contrast, overexpression of

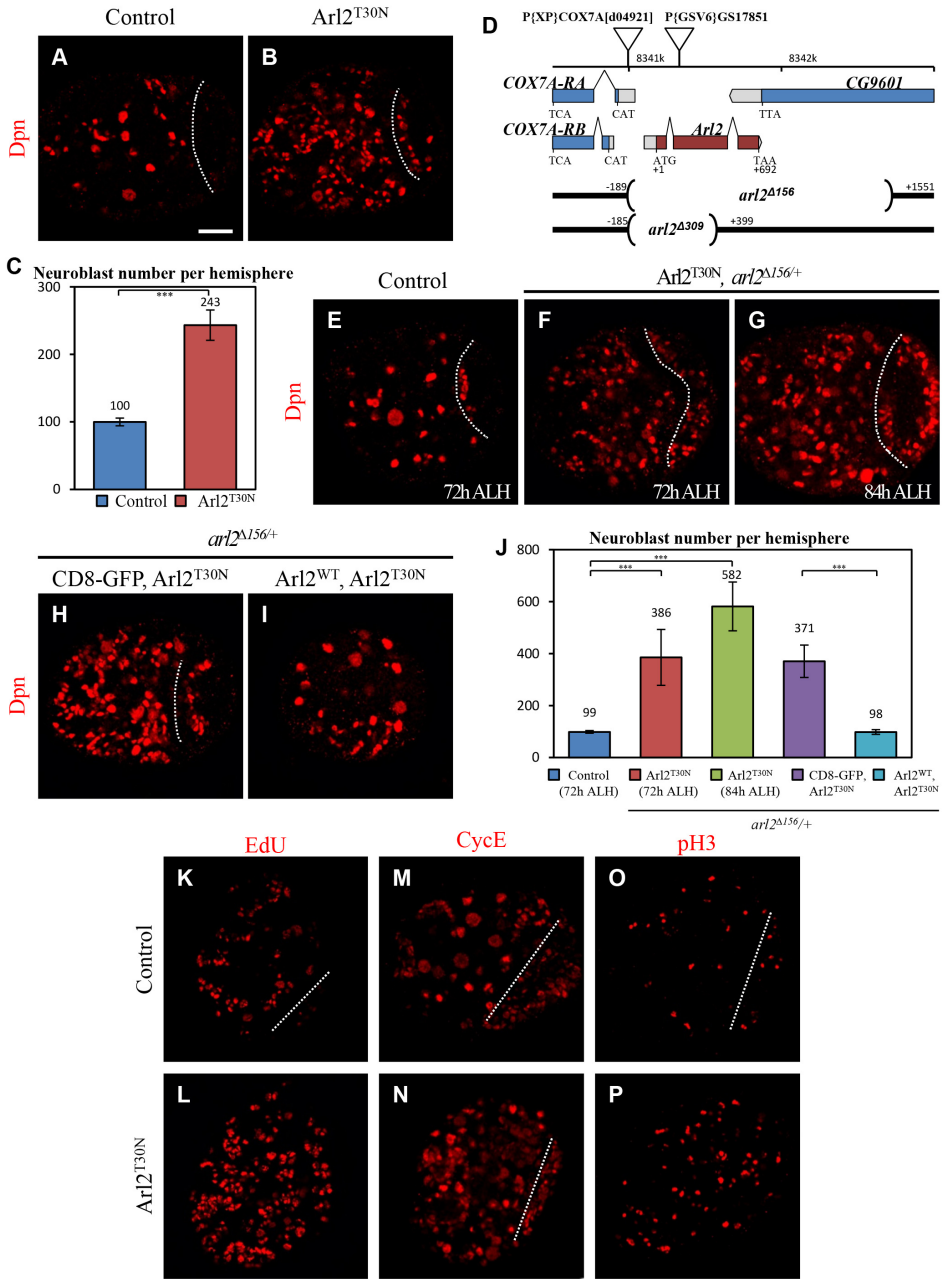

Figure 13. Overexpression of a dominant negative Arl2 (Arl2^{T30N}) causes neuroblast overgrowth.

(A, B) Control (A) and Arl2^{T30N}-overexpressing (B) larval brains labeled for Dpn. (C) Quantification of central brain neuroblast number per brain hemisphere for (A-B). Mean and SD are shown. (D) A schematic diagram of deleted regions in *arl2*$^{\Delta 156}$ and *arl2*$^{\Delta 309}$, with locations of the two P elements used. (E-G) Larval brains from a control at 72 h ALH (E), Arl2^{T30N}, *arl2*$^{\Delta 156}$/+ (overexpressed Arl2^{T30N}, *arl2*$^{\Delta 156}$/+) at 72 h ALH (F) and 84 h ALH (G) labeled for Dpn. (H, I) Larval brains from Arl2^{T30N}, *arl2*$^{\Delta 156}$/+ with CD8-GFP (H), and Arl2^{T30N}, *arl2*$^{\Delta 156}$/+ with Arl2^{WT} (I) labeled for Dpn. (J) Quantification of central brain neuroblast number per brain hemisphere for (E-I). Mean and SD are shown. (K-P) Larval brains from control (K, M, O) and Arl2^{T30N}-overexpressing (L, N, P) labeled for EdU (K, L), CycE (M, N) and pH3 (O, P). Central brain is to the left of the white dotted line. Scale bars, 20 μm. *** indicates P <0.001.

Arl2^{T30N} resulted in a significant increase in neuroblast number (Fig. 13B, C; 243±22, n=30), as judged by a neuroblast marker, Deadpan (Dpn). Consistent with the neuroblast overgrowth phenotype, the number of cells positive for EdU, phospho-Histone H3 (pH3) and Cyclin E (CycE) was significantly increased upon Arl2^{T30N} overexpression (Fig. 13K-P). Therefore, loss of *arl2* by either RNAi knockdown or overexpression of a dominant-negative *arl2* transgene caused neuroblast overgrowth.

To generate *arl2* deletion mutants, we mobilized a P element, P{XP}COX7A^{d04921}, which is inserted at 105 base pairs (bp) upstream of the transcription start site of *arl2* (Fig. 13D). Through imprecise excision, two embryonic-lethal alleles, *arl2$^{\Delta 156}$* and *arl2$^{\Delta 309}$*, were obtained (see 2.1.3). Introduction of heterozygous *arl2$^{\Delta 156}$* into Arl2^{T30N}-expressing brains enhanced the supernumerary neuroblast phenotype caused by *arl2* dominant-negative. At 72h after larval hatching (ALH) at 29°C, the central brain neuroblast number was increased to 386±108 in each brain hemisphere in Arl2^{T30N}, *arl2$^{\Delta 156}$/+* (Fig. 13F, J; n=25), compared to wild-type central brains that contained ~100 neuroblasts in each brain hemisphere (Fig. 13E, J; 99±5, n=23). Arl2^{T30N}, *arl2$^{\Delta 156}$/+* exhibited a slight extension of larval stage and neuroblast number was further increased to 582±94 at 84h ALH at 29°C (Fig. 13G, J; n=25). The neuroblast overgrowth phenotype was fully restored by co-expression of an Arl2^{WT} transgene (Fig. 13H-J).

There are at least two major types of neuroblast lineages in the *Drosophila* larval central brain. Type I and type II neuroblasts both divide asymmetrically to self-renewal, but type I neuroblasts give rise to a ganglion mother cell, whereas type II neuroblasts give rise to an intermediate neural progenitor (Bello et al., 2008; Boone and Doe, 2008; Bowman et al., 2008).

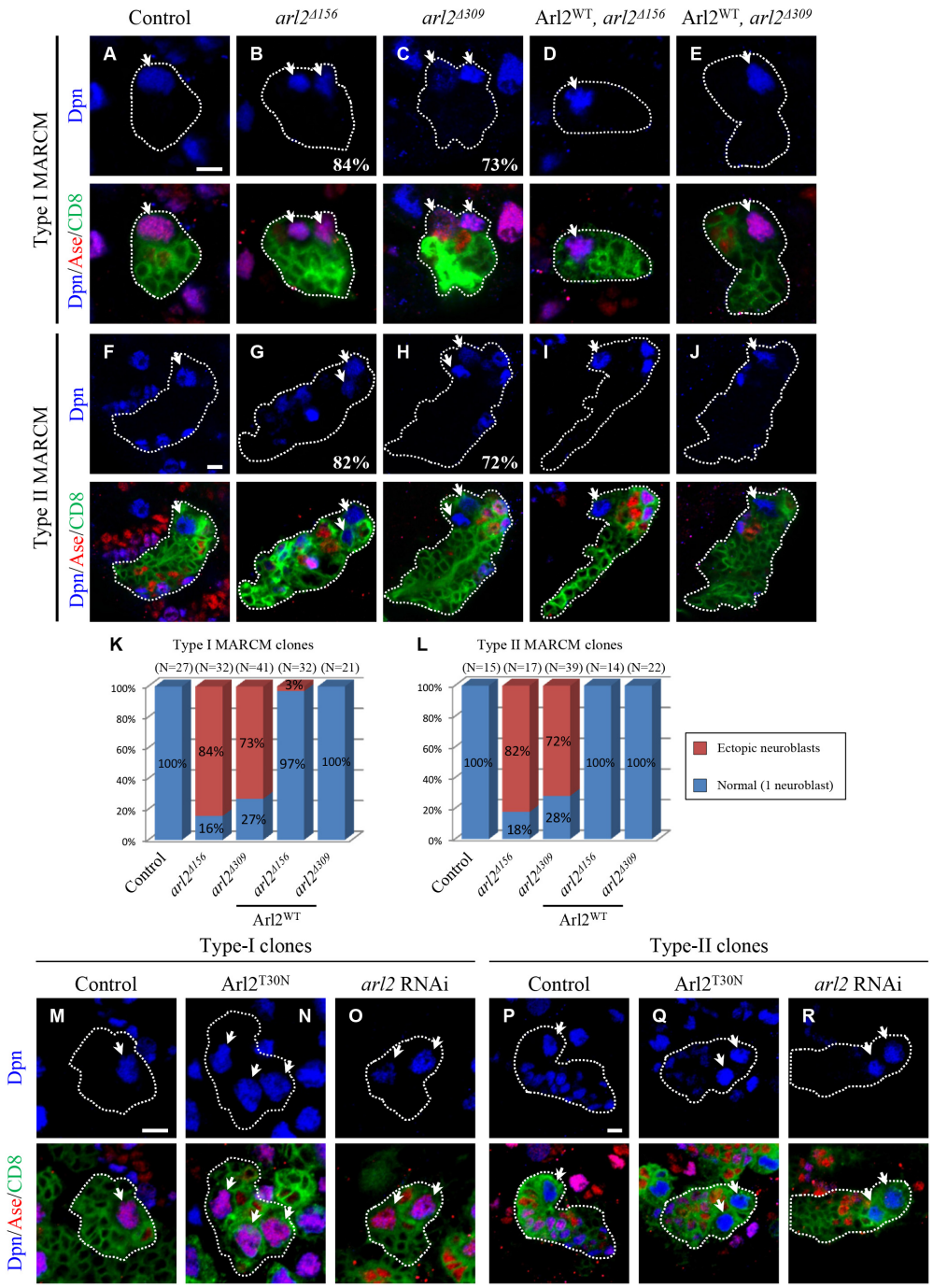

Figure 14. Arl2 inhibits the formation of ectopic neuroblasts in both type I and type II neuroblast lineages.

(A-J) Type-I (A-E) and Type-II (F-J) neuroblast MARCM clones in control (FRT82B) (A, F), *arl2*$^{\Delta 156}$ (B, G), *arl2*$^{\Delta 309}$ (C, H), Arl2^{WT} overexpression (O/E) in *arl2*$^{\Delta 156}$ (D, I) and Arl2^{WT} O/E in *arl2*$^{\Delta 309}$ (E, J) labeled for Dpn, Ase and CD8. (K, L) Quantification of neuroblast overgrowth phenotype in type I (K) and type II (L) MARCM clones. (M-R) Control (M, P), Arl2^{T30N} overexpression (Arl2^{T30N}) (N, Q) and *arl2* RNAi (44334GD) (O, R) using *ase*-Gal4 (M-O) or *wor*-Gal4, *ase*-Gal80 (P-R) labeled for Dpn, Ase and CD8. Cells in the clones are labeled by CD8-GFP and the outline of the neuroblast lineages is indicated by white dotted lines. Arrows indicate neuroblasts. Scale bars, 5 μm.

To ascertain the requirement of *arl2* for both types of neuroblast lineages, we generated $arl2^{\Delta 156}$ and $arl2^{309}$ clones using Mosaic Analysis with a Repressible Cell Marker (MARCM) (Lee and Luo, 1999). In contrast to a single neuroblast in control clones (FRT82B control: type I, 100%, n=27; type II, 100%, n=15), ectopic neuroblasts were observed in both type I (84%, n=32) and type II (82%, n=17) neuroblast lineages in $arl2^{\Delta 156}$ clones (Fig. 14A, B, F, G, K, L). Similarly, ectopic neuroblasts were found in 69% (n=28) of type I and 65% (n=29) of type II neuroblast lineages in $arl2^{\Delta 309}$ clones (Fig. 14C, H, K, L). This phenotype seen in *arl2* clones was largely rescued by overexpression of a wild-type *arl2* ($Arl2^{WT}$) transgene, suggesting that neuroblast self-renewal defects were caused by *arl2* loss-of-function ($Arl2^{WT}$ OE in $arl2^{\Delta 156}$: type I, 97%, n=32; type II, 100%, n=14; $Arl2^{WT}$ OE in $arl2^{\Delta 309}$: type I, 100%, n=21; type II, 100%, n=22) (Fig. 14D, E, I, J, K, L). Furthermore, ectopic neuroblasts were also found in *arl2* knockdown and upon $Arl2^{T30N}$ overexpression type I or type II lineages under type I- (*ase*-Gal4) or type II-specific drivers (*wor*-Gal4, *ase*-Gal80), respectively (Fig. 14M-R). Therefore, *arl2* is required to prevent neuroblast overgrowth in both type I and type II neuroblast lineages.

3.2.2 Arl2 regulates cell polarity and mitotic spindle orientation during neuroblast asymmetric division

We asked whether Arl2 is required for neuroblast asymmetric division, by first examining the localization of asymmetric proteins in *arl2* mutants. In metaphase neuroblasts of control clones, aPKC displayed a strong crescent at the apical cortex (Fig. 15A, G; 100%, n=33). However, 70% (n=50) of metaphase neuroblasts from $arl2^{\Delta 156}$ clones and 76% (n=52) of metaphase neuroblasts from $arl2^{\Delta 309}$ clones failed to form a robust aPKC crescent (Fig. 15B, C, G). In contrast, these metaphase neuroblasts in *arl2* mutant clones

no longer localized aPKC asymmetrically, or they only formed much weaker aPKC crescents. aPKC de-localization seen in *arl2* mutant clones was rescued by overexpression of an Arl2^{WT} transgene (Fig. 15D, G). *arl2*^{GS17851} is a putative *arl2* loss-of-function allele, which contains a P-element

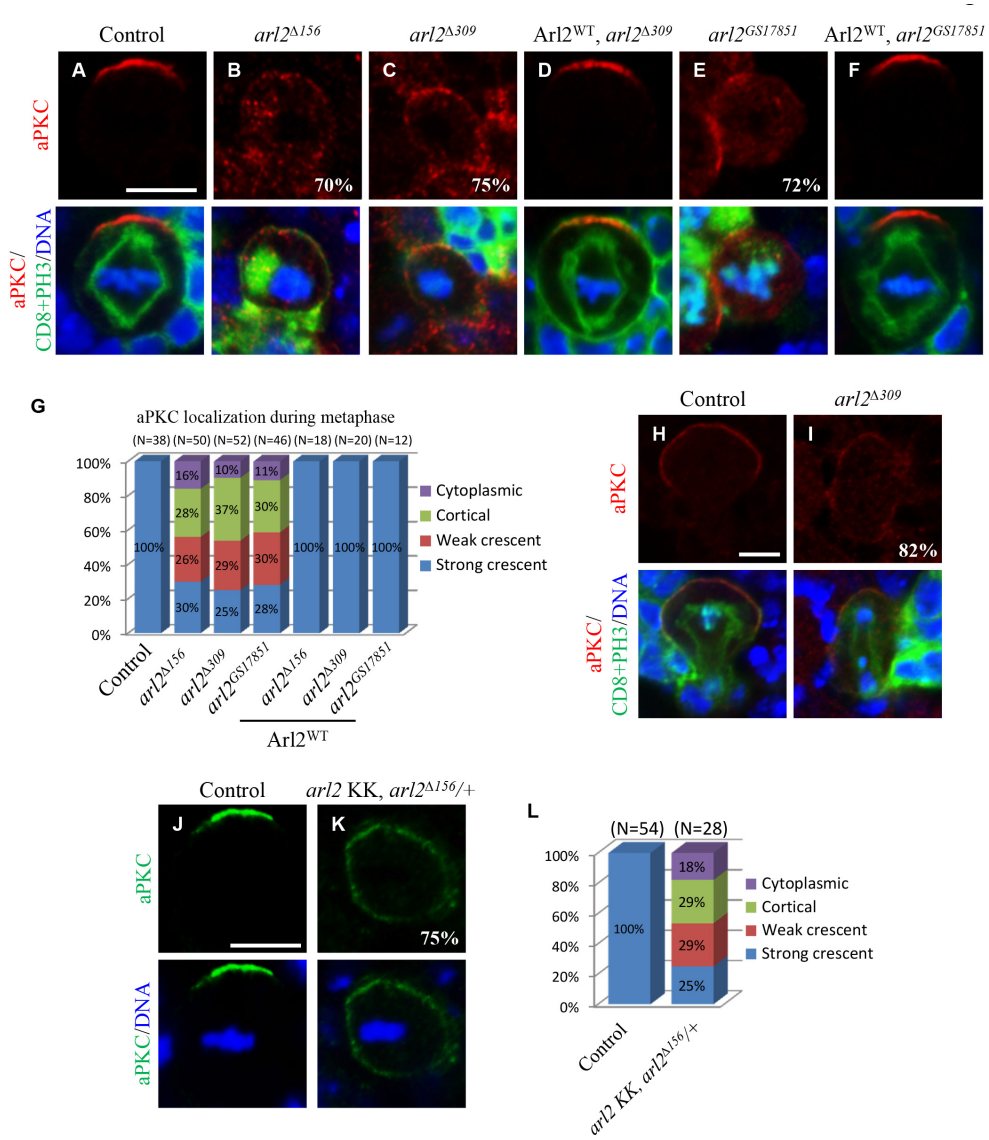

Figure 15. The apical localization of aPKC is disrupted upon *arl2* loss of function.
(A-F) Metaphase neuroblasts of control (FRT82B) (A), *arl2*$^{\Delta 156}$ (B), *arl2*$^{\Delta 309}$ (C), Arl2^{WT} overexpression (O/E) in *arl2*$^{\Delta 309}$ (D), *arl2*^{GS17865} (E) and Arl2^{WT} O/E in *arl2*^{GS17851} (F) MARCM clones labeled for aPKC, CD8, PH3 and DNA. (G) Quantification of aPKC localization in (A-F). (H, I) Telophase neuroblasts of control (H) and *arl2*$^{\Delta 309}$ (I) MARCM clones labeled for aPKC, CD8, PH3 and DNA. (J, K) Metaphase neuroblasts of control (J), *arl2* knockdown in *arl2*$^{\Delta 156}$/+ (*arl2* KK, *arl2*$^{\Delta 156}$/+) (K) labeled for aPKC and DNA. (L) Quantification of aPKC localization in (J-K). Scale bars, 5 μm.

inserted at the coding region of *arl2* (Fig, 13D). Consistently, aPKC polarity was disrupted in 72% (n=46) $arl2^{GS17851}$ metaphase neuroblasts, and this defect was restored by overexpression of $Arl2^{WT}$ transgene (Fig. 15E-G). In 75% (n=28) of metaphase neuroblasts with *arl2* RNAi knockdown in the $arl2^{\Delta 156/+}$ background, aPKC was not localized properly (Fig. 15J-L). In many previously reported mutants, such as *insc*, *pins* and *ctp* mutants (Kraut et al., 1996; Wang et al., 2011; Yu et al., 2000), the defective cell polarity can be largely restored during late mitosis, a phenomenon called 'telophase rescue' (Cai et al., 2001). In $arl2^{\Delta 309}$ telophase neuroblasts, aPKC was often mis-segregated to both daughter cells (Fig. 15I; n=11), suggesting that telophase rescue did not occur in *arl2* mutants.

Similarly, Baz was delocalized in 52% (n=62) of $arl2^{\Delta 156}$ clones and 60% (n=62) of $arl2^{\Delta 309}$ clones during metaphase (Fig. 16B, C, E). Another apically localized protein, Insc, was delocalized in 43% (n=35) and 49% (n=40) of metaphase neuroblasts in $arl2^{\Delta 156}$ and $arl2^{\Delta 309}$ clones, respectively (Fig. 16G, H, J). Arl2 is also required for proper localization of basal proteins during neuroblast asymmetric division. 58% of $arl2^{\Delta 156}$ (n=46) and 76% of $arl2^{\Delta 309}$ (n=51) neuroblasts displayed cortical Numb or no Numb crescent during metaphase (Fig. 16L, M, O). In control metaphase neuroblasts, Mira was targeted to the basal cortex (Fig. 16P, T; 100%, n=37). In contrast, the localization of Mira was disrupted in 33% (n=48) and 41% (n=54) of metaphase neuroblasts in $arl2^{\Delta 156}$ and $arl2^{\Delta 309}$ clones, respectively (Fig. 16Q, R, T). The defects of apico-basal polarity could be fully restored by overexpression of an $Arl2^{WT}$ transgene in neuroblasts (Fig. 16). Together, Arl2 is important for the apico-basal polarity during neuroblast asymmetric division.

We next examined whether spindle orientation was altered in *arl2* loss of function. In a wild-type metaphase neuroblast, the mitotic spindle, labeled by

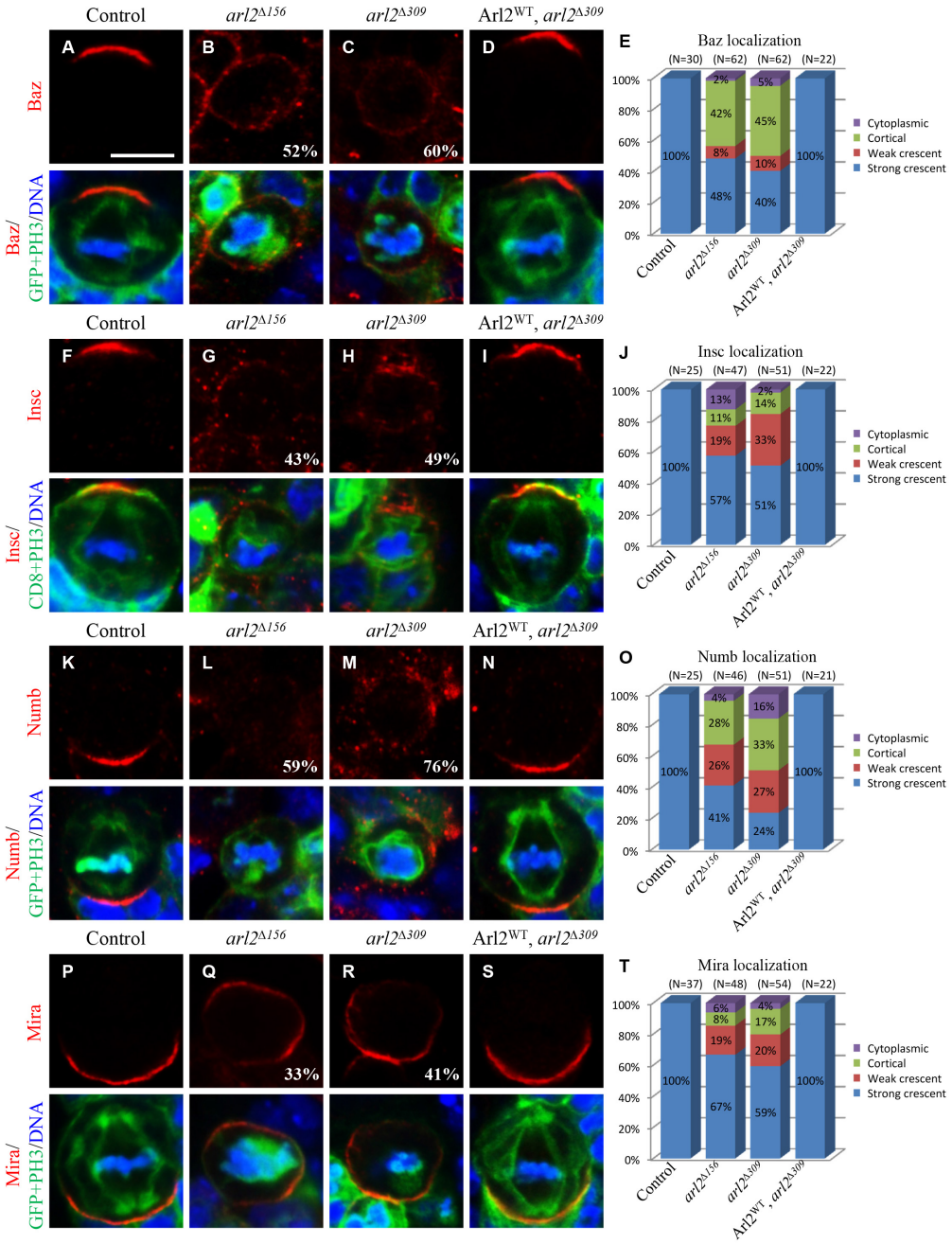

Figure 16. Cortical polarity defects seen in *arl2* mutant MARCM clones. (A-D) Metaphase neuroblasts of control (FRT82B) (A), *arl2*$^{\Delta 156}$ (B), *arl2*$^{\Delta 309}$ (C) and Arl2^{WT} overexpression (O/E) in *arl2*$^{\Delta 309}$ (D) MARCM clones labeled for Baz, GFP, PH3 and DNA. (E) Quantification of Baz localization in (A-D). (F-I) Metaphase neuroblasts of control (FRT82B) (F), *arl2*$^{\Delta 156}$ (G), *arl2*$^{\Delta 309}$ (H) and Arl2^{WT} O/E in *arl2*$^{\Delta 309}$ (I) MARCM clones labeled for Insc, CD8, PH3 and DNA. (J) Quantification of Insc localization in (H-M). (K-N) Metaphase neuroblasts of control (FRT82B) (K), *arl2*$^{\Delta 156}$ (L), *arl2*$^{\Delta 309}$ (M) and Arl2^{WT} O/E in *arl2*$^{\Delta 309}$ (N) MARCM clones labeled for Numb, GFP, PH3 and DNA. (O) Quantification of Numb localization in (K-N). (P-S) Metaphase neuroblasts of control (FRT82B) (P), *arl2*$^{\Delta 156}$ (Q), *arl2*$^{\Delta 309}$ (R) and Arl2^{WT} O/E in *arl2*$^{\Delta 309}$ (S) MARCM clones labeled for Mira, GFP, PH3 and DNA. (T) Quantification of Mira localization in (P-S). Scale bars, 5 μm.

α-tubulin, is oriented along the apico-basal axis inferred from the apically localized Insc crescent, to ensure the correct segregation of asymmetrically-localized proteins into two different daughter cells (Fig. 17A; 100%, n=83). In contrast, upon Arl2^{T30N} overexpression in *arl2*$^{\Delta 156}$/+, 57% (n=105) of mitotic spindles were no longer properly oriented, and 1% of metaphase neuroblasts were dividing orthogonally with mitotic spindles rotated by close to 90° from the apicobasal axis (Fig. 17B; n=105). Likewise, Arl2^{T30N} overexpression or *arl2* RNAi knockdown in neuroblasts also led to mis-orientation of mitotic spindle, albeit with slightly weaker phenotypes (Fig. 17C, D). Similar spindle

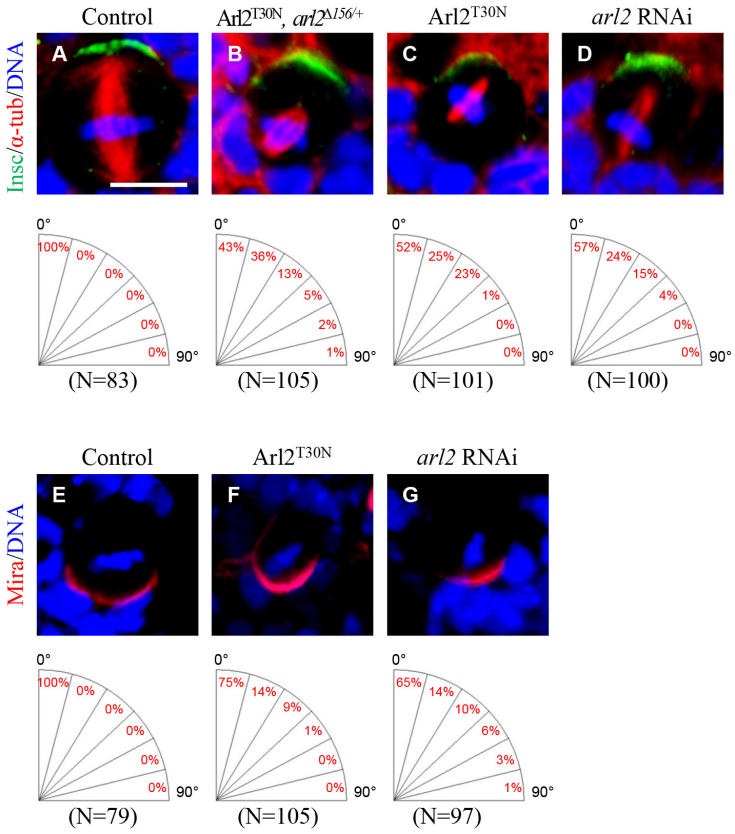

Figure 17. Loss of *arl2* disrupts proper mitotic spindle orientation in neuroblasts.
(A-D) Metaphase neuroblasts of control (A), Arl2^{T30N}, *arl2*$^{\Delta 156}$/+ (Arl2^{T30N} overexpression in *arl2*$^{\Delta 156}$/+) (B), Arl2^{T30N} (C) and *arl2* RNAi (44334GD) (D) labeled for Insc, α-tubulin and DNA. (E-G) Metaphase neuroblasts of control (E), Arl2^{T30N} (F) and *arl2* RNAi (44334GD) (G) labeled for Mira and DNA. Quantification of spindle orientation is shown in the lower panels. Scale bars, 5 μm.

mis-orientation was observed in *arl2* knockdown and Arl2^{T30N}-expressing metaphase neuroblasts, when the analysis was based on the metaphase plate and the apicobasal axis inferred from the Mira crescent (Fig. 17E-G). Taken together, Arl2 is required for the correct alignment of the mitotic spindle in neuroblasts.

In each round of asymmetric division, two daughter cells with distinct cell sizes are produced. To determine whether Arl2 is important for the cell-size asymmetry, we measured the diameters of the two daughter cells during telophase. In wild-type telophase neuroblasts, the two daughter cells had distinct cell sizes, with the ratio D1 (larger daughter)/D2 (smaller daughter) of 2.10±0.24 (Fig. 18A, D; n=55). However, upon Arl2^{T30N} overexpression, the ratio of daughter cell diameters was dramatically decreased to 1.65±0.29 (Fig. 18B, D; n=47). In telophase neuroblasts in Arl2^{T30N}, *arl2*$^{\Delta 156}$/+, the ratio of daughter cell diameters was further decreased to 1.51±0.19 (Fig. 18C, D; n=54), suggesting that *arl2* is essential for cell-size asymmetry during neuroblast asymmetric divisions. Time-lapse live cell imaging was carried out to analyze the asymmetric cell division in Arl2^{T30N}-expressing neuroblasts, using live whole-mounted brains expressing G147-GFP, which labels microtubules (Morin et al., 2001). The control neuroblasts always divided asymmetrically (Fig. 18E; n=18). However, symmetric divisions were found in13% of Arl2^{T30N}-expressing neuroblasts (Fig. 18F; n=23). These data suggest that Arl2 is essential for regulating neuroblast asymmetric division.

To examine the subcellular localization of Arl2 in neuroblasts, we generated an Arl2-Venus transgene. When expressed under *insc*-Gal4 driver, Arl2-Venus displayed cytoplasmic localization throughout different phases of neuroblast division (Fig. 19A-D). Mammalian Arl2 is predominantly cytosolic

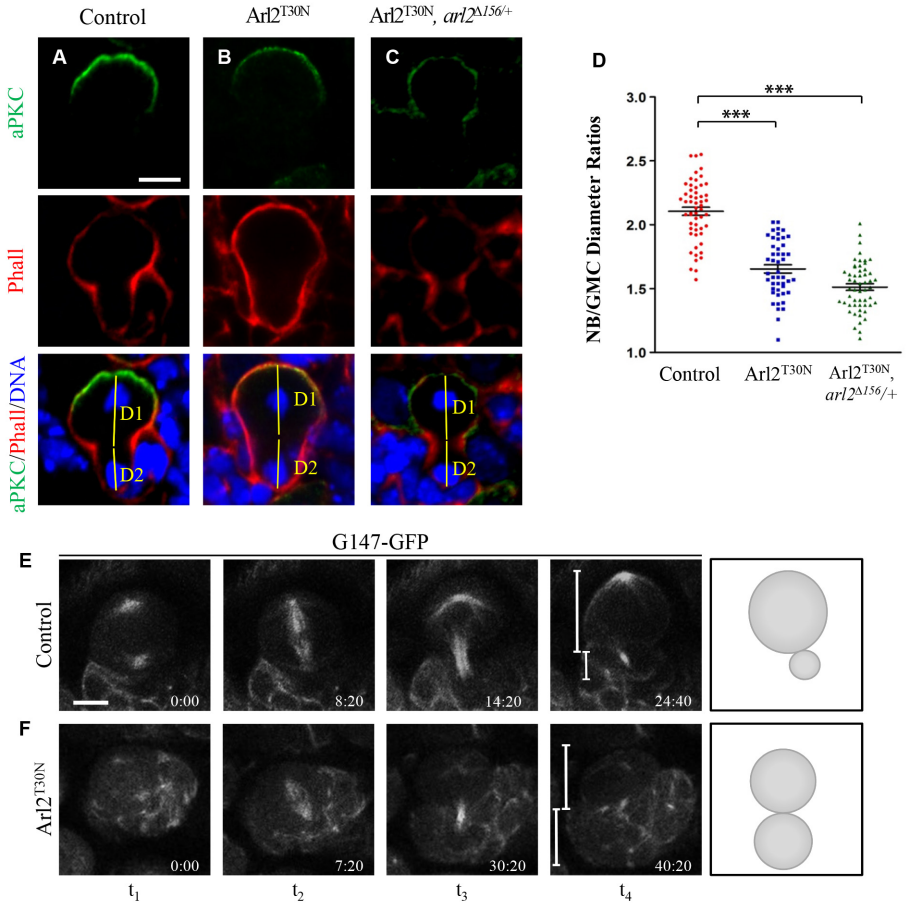

Figure 18. Symmetric divisions are observed in Arl2^{T30N}-expressing neuroblasts.
(A-C) Telophase neuroblasts of control (A), Arl2^{T30N} (B) and Arl2^{T30N}, *arl2^{Δ156}/+* (Arl2^{T30N} overexpression in *arl2^{Δ156}/+*) (C) labeled for aPKC, phalloidine (Phall) and DNA. D1 and D2 indicate the diameters of neuroblast daughter and GMC daughter, respectively. (D) Quantification of the ratio of D1/D2 for (A-C). Mean and SEM are shown. *** indicates P <0.001. (E, F) Time-lapse imaging of control (G147-GFP/+) (E) and Arl2^{T30N}-neuroblasts expressing G147-GFP (F). Scale bars, 5 µm

but is also found in mitochondria (Shern et al., 2003). However, *Drosophila* Arl2-Venus did not localize to the mitochondria labeled by the vital dye Mitotracker (Fig. 19E, F).

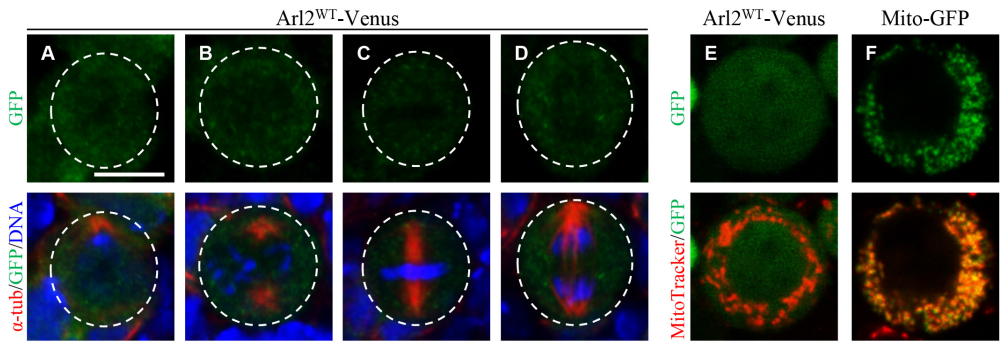

Figure 19. Arl2 is localized to the cytoplasm in neuroblasts.
(A-D) Neuroblasts expressing Arl2^{WT}-Venus (under *insc*-Gal4) at interphase (A), prophase (B), metaphase (C) and anaphase (D) labeled for GFP, α-tubulin and DNA. The white dotted circles indicate the neuroblast contours. (E, F) Live neuroblasts expressing Arl2^{WT}-Venus (E) and Mito-GFP (F) labeled with MitoTracker Red FM. Scale bars, 5 μm.

3.2.3 Arl2 is critical for the formation of interphase microtubule asters and mitotic spindles

In mammalian cells, Arl2 inhibits the Tubulin Binding Co-factor D (TBCD), thus prevents the dissociation of microtubules (Bhamidipati et al., 2000). We next asked whether Arl2 is required for microtubule nucleation and growth in neuroblasts. Indeed, we noticed that metaphase neuroblasts in Arl2^{T30N}, *arl2*$^{\Delta 156}$/+ assembled shorter mitotic spindles (Fig. 17B; 5.31±0.83μm, n=65) than in wild-type neuroblasts (Fig. 17A; 9.33±0.81μm, n=46), suggesting a defect in microtubule polymerization in *arl2* loss of function. We carried out a microtubule re-growth assay, depolymerizing mitotic spindles by cold treatment, followed by monitoring the microtubule re-growth at 25°C in Arl2^{T30N}-expressing neuroblasts (Fig. 20A). Treatment on ice for 30 min fully disrupted mitotic spindles in both control and Arl2^{T30N} neuroblasts, suggesting an efficient de-polymerization of microtubules (Fig. 20B, G; control, n=10; Arl2^{T30N}, n=14). After returning to 25°C for 30 seconds (s), re-growth of microtubules were observed around the centrosomes and the chromosomes in control metaphase neuroblasts (Fig. 20C; n=10). After 2 minutes' recovery,

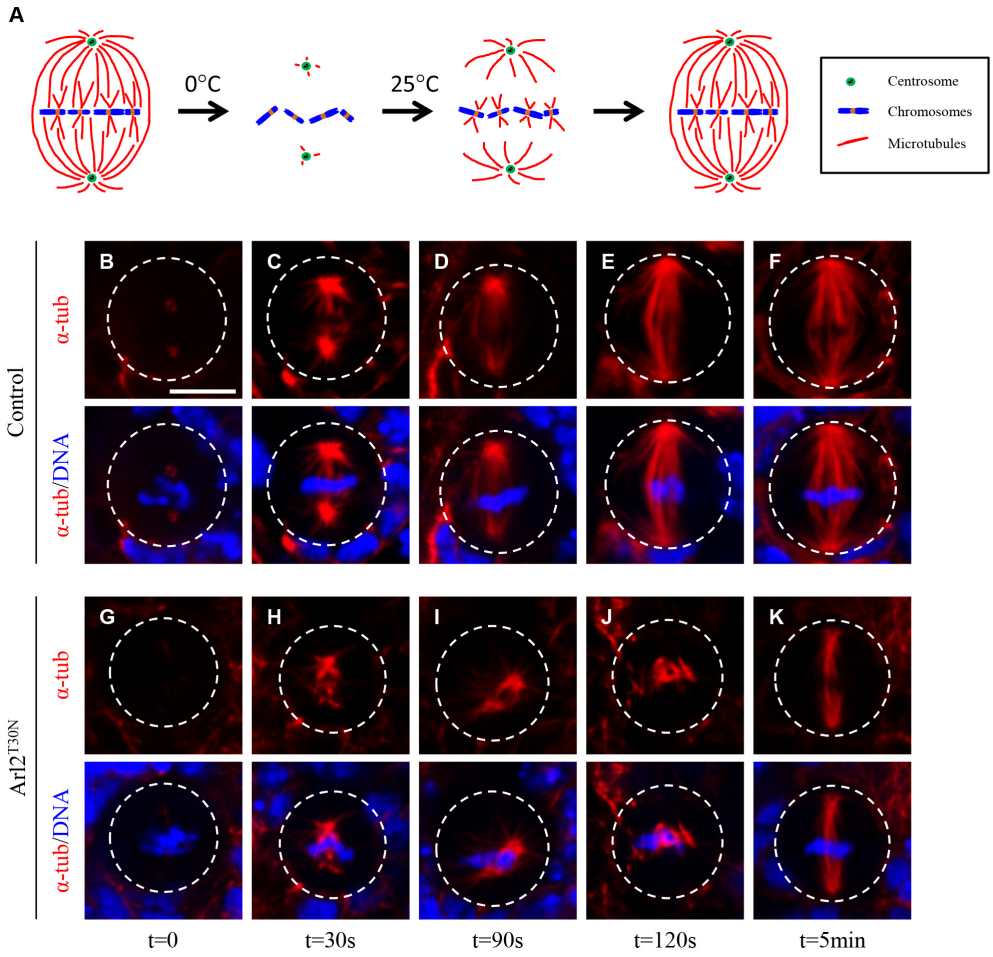

Figure 20. The re-assembly of mitotic spindles is disrupted in Arl2^{T30N}-expressing neuroblasts.
(A) A schematic of microtubule re-growth assay. (B-K) Control (B-F) and Arl2^{T30N}-expressing (G-K) metaphase neuroblasts labeled for α-tubulin and DNA after recovery for different times following treatment on ice. Times allowed for the recovery after ice treatment are indicated at lower panels. Scale bars, 5 μm.

all control metaphase neuroblasts were able to re-assemble normal-appearing mitotic spindles (Fig. 20E; n=22). In contrast, after 30s recovery, 40% of Arl2^{T30N} metaphase neuroblasts re- assembled less microtubule mass (Fig. 20H; n=15), and after 2 min, 54% (n=26) of metaphase neuroblasts still failed to form mitotic spindles (Fig. 20J). After 5 min, most Arl2^{T30N}-expressing metaphase neuroblasts re-assembled mitotic spindles, but they were shorter and narrower than in the control (Fig. 20F, K; n=20). These results suggest that Arl2 promotes microtubule nucleation and growth.

Next we ascertained whether defects of microtubule organization could be observed in *arl2* null mutants. A wild-type interphase neuroblast contained one major microtubule aster organized by the Centrosomin (CNN)-labeled centrosome (Fig. 21A, E; 100%, n=25). Strikingly, none of the interphase neuroblasts in *arl2*$^{\Delta 156}$ or *arl2*$^{\Delta 309}$ clones organized the microtubule aster (Fig. 21B, C, E; *arl2*$^{\Delta 156}$, n=34; *arl2*$^{\Delta 309}$, n=18), suggesting that Arl2 is critical for the formation of the interphase microtubule aster. In the wild-type metaphase neuroblast, the mitotic spindle is assembled with two centrosomes well separated and located at the two sides of the metaphase plate (Fig. 21F, J; 100%, n=13). None of the *arl2*$^{\Delta 156}$ or *arl2*$^{\Delta 309}$ metaphase neuroblast was able

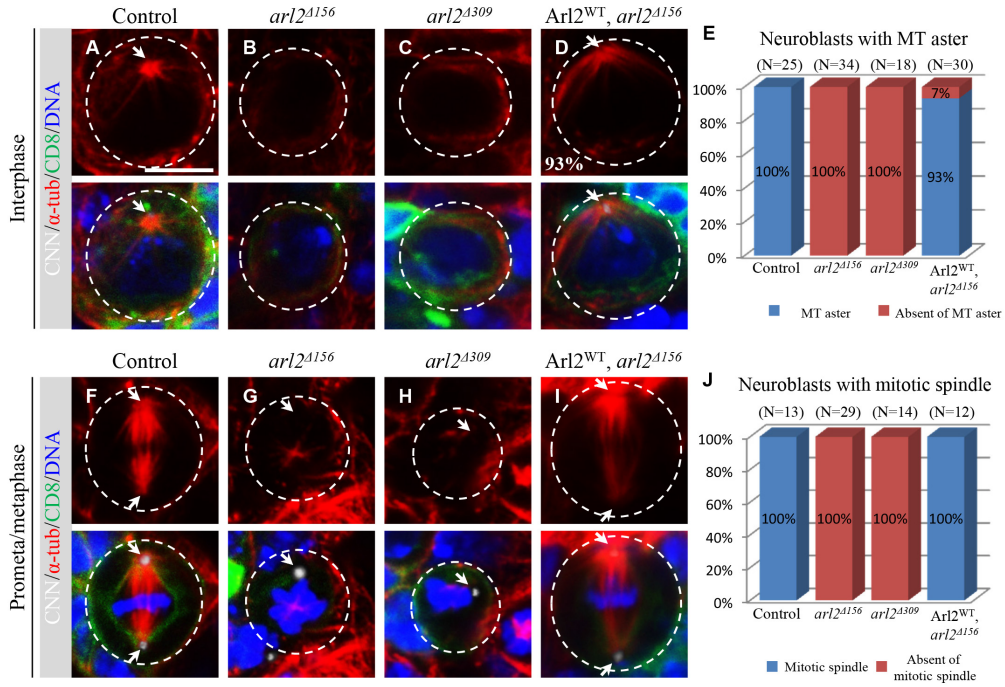

Figure 21. The formation of interphase microtubule asters and mitotic spindles is fully disrupted in *arl2* null mutant neuroblasts.
(A-D) Interphase neuroblasts in control (FRT82B) (A), *arl2*$^{\Delta 156}$ (B), *arl2*$^{\Delta 309}$ (C) and *arl2*$^{\Delta 156}$ with Arl2^{WT} overexpression (Arl2^{WT}, *arl2*$^{\Delta 156}$) (D) MARCM clones labeled for CNN, α-tubulin, CD8 and DNA. (E) Quantification of microtubule aster defects in (A-D). (F-I) Prometa/metaphase neuroblasts in control (FRT82B) (F), *arl2*$^{\Delta 156}$ (G), *arl2*$^{\Delta 309}$ (H) and Arl2^{WT}, *arl2*$^{\Delta 156}$ (I) MARCM clones labeled for CNN, α-tubulin, CD8 and DNA. (J) Quantification of mitotic spindle defects in (F-I). Scale bars, 5 μm.

to assemble the mitotic spindle (Fig. 21G, H, J; *arl2*$^{\Delta 156}$, n=29; *arl2*$^{\Delta 309}$, n=14). Interestingly, microtubules in *arl2* clones were not completely depleted, as residual microtubules labeled by α-tubulin were still found in interphase and mitotic neuroblasts in *arl2* clones (Fig. 21B, C, G, H). These microtubule abnormalities seen in *arl2*$^{\Delta 156}$ neuroblasts were rescued by Arl2^{WT} overexpression (93% in interphase, n=30; 100% in mitosis, n=12) (Fig. 21D, E, I, J). Similar microtubule defects were also observed in interphase and mitotic neuroblasts in *arl2*^{GS17851} MARCM clones (data not shown). Together, our results showed that Arl2 plays a central role in organizing both interphase microtubule asters and the mitotic spindle in neuroblasts.

Given that microtubule organization was disrupted in *arl2* loss of function, we asked whether overexpression of α-tubulin or β-tubulin could restore the microtubule defects in Arl2^{T30N}-expressing neuroblasts. We used a transgene of α-tubulin-GFP, which displayed microtubule asters during interphase and mitotic spindles during metaphase in control neuroblasts (Fig. 22A, C). Interestingly, when α-tubulin-GFP transgene was introduced in Arl2^{T30N}-expressing neuroblasts, the microtubule-localization was fully disrupted (Fig. 22B, D), despite similar expression levels of α- tubulin-GFP in control and Arl2^{T30N} brains (Fig. 22E). Similar defects were observed when a β-tubulin-Venus transgene was expressed in Arl2^{T30N} neuroblasts (Fig. 22F-K). Interestingly, compared to control, larval brains with different *arl2* loss-of-function conditions contained similar α-tubulin and β-tubulin protein levels (Fig. 29E, F), suggesting that microtubule growth, but not tubulin degradation, was likely affected under these conditions.

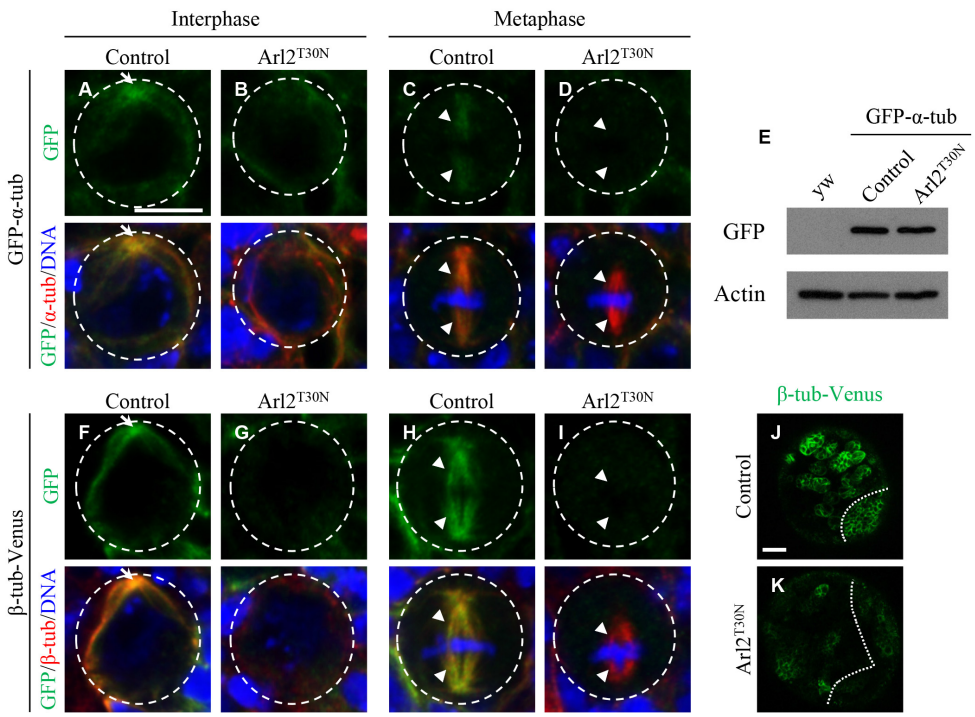

Figure 22. Microtubules are not properly assembled in Arl2^{T30N}-expressing neuroblasts.
(A-D) Interphase (A, B) and metaphase (C, D) neuroblasts from control (A, C) and Arl2^{T30N} (B, D) expressing GFP-α-tubulin labeled for GFP, α-tubulin and DNA. (E) Western blotting of GFP and Actin levels from larval brains of yw (1st lane), GFP- α-tubulin control (2nd lane) and GFP-α-tubulin with Arl2^{T30N} overexpression (3rd lane). (F-I) Interphase (F, G) and metaphase (H, I) neuroblasts from control (F, H) and Arl2^{T30N} (G, I) expressing β-tubulin-Venus labeled for GFP, β-tubulin and DNA. (J-K) Fluorescent signal of GFP in larval brains from control (J) and Arl2^{T30N} (K) expressing β-tubulin-Venus. Central brain is to the left of the white dotted line. The white dotted circles indicate the neuroblast contours, arrows indicate interphase microtubule asters, and arrowheads indicate mitotic spindles labeled by α-tubulin or β-tubulin in (A-D) and (F-I). Scale bars, 5 µm in (A-D) and (F-I), 20 µm in (J, K).

3.2.4 Loss of *arl2* results in defects in centriole biogenesis and recruitment of PCM proteins to the interphase centrosome

Severe centrosome defects were also found in *arl2* null mutants. In the wild-type interphase neuroblast, PCM proteins such as CNN were recruited to one of the centrosomes (Fig. 21A; n=25). In contrast, CNN was only observed in 9% or 11% of interphase *arl2*$^{\Delta 156}$ or *arl2*$^{\Delta 309}$ neuroblasts (Fig. 21B, C; *arl2*$^{\Delta 156}$, n=34; *arl2*$^{\Delta 309}$, n=18). Similarly, Aurora-A (AurA), Polo and Mini spindles

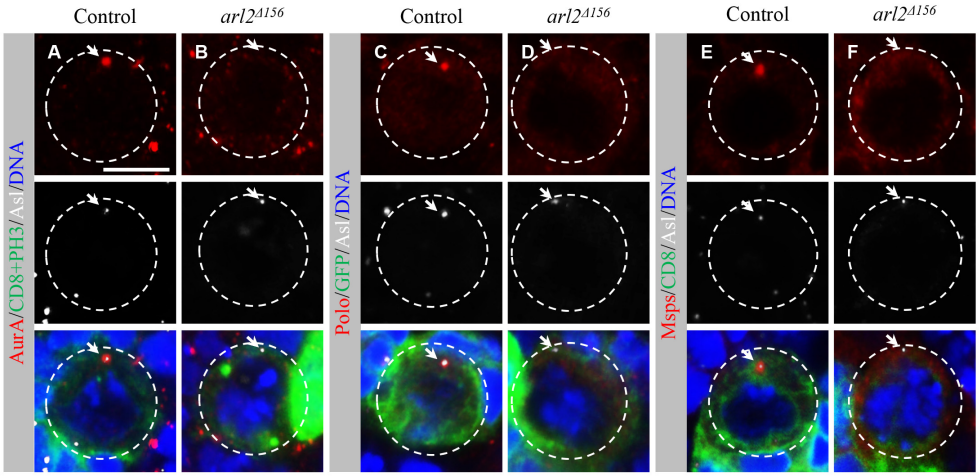

Figure 23. PCM proteins are not properly recruited to the centrosome in *arl2* interphase neuroblasts.
(A, B) Interphase neuroblasts in control (FRT82B) (A) and *arl2*$^{\Delta 156}$ (B) MARCM clones labeled for AurA, CD8, PH3, Asl and DNA. (C, D) Interphase neuroblasts in control (FRT82B) (C) and *arl2*$^{\Delta 156}$ (D) MARCM clones labeled for Polo, GFP, Asl and DNA. (E, F) Interphase neuroblasts in control (FRT82B) (E) and *arl2*$^{\Delta 156}$ (F) MARCM clones labeled for Msps, CD8, Asl and DNA. White dotted circles indicate the neuroblast contours, arrows indicate centrosomes. Scale bars, 5 μm.

(Msps) all failed to be recruited to the centrosomes in *arl2*$^{\Delta 156}$ interphase neuroblasts (Fig. 23).

Abnormal centrosome number in *arl2* null alleles may be a consequence of spindle abnormalities or a result of defects in centriole biogenesis. To assess whether Arl2 is required for centriole duplication, we labeled Asterless (Asl), a centriolar protein (Varmark et al., 2007), in wild-type and *arl2* mutant neuroblasts. In each control interphase neuroblast, there were two centrosomes marked by two Asl^{+} punctae (Fig. 24A; 100%, n=48) (Rebollo et al., 2007). However, 39% (n=38) of *arl2*$^{\Delta 156}$ interphase neuroblasts contained only one Asl^{+} puncta and 39% (n=38) of the mutant neuroblasts had no Asl^{+} centriole (Fig. 24B, B'). A similar phenotype was observed in *arl2*$^{\Delta 309}$ interphase neuroblasts, in which 45% neuroblasts were devoid of Asl^{+} centrioles and 32% contained only one Asl^{+} puncta (Fig. 24C, C'). The defect in centriole number seen in *arl2* null mutants could be fully restored when

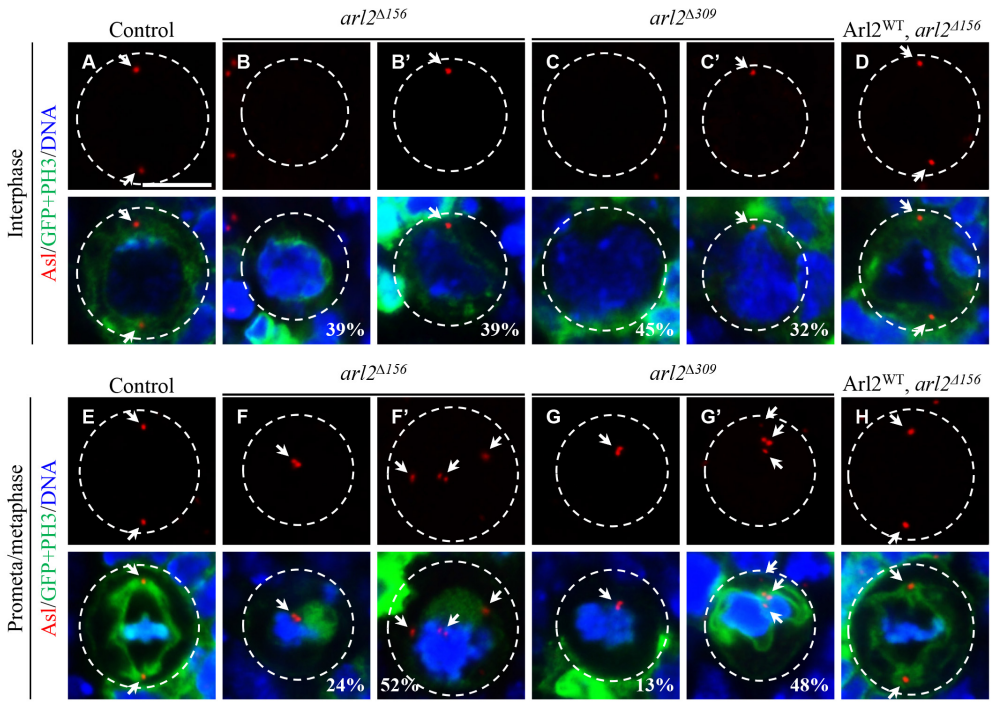

Figure 24. Centrosome biogenesis is disrupted in *arl2* null mutant neuroblasts.
Interphase (A-D) and prometa/metaphase (E-H) neuroblasts in control (FRT82B) (A, E), *arl2*$^{\Delta 156}$ (B, B', F, F'), *arl2*$^{\Delta 309}$ (C, C', G, G') and *arl2*$^{\Delta 156}$ with Arl2^{WT} overexpression (Arl2^{WT}, *arl2*$^{\Delta 156}$) (D, H) MARCM clones labeled for Asl, GFP, PH3 and DNA. Scale bars, 5 μm.

Arl2^{WT} transgene was introduced in the mutant background (Fig. 24D). These observations suggest that Arl2 is likely required for centriole biogenesis in neuroblasts.

In each wild-type mitotic neuroblast, the two pairs of centrioles were fully separated and localized to the two sides of cell (Fig. 24E; n=27). Surprisingly, in mitotic neuroblasts in *arl2* mutant clones, multiple centriole pairs were often observed (Fig. 24F', G'; *arl2*$^{\Delta 156}$: 52%, n=42; *arl2*$^{\Delta 309}$: 48%, n=38). Centrosome separation defects were also observed, as two or multiple centriole pairs that attached to each other were often seen in *arl2*$^{\Delta 156}$ (76%, n=42) and *arl2*$^{\Delta 309}$ (61%, n=38) clone mitotic neuroblasts (Fig. 24F-G'). We assumed that the phenotype of multiple centriole pairs in mitotic neuroblasts was due to failure of cell division in *arl2* mutant clone mitotic neuroblasts, thus

centriole pairs were accumulated in the cell. Further studies are needed to better understand the underlying mechanisms of Arl2 in regulating centriole duplication, centrosome function and microtubule organization.

3.2.5 Overactivation of Arl2 causes microtubule overgrowth and depletion of neuroblasts

We then determined the effect upon Arl2 overactivation in neuroblasts, by analyzing overexpression of $Arl2^{Q70L}$, a constitutively active GTP-bound form of Arl2. Surprisingly, overexpression of $Arl2^{Q70L}$ under *insc*-Gal4 driver resulted in a dramatic depletion of neuroblasts in central brains (Fig. 25A, B; control, 99±6, n=20; $Arl2^{Q70L}$, 53±12, n=24). Both type I and type II neuroblasts showed under-proliferation, as indicated by co-staining of Dpn and Ase in $Arl2^{Q70L}$-expressing brains (Fig. 25C, D). Consistently, the neuroblast in the type II neuroblast lineages was often lost when $Arl2^{Q70L}$ was expressed under *wor*-Gal4, *ase*-Gal80 induction (Fig. 25E-F'). By contrast, overexpression of $Arl2^{WT}$ did not alter neuroblast number (data not shown).

In $Arl2^{Q70L}$-expressing interphase and mitotic neuroblasts, microtubules were more abundant compared to in control neuroblasts (Fig. 26A-D). 52% of $Arl2^{Q70L}$-expressing neuroblasts formed monopolar spindles during mitosis (n=25), compared to control neuroblasts, all of which assembled bipolar spindles (Fig. 26C, D; n=25). In the microtubule-regrowth assay, after 30 s of recovery at 25°C, majority of $Arl2^{Q70L}$-expressing metaphase neuroblasts (Fig. 26J; 65%, n=17) nucleated more abundant microtubules from both centrosomes than control neuroblasts (Fig. 26F; n=30). Moreover, the distance between the two centrosomes in $Arl2^{Q70L}$-expressing neuroblasts (Fig. 26J; 7.44±2.01μm, n=14) was dramatically greater than in controls (Fig.

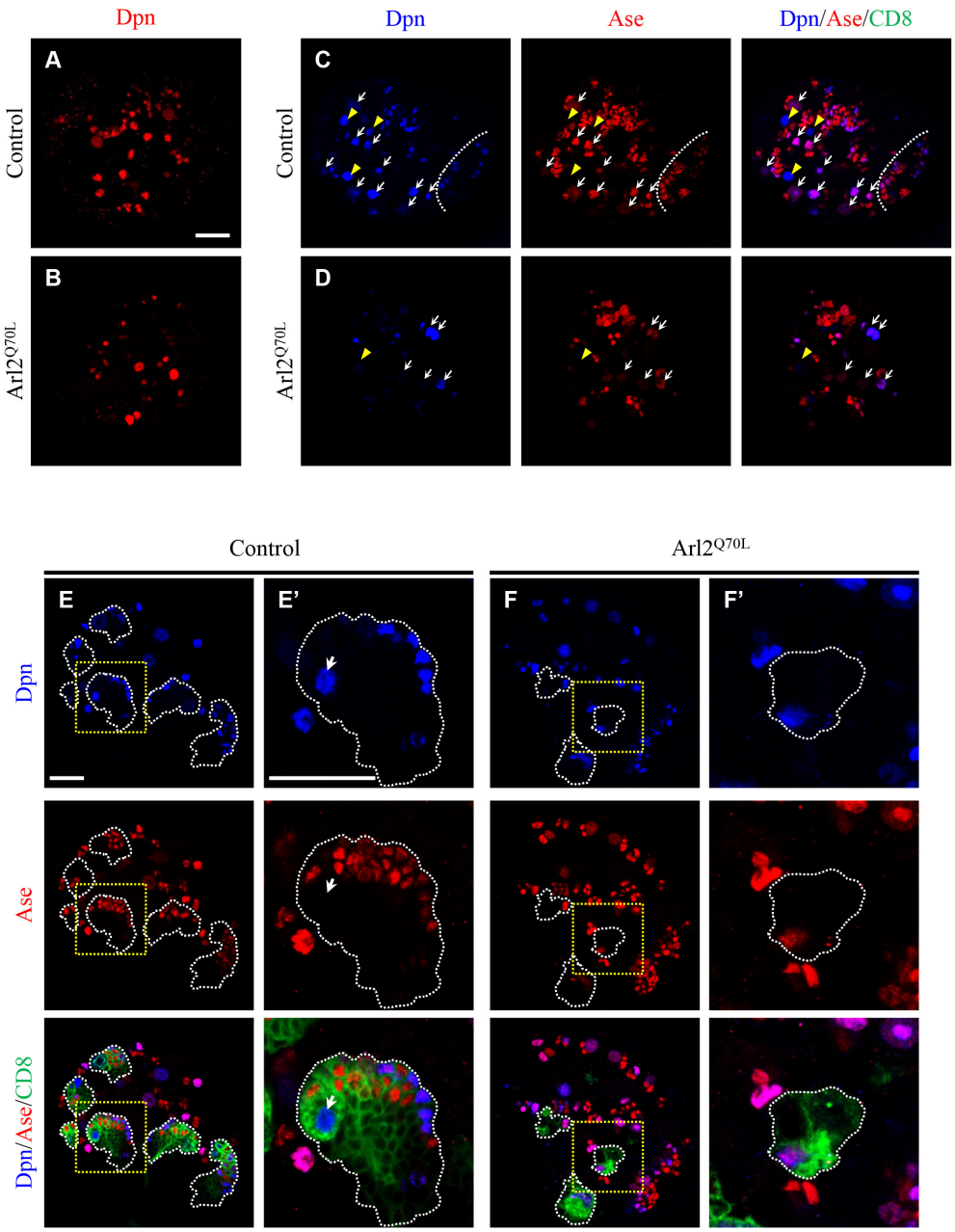

Figure 25. Overexpression of a constitutively active Arl2 (Arl2^{Q70L}) results in depletion of neuroblasts.
(A-D) Larval brains of control (A, C) and Arl2^{Q70L} overexpression (B, D) under *insc*-Gal4 labeled for Dpn (A, B), or co-labeled for Dpn and Ase (C, D). Central brain is to the left of the white dotted line. White arrows indicate type I neuroblasts and yellow arrowheads indicate type II neuroblasts in (C, D). (E-F') Larval brains of control (E) and Arl2^{Q70L} overexpression (F) under *wor*-Gal4, *ase*-Gal80 labeled for Dpn, Ase and CD8. Type II clones are indicated by white dotted lines, (E') and (F') are enlarged views of single type II neuroblast clones of (E) and (F). Scale bars, 20 μm.

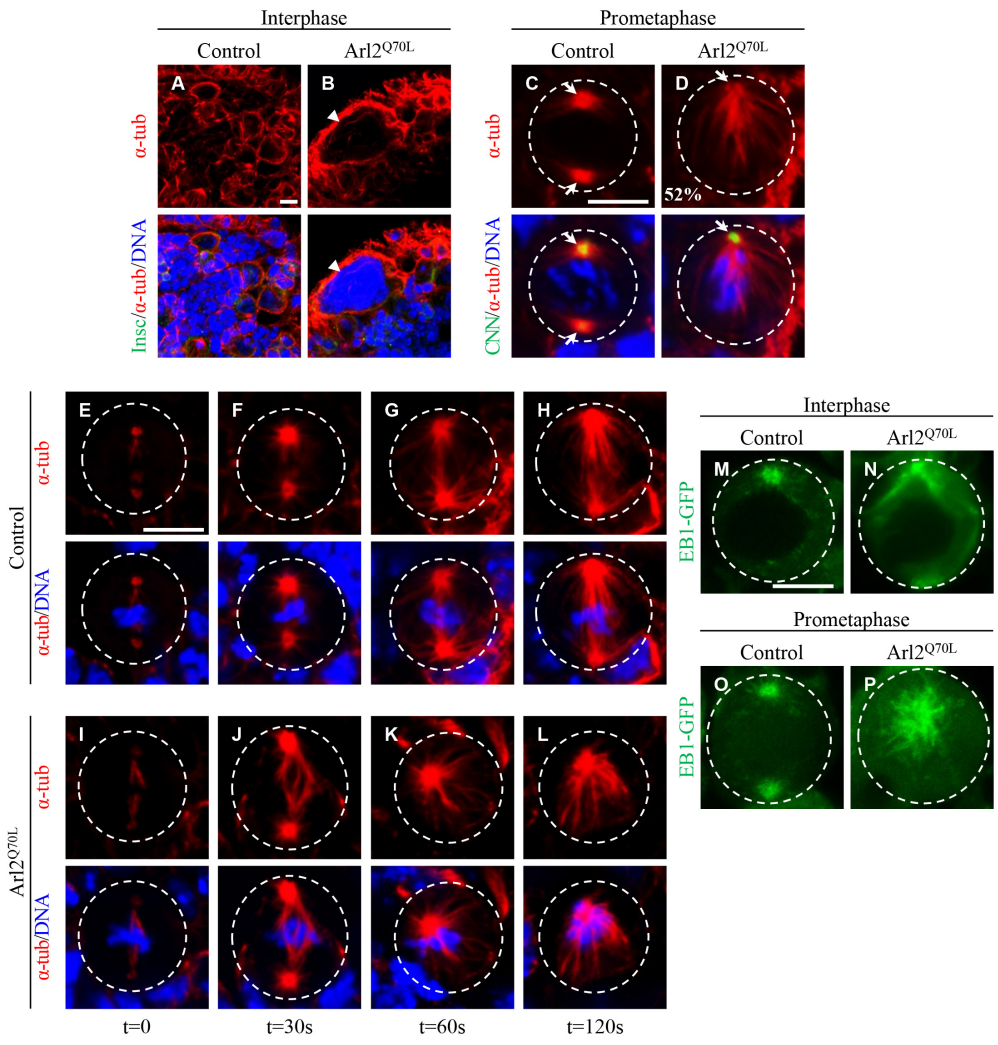

Figure 26. Overexpression of Arl2^{Q70L} causes microtubule overgrowth and severe mitotic defects.
(A, B) Control (A) and Arl2^{Q70L}-expressing (B) interphase neuroblasts labeled for Insc, α-tubulin and DNA. Arrowhead indicates the DNA mass. (C, D) Control (C) and Arl2^{Q70L}-expressing (D) prometaphase neuroblasts labeled for CNN, α-tubulin and DNA. Arrows indicate centrosomes. (E-L) α-tubulin and DNA staining in control (E-H) and Arl2^{Q70L}-expressing (I-L) metaphase neuroblasts from the microtubule regrowth assay. Times allowed for the recovery after ice treatment are indicated at lower panels. (M-P) Fluorescent signals of GFP in interphase (M, N) and prometaphase (O, P) neuroblasts of control (M, O) and Arl2^{Q70L} (N, P) expressing EB1-GFP. Cell outlines are indicated by the white dotted lines. Scale bars, 5 μm.

26F; 5.32±1.37μm, n=31), presumably due to the increased microtubule growth and forces between the two centrosomes. Interestingly, after 60s recovery, 64% (n=13) of Arl2^{Q70L}-expressing metaphase neuroblasts contained only one large centrosome located at the center of DNA mass.

After 120s recovery, this was observed in 88% (n=16) of metaphase neuroblasts in Arl2^{Q70L}-expressing brains (Fig. 26K, L). This data suggests that centrosomes in Arl2^{Q70L}-expressing neuroblasts initially tend to separate, but as centrosomal microtubules continued to overgrow, they were constrained by cell membranes and were pushed towards the center until they fuse together. We then examined the localization of EB1-GFP, which primarily binds to dynamic microtubule plus ends (Mimori-Kiyosue et al., 2000). In control neuroblasts, EB1-GFP showed punctate localization at microtubule plus ends. However, in Arl2^{Q70L}-expressing neuroblasts, stronger EB1-GFP signals were present along the microtubule length (Fig. 26M-P). In addition, Arl2^{Q70L} overexpression resulted in a defect in cytokinesis, as polyploidy cells with huge DNA mass were often observed in the central brains (Fig. 26B, arrowhead). These data suggest that Arl2 overactivation likely leads to overgrowth of microtubules and cell division defects, which may contribute to the depletion of neuroblasts.

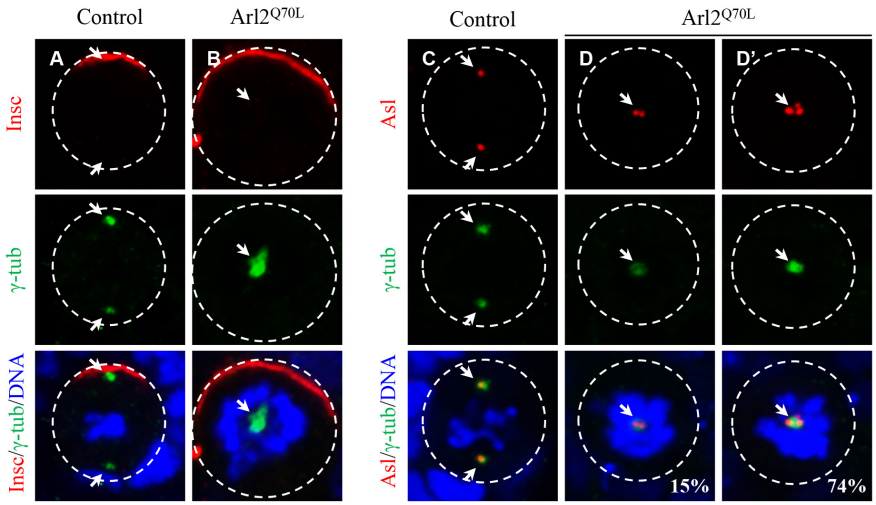

Figure 27. Excess amount of PCM proteins are recruited to the centrosomes in Arl2^{Q70L} mitotic neuroblasts.
(A, B) Control (A) and Arl2^{Q70L} (B) prometaphase neuroblasts labeled for Insc, γ-tubulin and DNA. (C-D') Control (C) and Arl2^{Q70L} (D, D') pro-metaphase neuroblasts labeled for Asl, γ-tubulin and DNA. Cell outlines are indicated by the white dotted lines. Arrows indicate the centrosomes. Scale bars, 5 μm.

The ability to nucleate larger amount of microtubule could be a result of increase PCM mass at the centrosome. Indeed, in Arl2^{Q70L}-expressing mitotic neuroblasts, larger amount of PCM was often observed (Fig. 27A, B). We then analyzed whether increased PCM amount at the centrosomes was due to over-duplication of centrioles upon Arl2 overactivation. Compared to control mitotic neuroblasts that contained two pairs of well-separated centrioles represented as two Asl positive punctate, 89% of Arl2^{Q70L}-expressing mitotic neuroblasts displayed abnormal centriolar clusters: they contained either two pairs or multiple pairs of centrioles that were clustered together (Fig. 27C-D'; control, n=27; Arl2^{Q70L}, n=34).

3.2.6 Arl2 and Tubulin Binding Co-factors function together to regulate microtubule growth and asymmetric division in neuroblasts

The human Arl2 homologue associates with TBCD, a tubulin binding co-factor (Bhamidipati et al., 2000). We tested whether *Drosophila* Arl2 binds to TBCD. Co-immunoprecipitation of FLAG-TBCD and Arl2-Venus was observed, confirming that Arl2 and TBCD physically associate with each other (Fig. 28A). Interestingly, we observed similar levels of TBCD associated with Arl2^{T30N}-Venus and Arl2^{Q70L}-Venus, suggesting that TBCD can tightly bind to both active and inactive forms of Arl2 (Fig. 28B). Moreover, co-immunoprecipitation of Myc-β-tubulin and Myc-α-tubulin with Arl2-Venus was detected (Fig. 28C, D). Interestingly, both β-tubulin and α-tubulin preferentially bind to Arl2-GDP than to Arl2-GTP, as higher amounts of Myc-β-tubulin and Myc-α-tubulin were associated with Arl2^{T30N}-Venus (Fig. 28C, D).

Consistently, Arl2 also physically associated with two other tubulin cofactors, TBCC (encoded by CG31961) and TBCE (encoded by CG7861)

(Fig. 29A, C). The fission yeast cofactor C, Tbc1, is associated with Arl2/Alp41 and acts as a GTPase- activating protein (GAP) for Arl2 (Mori and Toda, 2013). We detected a significantly higher amount of TBCC associated with Arl2^{Q70L}-Venus (by ~9.6-fold) than with Arl2^{T30N}-Venus (Fig. 29B). Therefore, *Drosophila* TBCC specifically binds to Arl2-GTP and may act as a GAP for Arl2. In contrast, a much higher level of TBCE was co-immunoprecipitated with Arl2^{T30N}-Venus (by ~3.1-fold fold) than that with

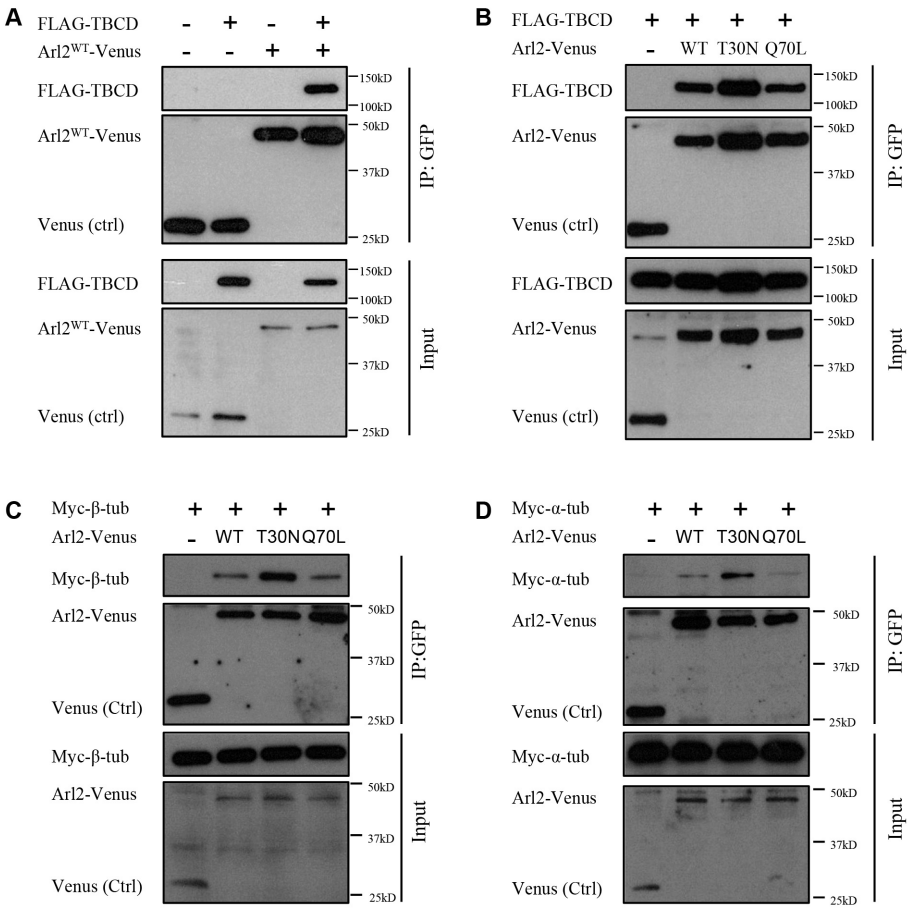

Figure 28. Arl2 physically interacts with TBCD, α-tub and β-tub.
(A) Co-immunoprecipitation (Co-IP) of S2 cells co-expressing Arl2^{WT}-Venus with FLAG-TBCD. Controls are either Venus or FLAG alone. (B) Co-IP of S2 cells co-expressing different forms of Arl2-Venus with FLAG-TBCD. Control is Venus and FLAG-TBCD. (C, D) Co-IP of S2 cells co-expressing different forms of Arl2-Venus with Myc-β-tub (C) or Myc-α-tub (D). Controls are Venus with Myc-β-tub (C) or Myc-α-tub (D). Immunoprecipitation was performed using anti-GFP antibodies, which recognized Venus. Western blotting was performed using anti-GFP, anti-FLAG and anti-Myc antibodies.

Arl2^{Q70L}-Venus (Fig. 29D), suggesting that TBCE preferentially binds to Arl2-GDP. Our data suggests that Arl2 forms complexes with tubulin cofactors C, D and E. Arl2 may interact with different cofactors sequentially, as each

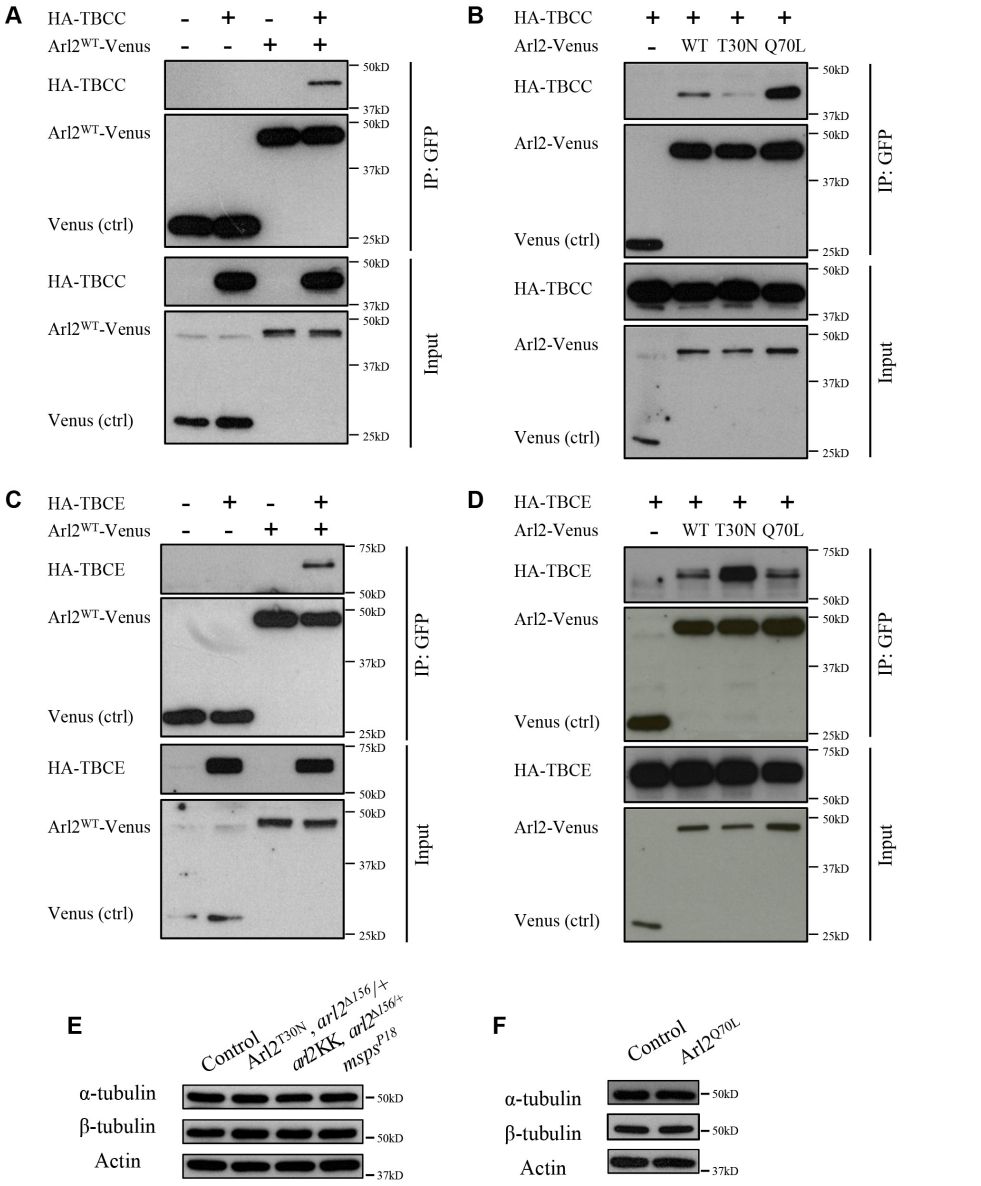

Figure 29. Arl2 physically interacts with TBCC and TBCE.
(A-D) Co-immunoprecipitation (Co-IP) of S2 cells co-expressing Arl2^{WT}-Venus with HA-TBCC (A) or HA-TBCE (C), different forms of Arl2-Venus with HA-TBCC (B) or HA-TBCE (D). Controls are either Venus or HA alone. Immunoprecipitation was performed using anti-GFP antibodies, which recognized Venus. Western blotting was performed using anti-GFP and anti-HA antibodies. (E, F) Western blotting of α-tub, β-tub and Actin levels from larval brains of control (1st lane), Arl2^{T30N}, *arl2*$^{\Delta 156}$*/+* (2nd lane), *arl2* KK, *arl2*$^{\Delta 156}$*/+* (3rd lane) and *msps*^{P18} (4th lane) (E), and from larval brains of control (1st lane) and Arl2^{Q70L} (2nd lane) (F).

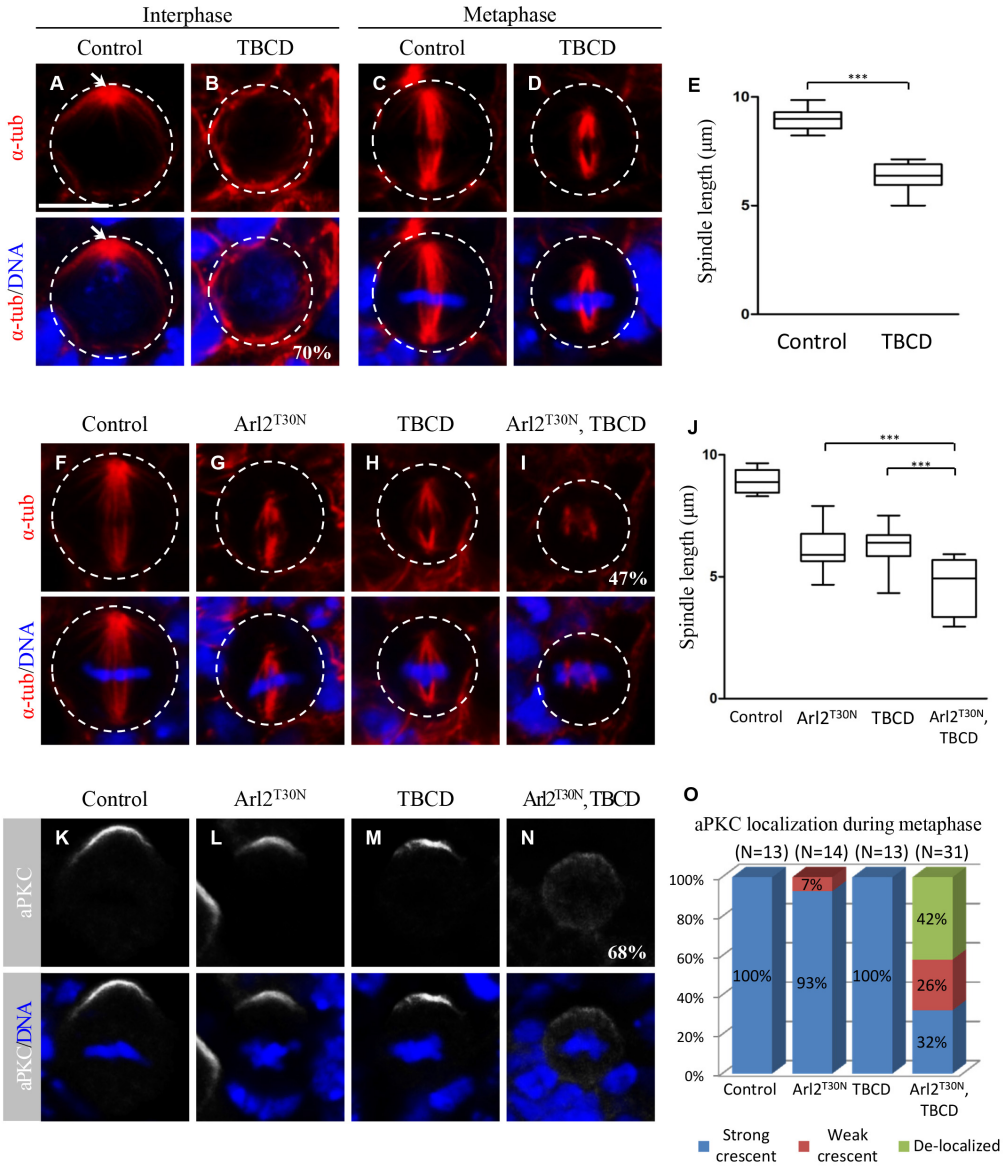

Figure 30. Co-expression of TBCD with Arl2^{T30N} disrupts mitotic spindle formation and cell polarity in metaphase neuroblasts.
(A-D) Interphase (A, B) and metaphase (C, D) neuroblasts of control (A, C) and TBCD overexpression (TBCD) (B, D) labeled for α-tubulin and DNA. (E) Quantification of spindle length in (C, D). (F-I) Metaphase neuroblasts of control (A), Arl2^{T30N} (B), TBCD (C) and Arl2^{T30N}, TBCD co-expression (D) labeled for α-tubulin and DNA. (J) Quantification of spindle length in (F-I). (K-N) Metaphase neuroblasts of control (G), Arl2^{T30N} (H), TBCD (I), and Arl2^{T30N}, TBCD co-expression (J) labeled for aPKC and DNA. (O) Quantification of aPKC localization in (K-N). UAS-CD8-GFP was introduced in controls to balance the number of UAS elements in (F-I) and (K-N). The white dotted circles label the cell outlines. Scale bars, 5μm. *** indicates P <0.001.

cofactor exhibits different preference to GTP- or GDP-bound form of Arl2. Western blotting results showed that in different *arl2* loss-of-function or over-activation conditions, the protein levels of α-tubulin and β-tubulin were not affected (Fig. 29E, F).

To ascertain whether excess TBCD can cause defects in microtubule growth, as shown for its mammalian orthologues (Bhamidipati et al., 2000), we overexpressed a TBCD transgene in neuroblasts. Notably, microtubule aster was absent in 70% of interphase neuroblasts (Fig. 30B, n=33) with overexpression of *Drosophila* TBCD under *insc*-Gal4 driver, suggesting a significant disruption of microtubule growth. In addition, during metaphase, TBCD-overexpressing neuroblasts assembled shorter mitotic spindles (Fig. 30C, D, E; control: 8.99±0.49μm, n=14; O/E TBCD: 6.37±0.57μm, n=20).

Mammalian Arl2-GDP sequesters TBCD, as Arl2-GDP can suppress microtubule defects caused by TBCD overexpression (Bhamidipati et al., 2000). Surprisingly, when $Arl2^{T30N}$ and TBCD were co-overexpressed in neuroblasts, a much more severe microtubule growth defect was observed: 53% (n=34) of metaphase neuroblasts formed shorter spindles (4.62±1.12 μm, n=14) and others (47%, n=34) were unable to assemble bipolar spindle (Fig. 30F-J). This suggests that defects in microtubule growth caused by overexpression of *Drosophila* $Arl2^{T30N}$ are not primarily attributed to sequestering TBCD, and GDP-bound Arl2 may represent the inactive form. The cortical polarity of aPKC was disrupted upon co-expression of $Arl2^{T30N}$ with TBCD in metaphase neuroblasts (Fig. 30N, O; 42%, n=31), compared to $Arl2^{T30N}$ or TBCD overexpression alone when aPKC polarity was not obviously affected (Fig. 30K-O; $Arl2^{T30N}$: n=14; TBCD: n=13).

Moreover, TBCD overexpression in $arl2^{\Delta 156}$ heterozygous background (TBCD $arl2^{\Delta 156}/+$) resulted in a more severe microtubule growth defect: 42%

(n=33) of metaphase neuroblasts failed to form bipolar spindles and the rest assembled severely shortened spindles (Fig. 31C, C', D; 4.41±0.82 μm, n=15). As a control, bipolar spindles (6.61±1.23μm, n=15) were still formed in all metaphase neuroblasts with TBCD overexpression alone (Fig. 31B, D; n=15). Furthermore, 60% (n=32) TBCD *arl2*$^{\Delta 156}$/+ metaphase neuroblasts

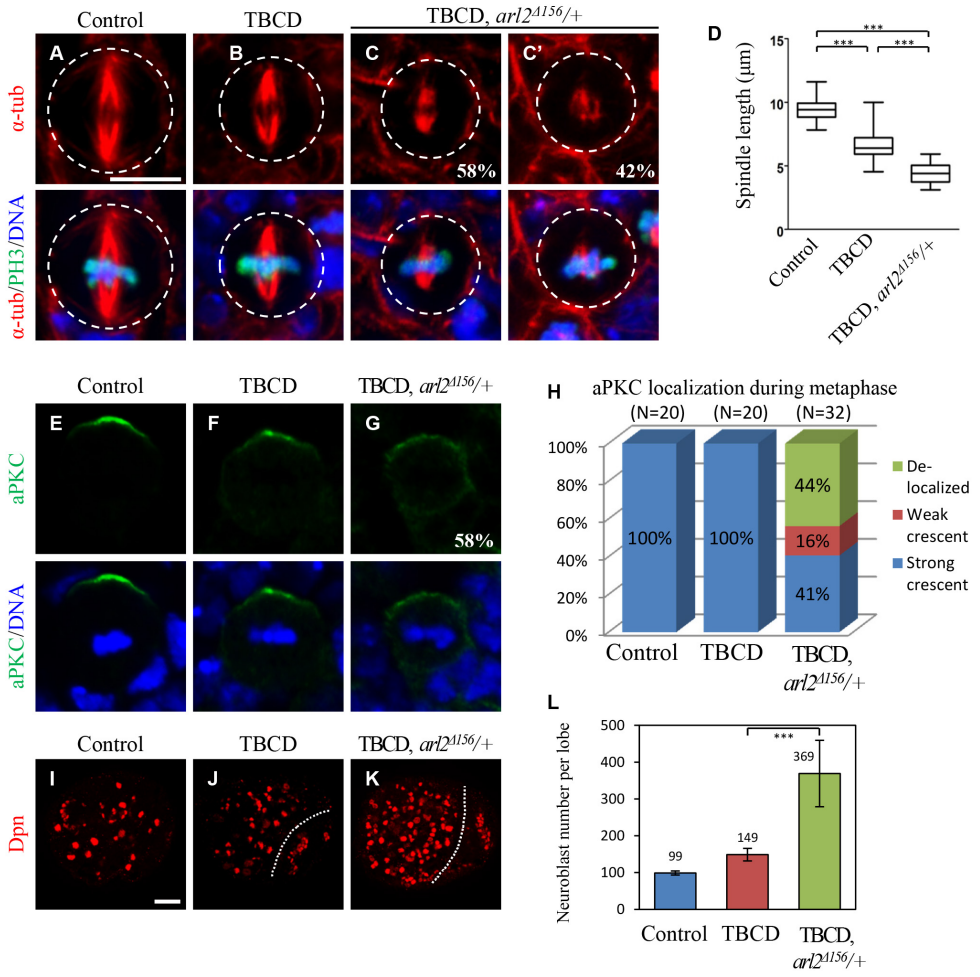

Figure 31. *arl2* heterozygosity enhances the microtubule abnormalities and asymmetric division defects in TBCD overexpression.
(A-C') Metaphase neuroblasts of control (A), TBCD overexpression (TBCD) (B), and TBCD O/E in *arl2*$^{\Delta 156}$ heterozygous background (TBCD, *arl2*$^{\Delta 156}$/+) (C, C') labeled for α-tubulin, PH3 and DNA. The white dotted circles label the cell outlines. (D) Quantification of spindle length in (A-C). (E-G) Metaphase neuroblasts of control (E), TBCD (F), and TBCD, *arl2*$^{\Delta 156}$/+ (G) labeled for aPKC and DNA. (H) Quantification of aPKC localization in (E-G). (I-K) Larval brains of control (I), TBCD (J), and TBCD, *arl2*$^{\Delta 156}$/+ (K) labeled for Dpn. Central brain is to the left of the white dotted line. (L) Quantification of neuroblast number in (I-K). Mean and SD are shown. Scale bars, 5μm in (A-C') and (E-G), 20μm in (I-K). *** indicates P <0.001.

failed to form a strong aPKC crescent at the apical cortex (Fig. 31G, H). TBCD *arl2*$^{\Delta 156}$/+ displayed neuroblast overgrowth in 54% of brains (Fig. 31K, L; n=24), with 369±90 (n=13) neuroblasts in each brain hemisphere, while TBCD overexpression alone only caused a very mild neuroblast overgrowth (Fig. 31J, L; 149±17, n=18) compared to wild-type (Fig. 31I, L; 99±5, n=20). These data indicate that Arl2 and TBCD function together to regulate microtubule growth, neuroblast polarity and self-renewal.

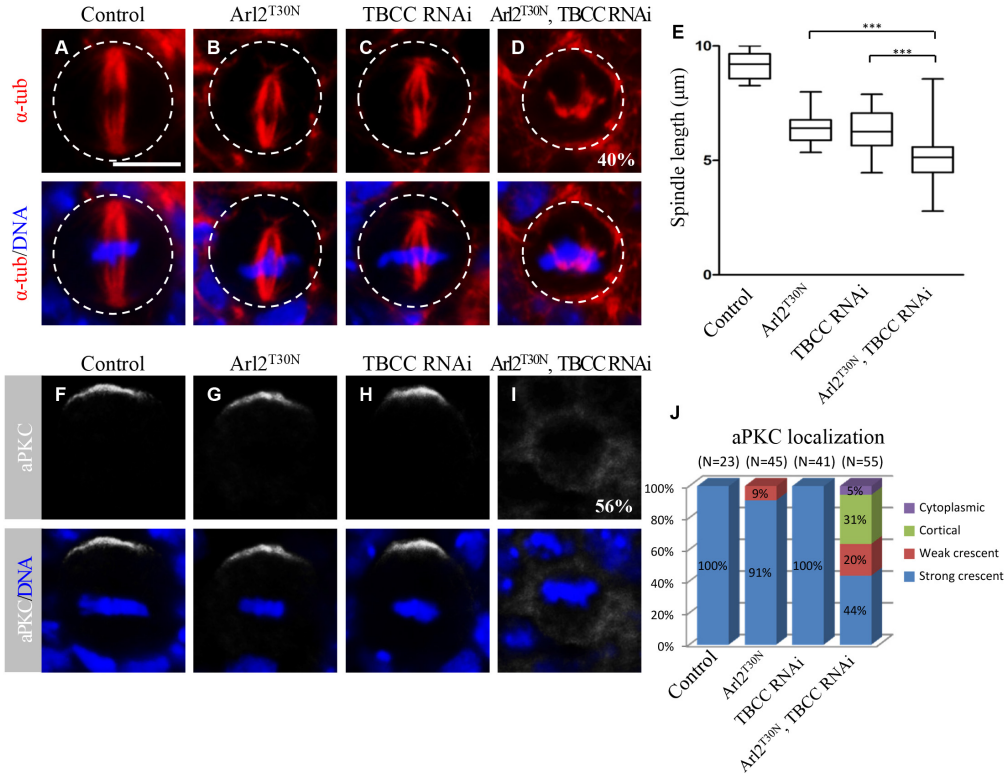

Figure 32. Knockdown of TBCC in Arl2^{T30N}-expressing neuroblasts disrupts mitotic spindle formation and cell polarity in metaphase neuroblasts.
(A-D) Metaphase neuroblasts of control (A), Arl2^{T30N} (B), TBCC RNAi (C), and TBCC RNAi with Arl2^{T30N} co-expression (D) labeled for α-tubulin and DNA. (E) Quantification of spindle length in (A-D). (F-I) Metaphase neuroblasts of control (F), Arl2^{T30N} (G), TBCC RNAi (H), and TBCC RNAi with Arl2^{T30N} co-expression (I) labeled with aPKC and DNA. (J) Quantification of aPKC localization in (E-H). UAS-CD8-GFP was introduced in controls to balance the number of UAS elements. The white dotted circles label the cell outlines. Scale bars, 5μm. *** indicates P <0.001.

Arl2 also interacts genetically with TBCC. Knockdown of TBCC in neuroblasts displayed mild defects of microtubule growth: shorter mitotic spindles were assembled during metaphase (Fig. 32C, E; 6.25±0.86, n=35), similar to what was seen upon $Arl2^{T30N}$ overexpression alone (Fig. 32B, E; 6.40±0.59μm, n=33). Notably, knockdown of TBCC in $Arl2^{T30N}$-expressing brains resulted in disruption of bipolar spindles in 40% of metaphase neuroblasts (Fig. 32D), and the remaining 60% of metaphase neuroblasts assembled even shorter spindles (Fig. 32E; 5.24±1.38μm; n=30). Overexpression of $Arl2^{T30N}$, or knockdown of TBCC alone did not cause obvious defects in aPKC asymmetric localization (Fig. 32G, H, J). However, when TBCC RNAi and $Arl2^{T30N}$ were co-expressed in neuroblasts, aPKC localization was disrupted in 56% (n=55) of metaphase neuroblasts (Fig. 32I, J). Together, we conclude that Arl2 functions together with tubulin binding co-factors to regulate microtubule organization and neuroblast asymmetric divisions.

3.2.7 Mini Spindles (Msps) regulates neuroblast asymmetric division and self-renewal

The phenotype of shorter mitotic spindles in *arl2* loss of function resembled what was reported previously for loss of *mini spindles (msps)*. Msps belongs to the XMAP215/ch-TOG family, which binds to microtubules and promotes microtubule polymerization (Lee et al., 2001). In a new *msps* allele ($msps^{P18}$) isolated from our lab, a nonsense mutation was found in the *msps* coding region and a truncated Msps protein which prematurely stops at Q1349 was generated (Koe CT and Wang H; Fig. 33E). Compared to wild-type brains that contained 99±7 neuroblasts in each brain hemisphere (Fig. 33A, F; n=21),

there were 296±50 in *msps*^{P18} (Fig. 33B, F; n=26). Similarly, neuroblast overgrowth was observed in trans-heterozygous mutant brains between *msps*^{P18} and *msps*^{P} (*msps*$^{P18/P}$), in which *msps*^{P} was a known loss-of-function *msps* allele (Cullen et al., 1999) (Fig. 33C, F; 303±47, n=26). The neuroblast overgrowth in larval central brains was fully rescued when an Msps-FL transgene was introduced in *msps*^{P18} mutants (Fig. 33D, F; 97±7, n=20). Loss of *msps* also resulted in increased proliferating cells in the brain labeled by EdU (Fig. 33G-I). To determine whether Msps regulates self-renewal of both type I and type II neuroblasts, we generated *msps*^{P18} MARCM clones. Ectopic

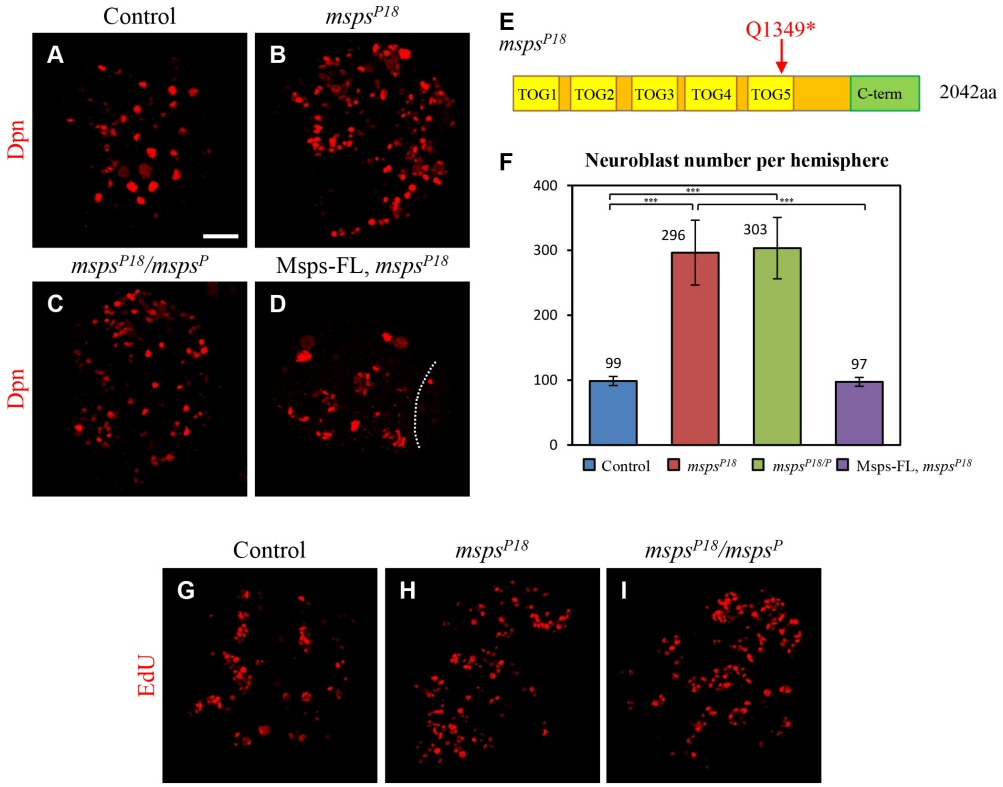

Figure 33. Loss of *msps* causes neuroblast overproliferation.
(A-D) Larval brains from control (A), *msps*^{P18} (B), *msps*$^{P18/P}$ (C) and *msps*^{P18} with Msps-FL overexpression (Msps-FL, *msps*^{P18}) (D) labeled for Dpn. Central brain is to the left of the white dotted line. (E) A schematic diagram of *msps* mutation in *msps*^{P18}. (F) Quantification of the neuroblast number per brain hemisphere for (A-D). Mean and SD are shown. *** indicates P <0.001. (G-I) Larval brains from control (G), *msps*^{P18} (H) and *msps*$^{P18/P}$ (I) labeled for EdU. Scale bars, 20 μm.

neuroblasts were found in both types of neuroblast lineages in *msps*^{P18} clones (Fig. 34A-D). Consistently, knockdown of Msps in either type I or type II lineage using *ase*-Gal4 or *wor*-Gal4, *ase*-Gal80 also caused neuroblast overgrowth (Fig. 34E-H). These data suggest that Msps is required in both neuroblast lineages to prevent the formation of ectopic neuroblasts.

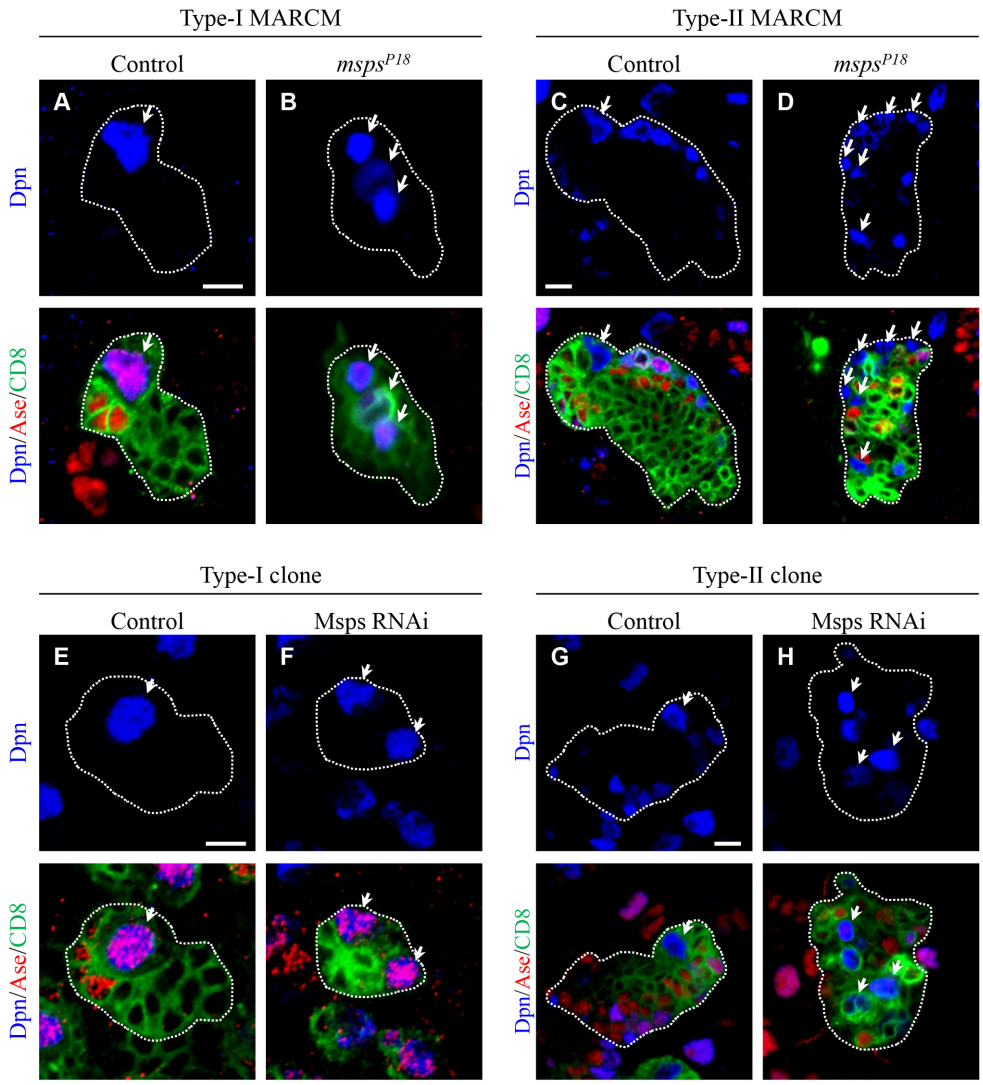

Figure 34. Msps inhibits neuroblast overgrowth in both type I and type II lineages.
(A-D) Control (A, C) and *msps*^{P18} (B, D) type I (A, B) and type II (C, D) MARCM clones labeled for Dpn, Ase and CD8. (E-H) Control (E, G) and *msps* RNAi (F, H) under the control of *ase*-Gal4 (E, F), or *wor*-Gal4, *ase*-Gal80 (G, H) labeled for Dpn, Ase and CD8. The neuroblast lineages are labeled by CD8-GFP and are indicated by white dotted lines. Arrows indicate neuroblasts. Scale bars, 5 μm.

In *msps*^{P18} and *msps*$^{P18/P}$ mutant brains, more than 70% of metaphase neuroblasts displayed random alignment of the mitotic spindles with respect to apico-basal polarity, whereas most wild-type neuroblasts properly aligned their spindle relative to the Insc crescent (Fig. 35B, C). Notably, around

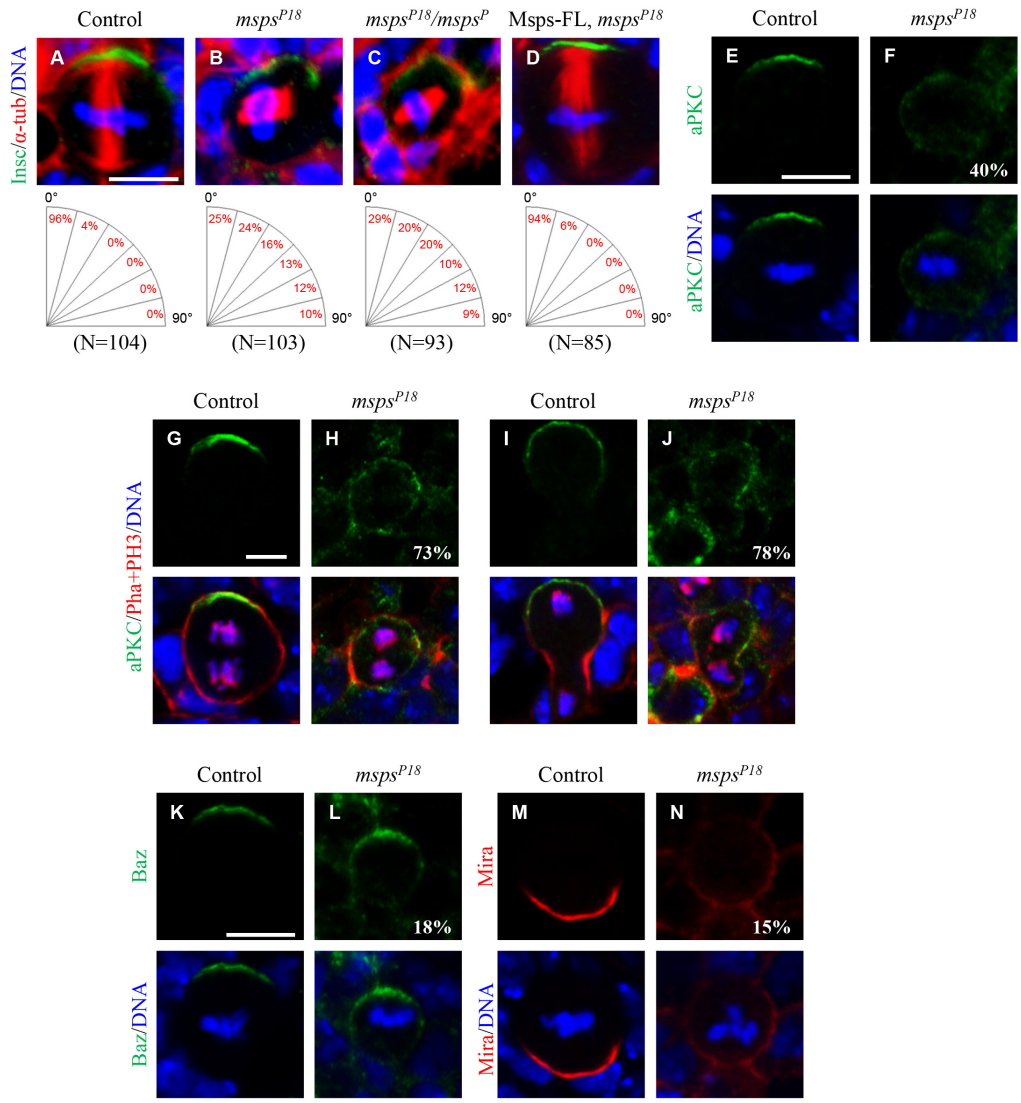

Figure 35. Loss of *msps* results in defects in neuroblast asymmetric division.
(A-D) Metaphase neuroblasts of control (A), *msps*^{P18} (B) and *msps*$^{P18/P}$ (C) and *msps*^{P18} with Msps-FL overexpression (Msps-FL, *msps*^{P18}) (D) labeled with Insc, α-tubulin and DNA. Quantification of spindle orientation is shown in lower panels. (E, F) Metaphase neuroblasts of control (E) and *msps*^{P18} (F) labeled for aPKC and DNA. (G-J) Anaphase (G, H) and telophase (I, J) neuroblasts of control (G, I) and *msps*^{P18} (H, J) labeled for aPKC, Phalloidin (Pha), PH3 and DNA. (K-N) Metaphase neuroblasts of control (K, M), *msps*^{P18} (L, N) labeled for Baz (K, L) or Mira (M, N). DNA was labeled by Topro-3 staining. Scale bars, 5 μm.

10% of neuroblasts in *msps*^{P18} and *msps*$^{P18/P}$ showed orthogonal division (Fig. 35B, C). This phenotype was largely restored by overexpression of Msps-FL (Fig. 35D), suggesting that Msps regulates spindle orientation. Cell polarity was also disrupted in *msps*^{P18} neuroblasts. Compared to wild-type neuroblasts that localized aPKC at the apical cortex (Fig. 35E; n=30), 40% of *msps*^{P18} metaphase neuroblasts failed to localize aPKC asymmetrically (Fig. 35F; n=40). The defects in aPKC localization were also found in anaphase and telophase neuroblasts in *msps*^{P18}. Compared to control anaphase (n=20) and telophase (n=57) that segregated aPKC to the neuroblast daughter cells, aPKC was mis-segregated to both daughter cells in 73% of anaphase (n=17) and 78% of telophase (n=23) neuroblasts in *msps*^{P18} (Fig. 35G-J). Similarly, Baz localization was disrupted in 18% of metaphase neuroblasts in *msps*^{P18} (Fig. 35K, L; control, n=15; *msps*^{P18}, n=55). In addition, the basal localization of Mira was also disrupted in 15% of metaphase neuroblasts in *msps*^{P18} (Fig. 35M, N; control, n=44; *msps*^{P18}, n=85). Taken together, Msps is essential for both neuroblast polarity and spindle orientation.

3.2.8 Arl2 functions together with TBCD to regulate the centrosomal localization of D-TACC and Msps

We then determined whether Arl2 is required for Msps localization in neuroblasts. Consistent with previous reports (Cullen et al., 1999), in wild-type neuroblasts Msps was co-localized with γ-tubulin on the centrosome during interphase (Fig. 36A; 100%, n=20), and was concentrated at centrosomes and weakly labeled along the mitotic spindle during metaphase (Fig. 36D; 100%, n=35). However, upon Arl2^{T30N} overexpression, Msps was absent from the centrosome(s) in 51% of neuroblasts during interphase (Fig. 36B; n=31) and 72% of neuroblasts during metaphase (Fig. 36E; n=32).

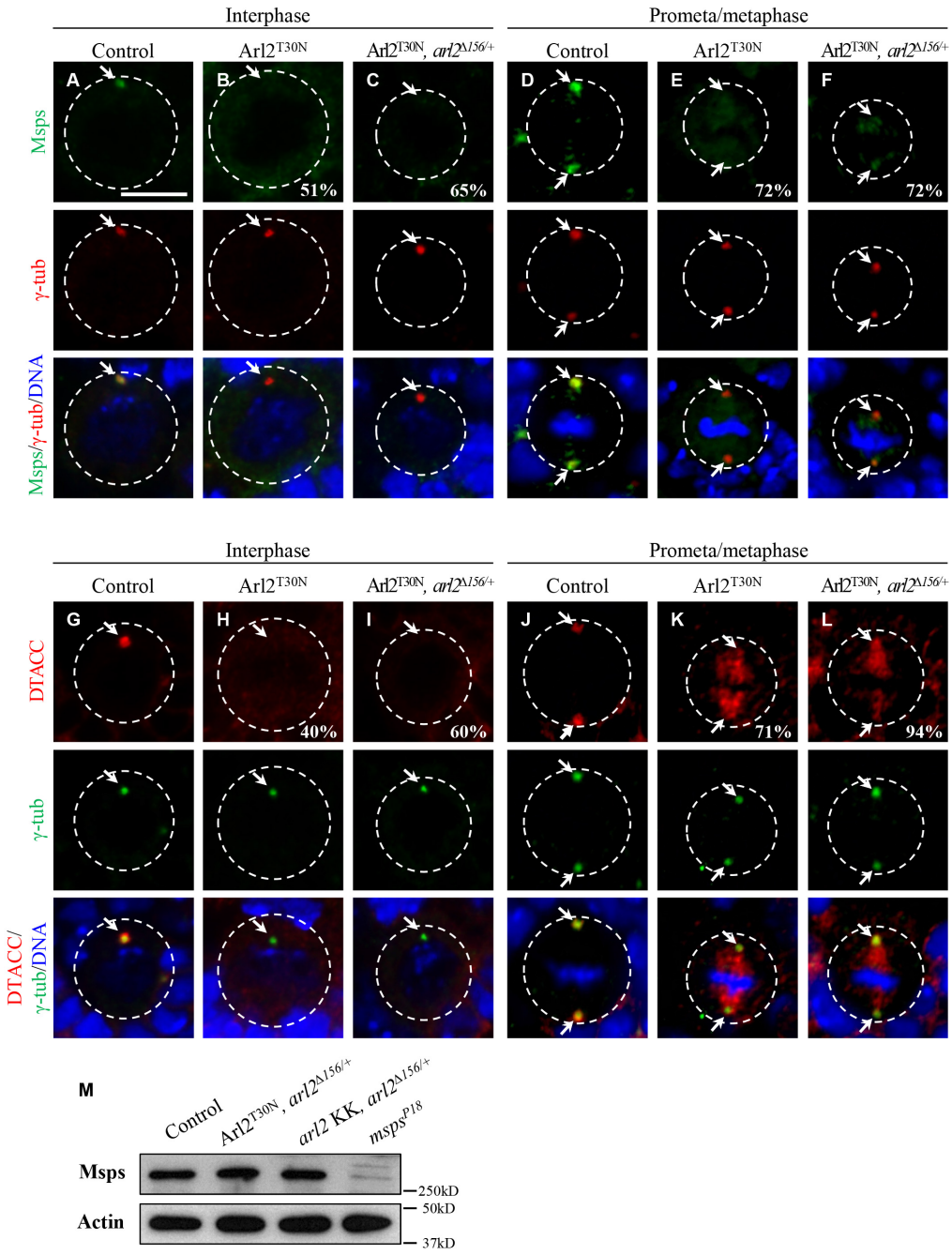

Figure 36. The centrosomal localization of Msps and D-TACC is disrupted in Arl2^{T30N}-expressing neuroblasts.

(A-F) Interphase (A-C) and metaphase (D-F) neuroblasts from control (A, D), Arl2^{T30N} (B, E) and Arl2^{T30N}, *arl2*$^{\Delta 156}$/+ (C, F) labeled for Msps, γ-tubulin and DNA. (G-L) Interphase (G-I) and metaphase (J-L) neuroblasts from control (G, J), Arl2^{T30N} (H, K) and Arl2^{T30N}, *arl2*$^{\Delta 156}$/+ (I, L) labeled for D-TACC, γ-tubulin and DNA. (M) Western blotting of Msps and Actin levels from larval brains of control (1st lane), Arl2^{T30N}, *arl2*$^{\Delta 156}$/+ (2nd lane), *arl2* KK, *arl2*$^{\Delta 156}$/+ (3rd lane) and *msps*^{P18} (4th lane). The white dotted circles label the cell outlines. Arrows indicate the centrosomes. Scale bars, 5μm.

Similarly, in Arl2^{T30N}, *arl2$^{\Delta 156}$/+*, Msps was delocalized from the centrosomes in both interphase (Fig. 36C; 65%, n=34) and metaphase (Fig. 36F; 72%, n=51). In these neuroblasts, γ-tubulin was still properly localized at the centrosomes (Fig. 36B, C, E, F), suggesting a specific requirement for Msps localization in these *arl2* loss-of-function conditions. Msps protein levels remained the same in Arl2^{T30N}, *arl2$^{\Delta 156}$/+* and *arl2* knockdown with *arl2$^{\Delta 156/+}$* (Fig. 36M).

The efficient centrosomal localization of Msps relies on D-TACC, a microtubule-binding centrosomal protein (Lee et al., 2001). We then examined whether Arl2 is required for D-TACC localization on centrosomes. In control neuroblasts D-TACC was mainly concentrated at the centrosomes (Fig. 36G, J) in both interphase and metaphase. However, D-TACC was de-localized from the centrosomes in 40% of Arl2^{T30N}-expressing neuroblasts during interphase (Fig. 36H, n=20). In metaphase Arl2^{T30N} neuroblasts, centrosomal localization of D-TACC was dramatically reduced and accumulated strongly along the spindles (Fig. 36K; 71%, n=28). Likewise, D-TACC was strongly reduced at centrosomes in Arl2^{T30N}, *arl2$^{\Delta 156}$/+* neuroblasts in interphase (Fig. 36I; 60%, n=15) and metaphase (Fig. 36L; 94%, n=31). Together, Arl2 is required for the centrosomal localization of D-TACC and Msps.

Overexpression of TBCD also disrupted the proper localization of D-TACC and Msps in neuroblasts, and this defect could be efficiently enhanced in *arl2$^{\Delta 156}$/+* background. Remarkably, during interphase, D-TACC localization was disrupted in 90% (n=32) TBCD *arl2$^{\Delta 156}$/+* neuroblasts, compared to 46% (n=52) of delocalization in TBCD overexpression alone (Fig. 37B, C). Similarly, during metaphase, D-TACC delocalization was

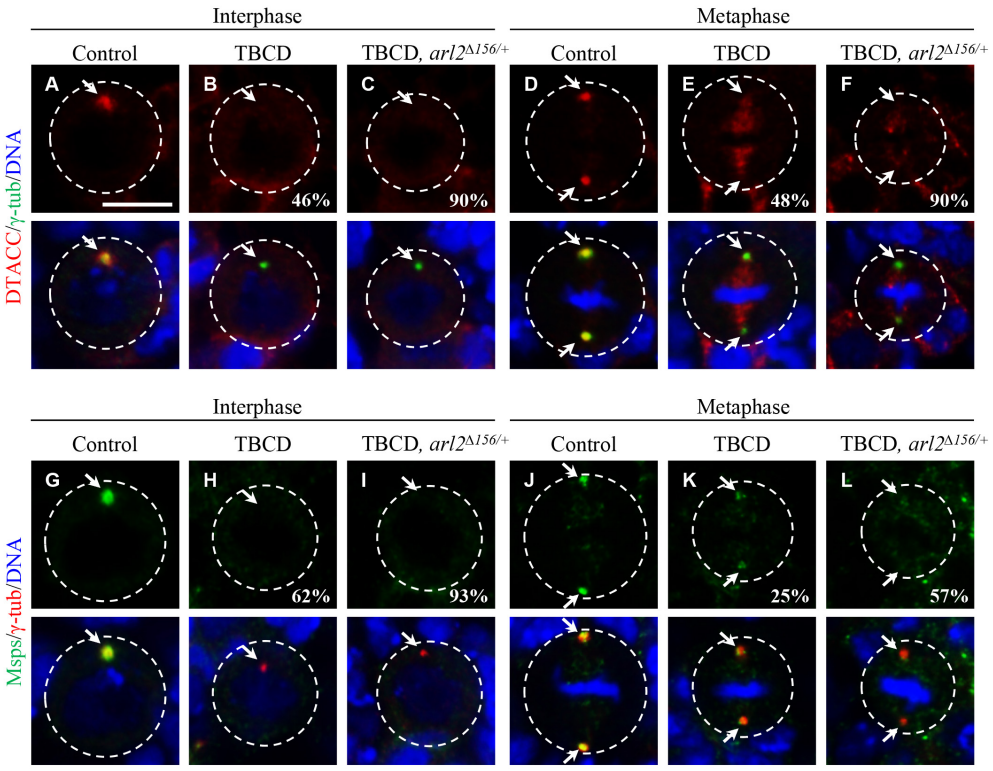

Figure 37. *arl2* heterozygosity enhances D-TACC and Msps localization defects caused by TBCD overexpression.
(A-F) Interphase (A-C) and metaphase (D-F) neuroblasts from control (A, D), TBCD (B, E) and TBCD, *arl2*$^{\Delta 156}$/+ (C, F) labeled for D-TACC, γ-tubulin and DNA. (G-L) Interphase (G-I) and metaphase (J-L) neuroblasts from control (G, J), TBCD (H, K) and TBCD, *arl2*$^{\Delta 156}$/+ (I, L) labeled for Msps, γ-tubulin and DNA. The white dotted circles label the cell outlines. Arrows indicate the centrosomes. Scale bars, 5μm.

dramatically enhanced to 90% (Fig. 37F; n=31) in TBCD *arl2*$^{\Delta 156}$/+ neuroblasts, compared with 48% (Fig. 37E; n=21) with TBCD overexpression alone. Likewise, the severity of Msps delocalization was significantly enhanced in TBCD *arl2*$^{\Delta 156}$/+, compared to TBCD overexpression alone or wild-type (Fig. 37G-L). These results indicate that Arl2 and TBCD function together to regulate D-TACC and Msps localization.

3.2.9 Arl2 regulates microtubule growth and neuroblast asymmetric division through Msps

As Arl2 was primarily localized at the cytoplasm, we presumed that Arl2 regulates D-TACC and Msps localization in an indirect manner. We tested the possibility that Arl2 regulates the centrosomal localization of D-TACC and Msps through dynein, which is a motor protein complex that normally carries cargo proteins to the minus-ends of microtubules (Dick et al., 1996). We first examined the localization of Cut up (Ctp), a *Drosophila* dynein light chain 1 (Ddlc-1). Venus-Ctp was observed at both centrosomes and spindle microtubules in wild-type metaphase neuroblasts, consistent with previous report (Fig. 38A; 100%, n=25) (Wang et al., 2011). In contrast, in $Arl2^{T30N}$, $arl2^{\Delta 156}/+$, the microtubule-localization of Venus-Ctp was strongly reduced in 75% of metaphase neuroblasts (Fig, 38B; n=24), while the centrosomal localization was not obviously affected. Conversely, overexpression of $Arl2^{Q70L}$ resulted in greater intensity of Venus-Ctp on microtubules (Fig. 38C;

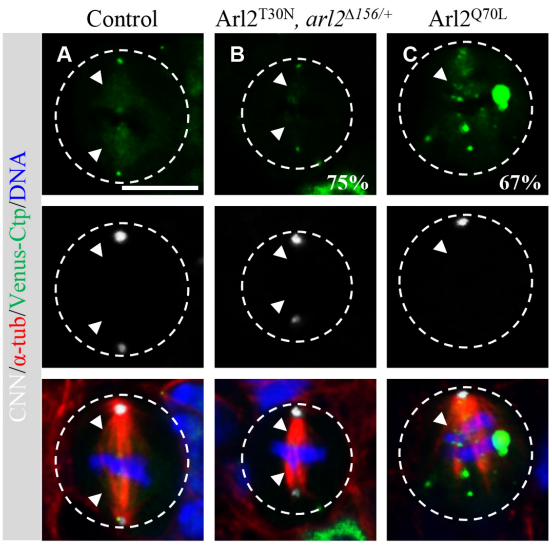

Figure 38. Arl2 regulates microtubule localization of Venus-Ctp.
Metaphase neuroblasts of control (A), $Arl2^{T30N}$, $arl2^{\Delta 156}/+$ (B) and $Arl2^{Q70L}$ (C) labeled for Venus-Ctp, CNN, α-tubulin and DNA. The white dotted circles label the cell outlines. Arrowheads indicate Venus-Ctp observed on spindle microtubule. Scale bars, 5μm.

67%, n=9). In addition, Venus-Ctp was often observed as multiple punctate dots in the cytoplasm of Arl2^{Q70L}-expressing neuroblasts (Fig. 38C). The number and size of Venus-Ctp dots increased as temperature increased (data not shown), suggesting that upon Arl2 over-activation either the expression

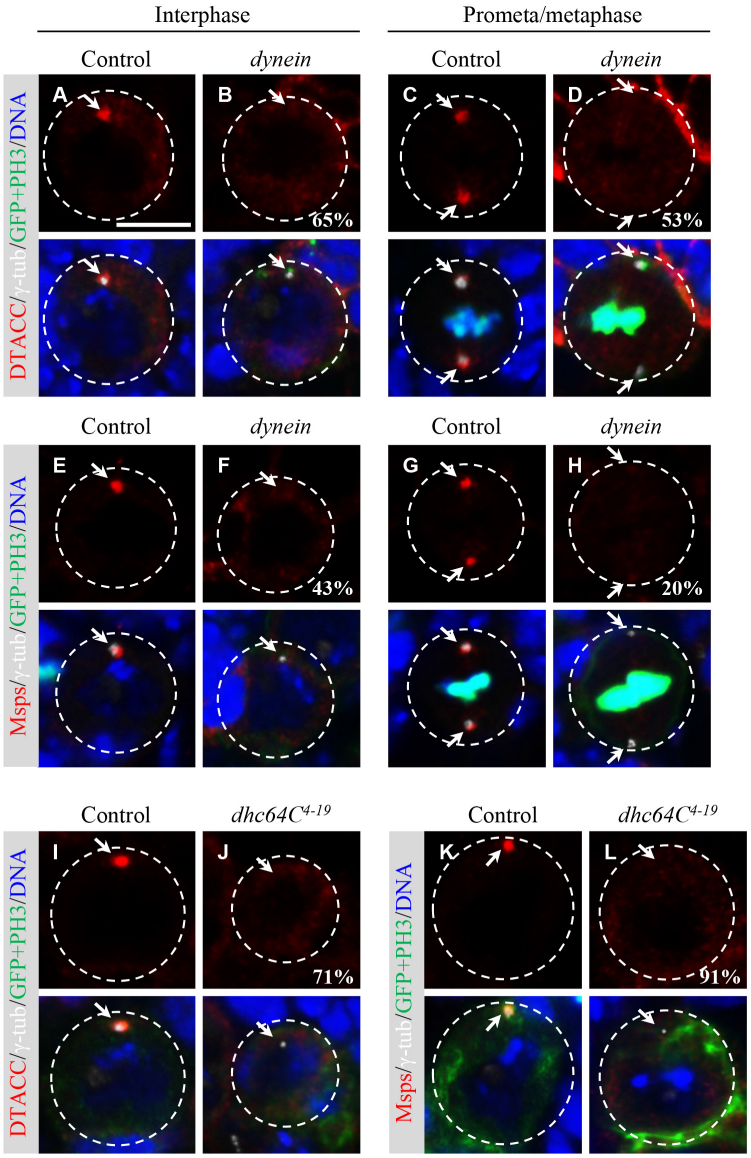

Figure 39. The centrosomal localization of D-TACC and Msps is dependent on dynein.
(A-D) Interphase (A, B) and metaphase (C, D) neuroblasts of control (A, C) and *dynein* (Venus-Ctp-CAAX overexxpression in *ctp*^{exc6}) (B, D) labeled for D-TACC, γ-tub, GFP, PH3 and DNA. (E-H) Interphase (E, F) and metaphase (G, H) neuroblasts of control (E, G) and *dynein* (F, H) labeled for Msps, γ-tub, GFP, PH3 and DNA. (I-L) Interphase neuroblasts of control (I, K) and *dhc64C*$^{4-19}$ (J, L) labeled with D-TACC, γ-tubulin, GFP, PH3 and DNA (I, J), or Msps, γ-tubulin, GFP, PH3 and DNA (K, L). The white dotted circles label the cell outlines. Arrows indicate the centrosomes. Scale bars, 5μm.

levels or the protein folding of Venus-Ctp was changed. Therefore, Arl2 likely determines the amount of Ctp on the microtubules.

We next ascertained whether the dynein complex is required for proper localization of D-TACC/Msps on the centrosomes. We analyzed a genetic background of *ctp* mutant with overexpression of Venus-Ctp^{CAAX}, which is known to disrupt the dynein function (Wang et al., 2011). In this mutant, D-TACC was no longer localized to the centrosomes in 65% (n=29) interphase and 53% (n=17) metaphase neuroblasts (Fig. 39B, D). Likewise, the centrosomal Msps localization was disrupted in 43% (n=12) of interphase and 20% (n=25) of metaphase neuroblasts in *ctp^{exc6}*; Venus-Ctp^{CAAX} mutant (Fig. 39F, H). In addition, in a *dynein heavy chain* mutant, *dhc64C$^{4-19}$*, both D-TACC (71%, n=17) and Msps (91%, n=11) were strongly de-localized in interphase neuroblasts (Fig. 39J, L). Taken together, our data suggest that Arl2 likely regulates D-TACC and Msps localization through regulating dynein complex.

To investigate whether Arl2 functions upstream of Msps, we first tested whether overexpression of Msps in *arl2* loss of function can suppress the defects in microtubule growth and neuroblast asymmetric division. Control line of Arl2^{T30N}, *arl2$^{\Delta 156}$/+* (Arl2^{T30N}, *arl2$^{\Delta 156}$/+* with CD8-GFP) contained 402±80 neuroblasts in the central brain (Fig. 40B, D; n=20), while overexpression of Msps-FL with CD8-GFP was similar to wild-type (Fig. 40A, D; 97±6, n=20). Overexpression of Msps-FL in Arl2^{T30N}, *arl2$^{\Delta 156}$/+* resulted in a dramatic reduction of neuroblast number (Fig. 40C, D; 100±26, n=20), suggesting a significant rescue of neuroblast overgrowth. In addition, spindle orientation was largely restored upon Msps-FL overexpression in Arl2^{T30N}, *arl2$^{\Delta 156}$/+* metaphase neuroblasts, with about 91% showing proper alignment of the mitotic spindle along the apico-basal axis (Fig. 40E-G). Notably, over-

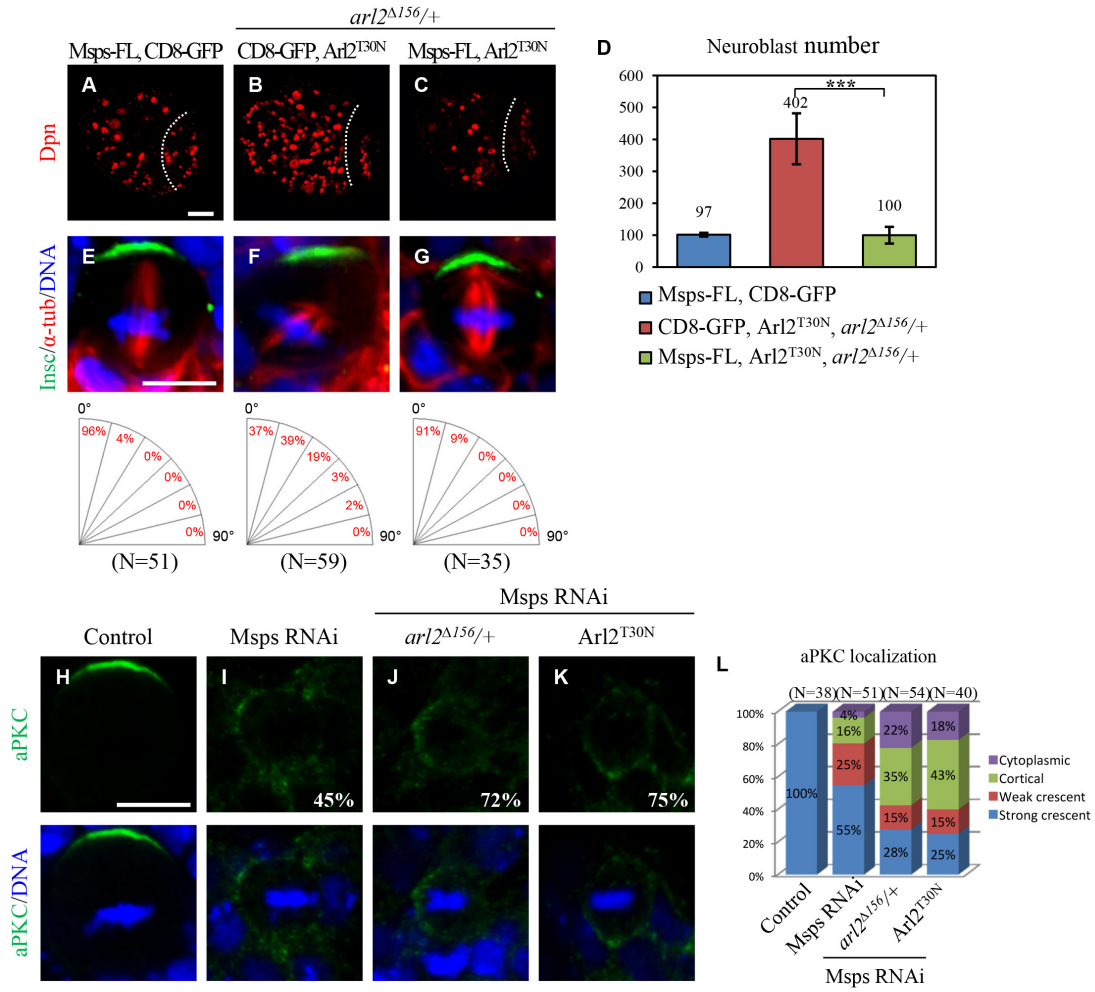

Figure 40. Arl2 regulates neuroblast asymmetric division through Msps. (A-C) Larval brains of Msps-FL, CD8-GFP (A), Arl2^{T30N}, CD8-GFP in *arl2$^{\Delta 156}$/+* (B) and Arl2^{T30N}, Msps-FL in *arl2$^{\Delta 156}$/+* (C) labeled for Dpn. Central brain is to the left of the white dotted line. (D) Quantification of neuroblast number per brain hemisphere in (A-C). Mean and SD are shown. *** indicates P <0.001. (E-G) Metaphase neuroblasts of Msps-FL, CD8-GFP (E), Arl2^{T30N}, CD8-GFP in *arl2$^{\Delta 156}$/+* (F) and Arl2^{T30N}, Msps-FL in *arl2$^{\Delta 156}$/+* (G) labeled for Insc, α-tubulin and DNA. Quantification of spindle orientation is shown in lower panels. (H-K) Metaphase neuroblasts of control (H), Msps RNAi alone (I), Msps RNAi in *arl2$^{\Delta 156}$/+* (J), and Msps RNAi with Arl2^{T30N} co-expression (K) labeled for aPKC and DNA. (L) Quantification of aPKC localization in (H-K). Scale bars, 10μm in (A-C) and 5μm in (E-K).

expression of Msps-FL also dramatically rescued the microtubule abnormalities in Arl2^{T30N} neuroblasts. 95% of interphase neuroblasts with Arl2^{T30N} and Msps co- expression organized robust microtubule asters (Fig. 41D, E; n=22), which were present in all interphase neuroblasts in wild-type or Msps-FL overexpression (Fig. 41A, B, E; n=30), but were absent in 68% of

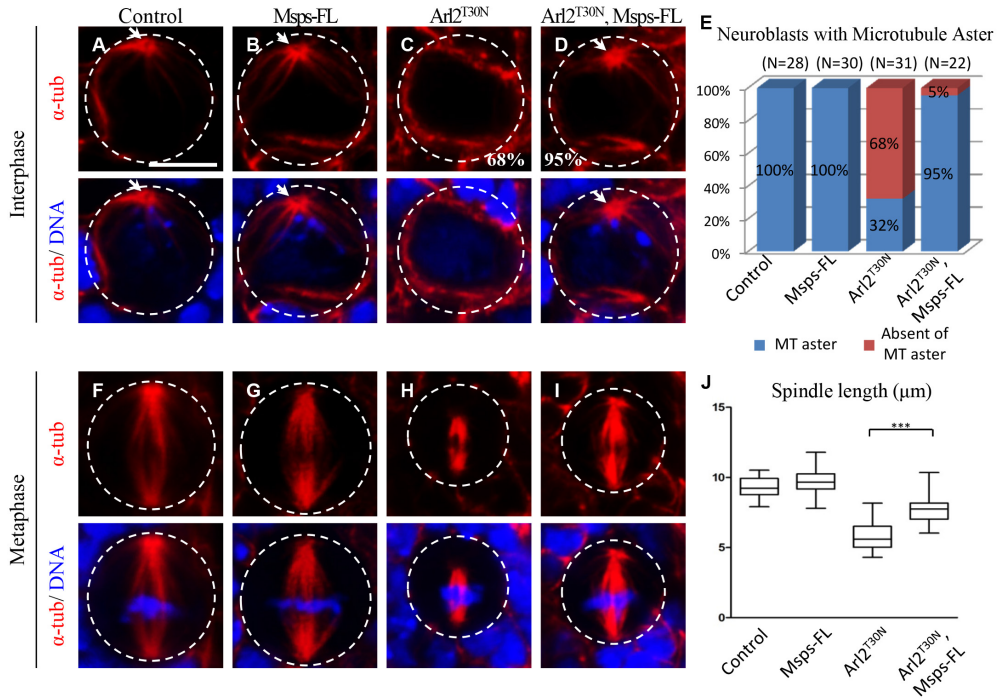

Figure 41. Co-expression of Msps-FL rescues the microtubule abnormalities in Arl2^{T30N}-expressing neuroblasts.
(A-D) Interphase neuroblasts of control (A), Msps-FL (B), Arl2^{T30N} (C) and Msps-FL, Arl2^{T30N} co-expression (D) labeled with α-tubulin and DNA. (E) Quantification of microtubule aster defects in (A-D). (F-I) Metaphase neuroblasts of control (F), Msps-FL (G), Arl2^{T30N} (H) and Msps-FL, Arl2^{T30N} co-expression (I) labeled with α-tubulin and DNA. (J) Quantification of spindle length in (F-I). *** indicates P <0.001. UAS-CD8-GFP was introduced in controls to balance the number of UAS elements. The white dotted circles label the cell outlines. Arrows indicate microtubule asters. Scale bars, 5μm.

Arl2^{T30N}-expressing interphase neuroblasts (Fig. 41C, E; n=31). Importantly, compared to Arl2^{T30N} neuroblasts that formed shorter spindles during metaphase (Fig. 41H, J; 5.78±1.00μm, n=27), co-expression of Msps-FL with Arl2^{T30N} restored spindle length to 7.77±1.06μm (Fig. 41I, J; n=19), suggesting that Arl2 functions upstream of Msps to regulate microtubule growth, which is required for the maintenance of neuroblast asymmetric division.

More severe defect in cell polarity was resulted from disruption of both Arl2 and Msps in neuroblasts. Knockdown of Msps alone under *insc*-Gal4 driver disrupted asymmetric localization of aPKC in 45% of metaphase neuroblasts (Fig. 40I, L, n=51). This phenotype was significantly enhanced in

arl2$^{\Delta 156/+}$ heterozygous background (Fig. 40J, L; 72%, n=54) or in co-expression with Arl2^{T30N} (Fig. 40K, L; 75%, n=40), suggesting that Arl2 and Msps function together to regulate cell polarity. Introduction of *msps*^{P18}/+ heterozygous was able to slightly enhance the neuroblast overgrowth and

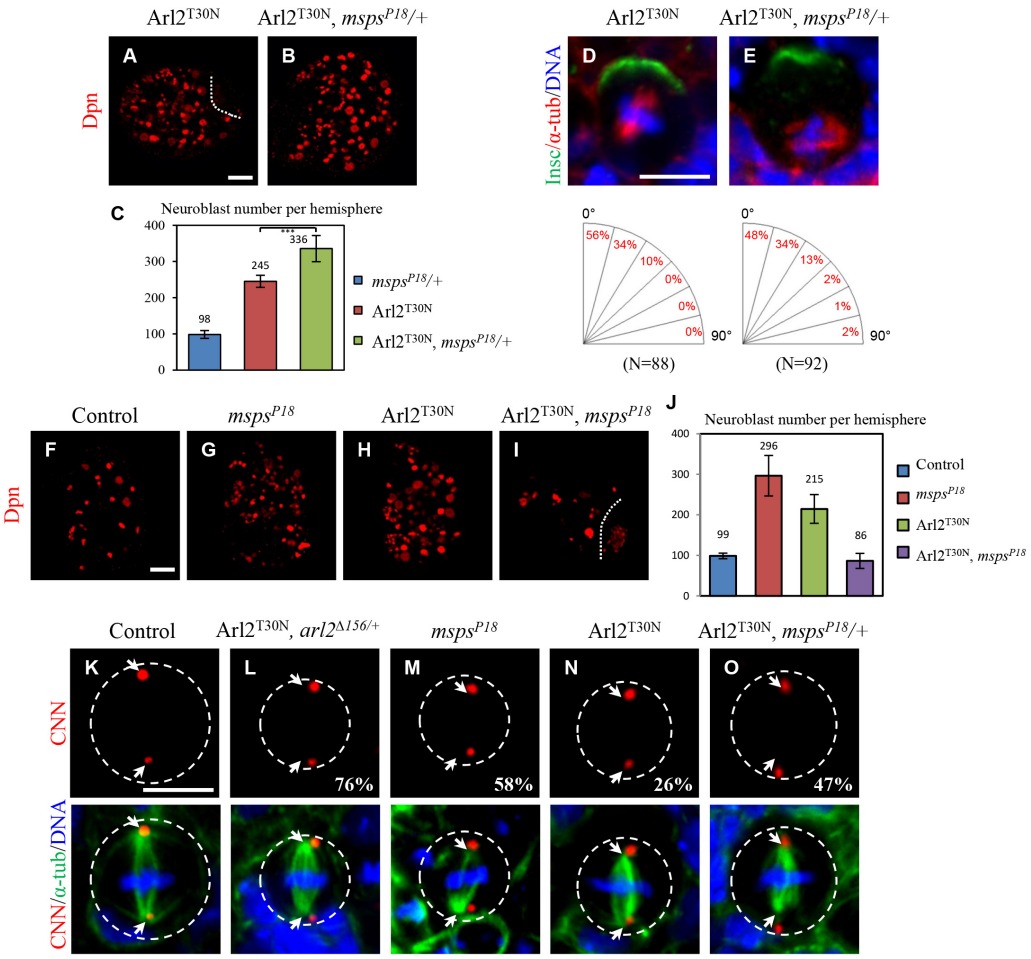

Figure 42. Genetic interaction between Arl2 and Msps.
(A, B) Larval brains of Arl2^{T30N} (A) and Arl2^{T30N} in *msps*^{P18}/+ (B) labeled for Dpn. Central brain is to the left of the white dotted line. (C) Quantification of neuroblast number per brain hemisphere in (A, B). Mean and SD are shown. *** indicates P <0.001. (D, E) Metaphase neuroblasts of Arl2^{T30N} (D) and Arl2^{T30N} in *msps*^{P18}/+ (E) labeled for Insc, α-tubulin and DNA. Quantification of spindle orientation is shown in lower panels. (F-I) Larval brains of control (F), *msps*^{P18} (G), Arl2^{T30N} (H) and Arl2^{T30N} in *msps*^{P18} (I) labeled for Dpn. Central brain is to the left of the white dotted line.
(J) Quantification of neuroblast number per brain hemisphere in (F-I). Mean and SD are shown. (K-O) Metaphase neuroblasts of control (K), Arl2^{T30N} in *arl2*$^{\Delta 156}$/+ (L), *msps*^{P18} (M), Arl2^{T30N} (N) and Arl2^{T30N} in *msps*^{P18}/+ (O) labeled for CNN, α-tubulin and DNA. The white dotted circles label the cell outlines. Arrows indicate centrosomes. Scale bars, 10μm in (A, B) and (F-I), 5μm in (D, E, K-O).

spindle mis-orientation phenotype caused by overexpression of Arl2^{T30N} (Fig. 42A-E). Surprisingly, overexpression of Arl2^{T30N} in *msps^{P18}* homozygous did not display overproliferation of neuroblast in the central brains (Fig. 42F-J), presumably due to severe cell division defects caused by loss of both *arl2* and *msps*.

In wild-type mitotic neuroblasts, the spindle poles are always focused and centrosomes are localized at the center of the spindle poles. We co-stained α-tubulin and CNN to label spindle poles and centrosomes, respectively, in *arl2* and *msps* metaphase neuroblasts. Consistent with previous reports, in wild-type metaphase neuroblasts, centrosomes marked by CNN were always localized at the center of the spindle poles (Fig. 42K). In contrast, 76% (n=58) of metaphase neuroblasts in Arl2^{T30N}, *arl2$^{\Delta 156}$/+* displayed dis-attachment of spindle poles from the centrosomes (Fig. 42L). Similar phenotype was observed in *msps^{P18}*: 58% (n=36) of metaphase neuroblasts that contained two centrosomes displayed dis-attachment of spindle poles from the centrosomes (Fig. 42M). Remarkably, Arl2^{T30N} overexpression in *msps^{P18}/+* heterozygous displayed more severe centrosome-spindle pole dis-engagement phenotype when compared to Arl2^{T30N} overexpression alone (Fig. 42N, O; Arl2^{T30N}: 26.5%, n=54; Arl2^{T30N}, *msps^{P18}/+*: 47.3%, n=36). The attachment of spindle poles to the centrosomes is an important event for the proper spindle orientation (Wang et al., 2011). Therefore, these results suggested that Arl2 and Msps are both required for the centrosome-spindle pole attachment, which may, in turn, contributes to their roles in spindle orientation. Altogether, we proposed that Arl2 functions upstream of Msps to regulate microtubule growth and neuroblast homeostasis.

3.2.10 Arl2 interacts genetically with Mushroom body defects (Mud) to regulate spindle orientation and neuroblast self-renewal

A *Drosophila* homologue of NuMA, Mushroom body defects (Mud), is a critical regulator of spindle orientation during neuroblast asymmetric division (Bowman et al., 2006; Izumi et al., 2006; Siller et al., 2006). Mud is recruited to the spindle pole during mitosis, which is dependent on the centrosomal proteins Ana2 and Ctp (Wang et al., 2011). We asked whether Arl2-Msps pathway interacts genetically with Mud to regulate neuroblast homeostasis. Interestingly, overexpression of Arl2^{T30N} in *mud*^{1} mutant caused a more severe neuroblast overproliferation in the central brains. In *mud*^{1}; Arl2^{T30N} brains, there was more than 600 neuroblasts in each central brain hemisphere, which was significant increased compared to *mud*^{1} mutant alone

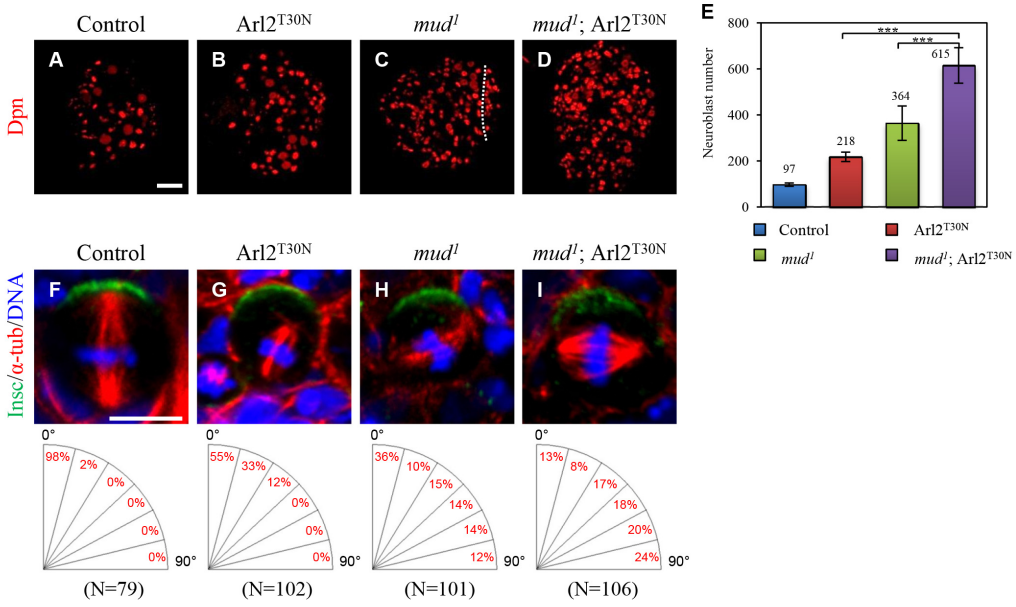

Figure 43. Genetic interaction between Arl2 and Mud.
(A-D) Larval brains of control (A), Arl2^{T30N} (B), *mud*^{1} (C) and Arl2^{T30N} in *mud*^{1} (D) labeled for Dpn. Central brain is to the left of the white dotted line. (E) Quantification of neuroblast number per brain hemisphere in (A-D). Mean and SD are shown. *** indicates P <0.001. (F-I) Metaphase neuroblasts of control (F), Arl2^{T30N} (G), *mud*^{1} (H) and Arl2^{T30N} in *mud*^{1} (I) labeled for Insc, α-tubulin and DNA. Quantification of spindle orientation is shown in lower panels. Scale bars, 10μm in (A-D) and 5μm in (F-I).

and Arl2^{T30N} overexpression alone (Fig. 43A-E, control: 97±7, n=20; Arl2^{T30N}: 218±21, n=16; *mud*^{1}: 364±75, n=20; *mud*^{1}, Arl2^{T30N}: 615±77, n=18). Overexpression of Arl2^{T30N} also caused an enhancement of spindle misorientation in *mud*^{1} metaphase neuroblasts: 87% manifested spindle misorientation, and 24% displayed orthogonal division (Fig. 43F-I). This data suggested that Arl2-Msps functions genetically with Ana2-Ctp-Mud complex.

3.2.11 Arl2 interacts with the catalytic subunit of Protein Phosphatase 2A – Microtubule star (Mts)

In the soluble fraction from bovine brain, Arl2 is associated with TBCD and different subunits of Protein Phosphatase 2A (PP2A) (Shern et al., 2003). In *Drosophila*, PP2A mediates asymmetric divisions and inhibits neuroblast self-renewal (Wang et al., 2009a). To determine whether Arl2 and PP2A function together, we first test if Arl2 is physically associated with the catalytic subunit of PP2A, Microtubule star (Mts). Interestingly, Mts co-immunoprecipitated with Arl2^{T30N}-Venus, but not with Arl2^{Q70L}-Venus or Arl2^{WT}-Venus, suggest a preference binding of Mts with Arl2-GDP (Fig. 44A). Consistently, we also observed co-immunoprecipitation of Mts with TBCE, which also binds preferentially with Arl2-GDP (Fig. 44B). We next examine whether Arl2 and Mts interact genetically. Overexpression of Arl2^{T30N} in *mts*^{XE2258}*/+* background resulted in disruption of aPKC localization in 51% (n=57) of metaphase neuroblasts, compared to Arl2^{T30N}-expressing alone which did not effectively alter cell polarity, with only 8% (n=62) of metaphase neuroblasts showing weaker but still asymmetrically localized aPKC (Fig. 44C-F). Interestingly, the heterozygosity of *mts* did not enhance the microtubule abnormalities or neuroblast overgrowth phenotype caused by Arl2^{T30N} overexpression (Fig.

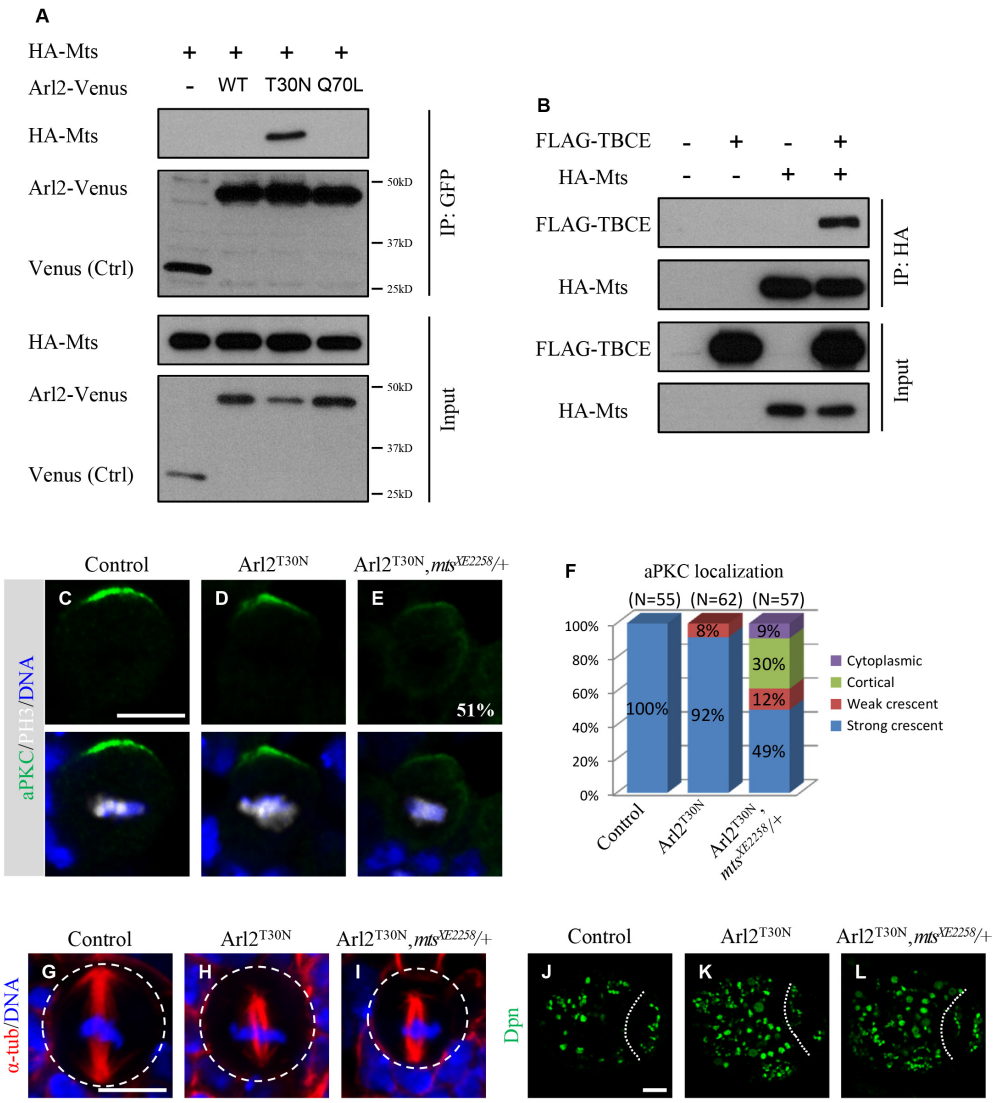

Figure 44. Arl2 and Mts function genetically to regulate cell polarity in neuroblasts.

(A) Co-immunoprecipitation (Co-IP) of S2 cells co-expressing different forms of Arl2-Venus with HA-Mts. Control is Venus and HA-Mts. (B) Co-IP of S2 cells co-expressing FLAG-TBCE with HA-Mts. Controls are either FLAG or HA alone. Immunoprecipitation was performed using anti-GFP (A) or anti-HA (B) antibodies. Western blotting was performed using anti-GFP, anti-HA and anti-FLAG antibodies. (C-E) Metaphase neuroblasts of control (C), Arl2^{T30N} (D) and Arl2^{T30N} in *mts*^{XE2258}/+ (E) labeled for aPKC and DNA. (F) Quantification of aPKC localization in (C-E). (G-I) Metaphase neuroblasts of control (G), Arl2^{T30N} (H) and Arl2^{T30N} in *mts*^{XE2258}/+ (I) labeled for α-tub and DNA. The white dotted circles label the cell outlines. (J-L) Larval brains of control (J), Arl2^{T30N} (K) and Arl2^{T30N} in *mts*^{XE2258}/+ (L) labeled for Dpn. Central brain is to the left of the white dotted line. Scale bars, 5μm in (C-E) and (G-I), 10μm in (J-L).

44G-L). Therefore, our data suggested genetic interactions between Arl2 and Mts in regulating cell polarity during neuroblast asymmetric division.

3.2.12 Arl2 may have a conserved role in regulation of microtubule growth and brain development

Arl2 is a highly conserved gene, with 74% identities between mouse and *Drosophila* homologue. To test whether mammalian Arl2 has a similar function for microtubule growth, we generated a transgene with mouse Arl2

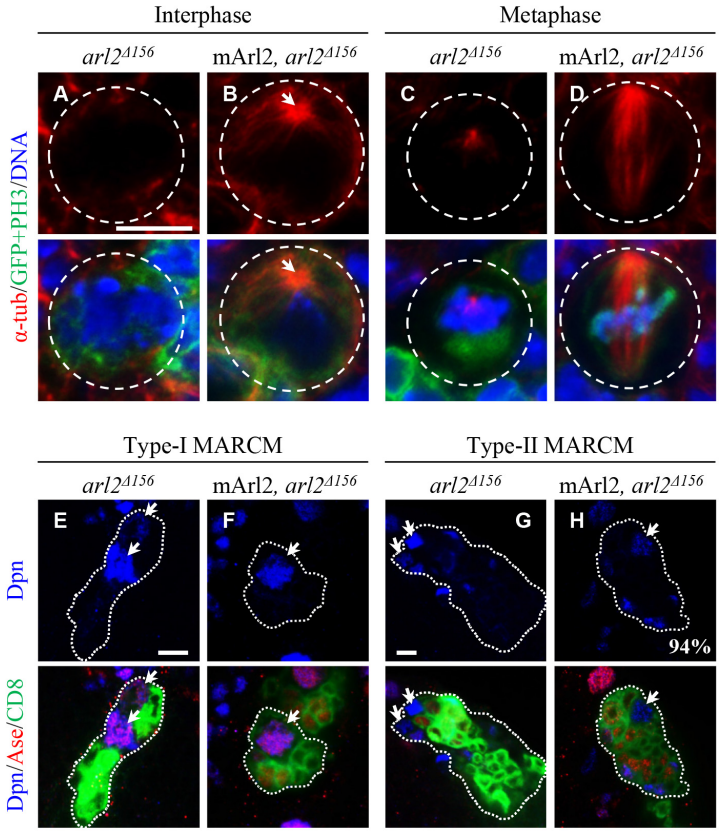

Figure 45. Arl2 plays a conserved role in regulating microtubule growth and neuroblast homeostasis.
(A-D) Interphase (A, B) and metaphase (C, D) neuroblasts of *arl2*$^{\Delta 156}$ (A, C) and *arl2*$^{\Delta 156}$ with overexpression of mouse Arl2 (mArl2) (B, D) labeled with α-tubulin, GFP, PH3 and DNA. The white dotted circles label the cell outlines. Arrows indicate microtubule asters. (E-H) Type I (E, F) and type II (G, H) neuroblasts of *arl2*$^{\Delta 156}$ (E, G) and *arl2*$^{\Delta 156}$, mArl2 (F, H) labeled with Dpn, Ase, and CD8. Cells in the clones are labeled by CD8-GFP and outline of the neuroblast lineages is indicated by white dotted lines. Arrows indicate neuroblasts. Scale bars, 5μm.

homologue. Remarkably, microtubule abnormalities seen in *arl2*$^{\Delta 156}$ mutant neuroblasts were completely restored by overexpression of mouse-Arl2 (Fig. 45A-D; interphase, 100%, n=22; metaphase, 100%, n=6). Moreover, mouse-Arl2 also rescued the neuroblast overgrowth phenotype in *arl2*$^{\Delta 156}$ clones (Fig. 45E-H; Type-I, 100%, n=38; Type-II, 94%, n=18), suggesting a conserved role of Arl2 in microtubule growth and brain development. Altogether, the results suggested that Arl2- and Msps-dependent microtubule growth plays an essential role for the regulation of neuroblast asymmetric division, and this work has been published in The Journal of Cell Biology (Chen et al., 2016).

CHAPTER 4: DISCUSSION AND CONCLUSION

Drosophila melanogaster has been used extensively for the *in vivo* studies of developmental biology and disease modeling. Particularly, the *Drosophila* neural stem cell (neuroblast) has emerged as an excellent model for the studies of self-renewal *vs.* differentiation in stem cells. Evidence has indicated the link between defective neuroblast asymmetric division and tumorigenesis, and a series of cell cycle regulators and centrosome proteins have been identified as critical regulators of asymmetric division and homeostasis in neuroblasts (Knoblich, 2010; Li et al., 2014b). In this thesis, I have provided a series of data showing that microtubule growth, which is dependent on Arl2 and Msps, plays essential roles in the asymmetric division of neural stem cells. Loss of *arl2* and *msps* both results in defects of cell polarity and spindle orientation, which are two key features of the asymmetric division. Moreover, disruption of *arl2* and *msps* causes neuroblast overgrowth in the larval central brain, indicating the roles of Arl2 and Msps in regulating neural stem cell self-renewal.

4.1 Arl2 plays a critical role in regulating microtubule growth

Arl2 is a small GTPase that belongs to the ADP Ribosylation Factor (ARF) family (Kahn et al., 2005). Unlike most other members of the ARF family that are involved in cellular processes of membrane trafficking, Arl2 is notably distinct. Lacking the N-terminal myristoylation (Sharer et al., 2002), Arl2 is often implicated in the regulation of microtubule formation (Antoshechkin and Han, 2002; Bhamidipati et al., 2000; Mori and Toda, 2013; Shern et al., 2003). Loss of the *arl2* homologue, *evl-20*, results in severe microtubule defects and

failure of cytokinesis in *C. elegans* (Antoshechkin and Han, 2002). In fission yeast, the continuous cycling of Alp41 (Arl2 homologue) between GTP- and GDP-bound forms is important for microtubule formation (Mori and Toda, 2013). In mammalian cell lines, Arl2 seems to function in an indirect manner to prevent the destruction of microtubules when an excess amount of chaperone protein TBCD is present (Bhamidipati et al., 2000).

The first functional study of *Drosophila* Arl2 is presented in this thesis. Overexpression of a dominant negative form of Arl2 results in formation of shorter mitotic spindles and absence of interphase microtubule asters in neural stem cells (Fig. 17 and Fig. 41). In a microtubule re-growth assay, $Arl2^{T30N}$-expressing neuroblasts fail to efficiently re-assemble mitotic spindles (Fig. 20). Similarly, GFP-α-Tub or β-Tub-Venus is not efficiently assembled onto microtubules in $Arl2^{T30N}$-expressing neuroblasts (Fig. 22). Moreover, none of the neuroblasts in *arl2* null mutants assembles interphase microtubule aster or mitotic spindle, albeit residual microtubules are still present in these neuroblasts (Fig. 21). Conversely, overexpression of a constitutively active Arl2 results in microtubule overgrowth and severe cell division defects (Fig. 26). All these data support that *Drosophila* Arl2 plays pivotal roles in regulating microtubule growth.

Data from mass spectrometry followed by tandem affinity purification suggests the conserved binding between Arl2 and TBCD in *Drosophila* (data from Tian X and Wu C) (Chen et al., 2016). In mammalian cells, Arl2-GDP but not Arl2-GTP inhibits the dissociation of tubulin heterodimers caused by TBCD (Bhamidipati et al., 2000). Surprisingly, in *Drosophila* neuroblasts, overexpression of $Arl2^{T30N}$ dramatically enhances the microtubule defects caused by TBCD, whereas co-expression of $Arl2^{WT}$ with TBCD restores the phenotype (Fig. 30 and unpublished data). This data is also consistent with

the finding that *Drosophila* TBCD forms complexes with both GTP- and GDP-bound Arl2 in the co-immunoprecipitation assay (Fig. 28), whereas in mammalian cells TBCD is preferentially associated with Arl2-GDP (Bhamidipati et al., 2000; Shern et al., 2003). In mammalian cells, overexpression of Arl2-GDP or Arl2-GTP alone does not result in any obvious effects on microtubules (Bhamidipati et al., 2000). By contrast, I have shown that overexpression of $Arl2^{T30N}$ or $Arl2^{Q70L}$ in neuroblasts causes dramatic effects in microtubules (Fig. 20, 22 and 26). These *in vivo* data suggest that *Drosophila* Arl2 plays an essential and likely a more direct role in microtubule growth, in addition to its known functions in suppressing the destruction effect of TBCD.

In addition, I also showed that Arl2 physically associates with tubulin binding cofactors C and E (Fig. 29). TBCE seems to preferentially bind to Arl2-GDP, whereas TBCC has higher affinities towards Arl2-GTP (Fig. 29). This is consistent with the previously reported function of yeast TBCC as a GAP for Arl2 (Mori and Toda, 2013). Moreover, Arl2 also genetically interacts with TBCC to regulate microtubule growth (Fig. 32), suggesting that Arl2 may function together with all three cofactors. TBCC, TBCD and TBCE are key components required for the *de novo* assembly of tubulin heterodimers (Tian et al., 1999). However, we are still unable to provide direct evidence to show that Arl2 is required for the *de novo* tubulin assembly pathway. An alternative model is provided by a recently published structural and biochemical study, which shows that the yeast homologue of Arl2, TBCD and TBCE form a stable cytosolic complex (Nithianantham et al., 2015). This complex is able to bind to tubulin dimer and TBCC sequentially to regulate the maintenance of soluble αβ-tubulin in the cytoplasm (Nithianantham et al., 2015). This alternative paradigm helps to explain the role of Arl2 in *Drosophila*, as our

results show different binding preferences of TBCC, TBCD and TBCE towards Arl2-GTP or Arl2-GDP (Fig. 28 and 29), which is consistent with the hypothesis that Arl2 binds to TBCD, TBCE and TBCC sequentially.

4.2 Arl2 and Tubulin Binding Co-factors are important for the centrosomal localization of D-TACC and Msps

In addition to defective microtubule growth, loss of *arl2* also displays impairment of centrosome functions. In *arl2* mutant interphase neuroblasts, most PCM proteins including CNN, γ-tubulin, AurA, Polo and Msps are not efficiently recruited to the daughter centrosomes (Fig. 21 and 23). This defect can be a result of failure in centrosome cycle, as *arl2* mutant interphase neuroblasts often contain only one Asl-positive centriole or show absence of centriole (Fig, 24). Consistently, over-activation of Arl2 caused accumulation of PCM proteins at the centrosomes (Fig. 27). However, it remains unknown how Arl2 affects centriole biogenesis, as an Arl2-Venus transgene is mainly localized at the cytoplasm (Fig. 19). Interestingly, studies carried out in human cell lines have shown that TBCD is localized to the centrosomes and is implicated in the regulation of centriologenesis, PCM recruitment and organization of mitotic spindle (Cunningham and Kahn, 2008; Fanarraga et al., 2010). Given that Arl2 and TBCD are closely associated to regulate microtubule formation, it is speculated that the centriole defect seen in *arl2* mutants is a secondary effect caused by microtubule loss, as centrioles are microtubule-based structures (Nigg and Stearns, 2011).

In a relatively milder *arl2* loss-of-function condition ($Arl2^{T30N}$ overexpression), 68% (n=39) of neuroblasts fail to assemble interphase microtubule asters (Fig. 41C), while recruitment of most PCM proteins such as CNN and γ-tubulin, or centriole duplication remains largely unaffected

(data not shown). In these Arl2^{T30N}-expressing interphase neuroblasts, loss of microtubule aster could be mainly due to defective microtubule growth. In *arl2* null mutants, centriole function is impaired and PCM proteins are not recruited to the centrosomes, which may further contribute to a complete loss of microtubule asters in all interphase neuroblasts (Fig. 24). Surprisingly, multiple centriole pairs are often found in *arl2* mutant mitotic neuroblasts (Fig. 24), presumably due to an accumulation effect of cell division defects. To further elucidate the effect of Arl2 on the function of mitotic centrosome, probably *arl2* null mutant clones at an earlier developmental stage are needed to be examined.

The centrosomal localization of D-TACC and Msps is ultimately disrupted in Arl2^{T30N}-expressing neuroblasts (Fig. 36). Introduction of the *arl2*$^{\Delta 156}$/+ heterozygous is able to significantly enhance the D-TACC and Msps de-localization caused by TBCD overexpression (Fig. 37), suggesting that Arl2 and TBCD function together to regulate this centrosomal localization. The results also showed that Arl2 regulates D-TACC and Msps localization through dynein complex (Fig. 38 and 39). However, I was not yet able to detect co-immunoprecipitation of Arl2 with Ctp. It remains uncertain of how Arl2 and/or tubulin binding co-factors regulate dynein functions. Interestingly, it has been shown that in 293 T cell lines, tubulin binding co-factor B (TBCB) is a direct interaction partner of the dynactin p150^{Glued} subunit (Kuh et al., 2012). Further experiments can be carried out to test whether Arl2 and tubulin binding co-factors can bind to dynein regulators such as the dynactin complex, which in turn regulates the function of the dynein complex.

In *Drosophila* syncytial embryos, de-polymerization of microtubules by Colchicine treatment does not alter Msps localization to the centrosomes, indicating that long microtubules are not essential for the centrosomal

localization of Msps (Cullen et al., 1999). However, it is still possible that short microtubules or cytosolic tubulin may play essential roles for D-TACC and Msps localization. A recently published study has uncovered an unexpected role of soluble tubulin in regulating PCM proteins' localization (Gopalakrishnan et al., 2012). Independent from its well-known role as building blocks of microtubules, soluble tubulin negatively regulates PCM recruitment to the centrosome through a Sas-4-dependent manner. Through different guanine-bound state, tubulin acts as a molecular switch for the PCM recruitment (Gopalakrishnan et al., 2012). Several lines of evidence have indicated that Arl2 and tubulin binding co-factors play crucial roles in maintaining the cytosolic pool of tubulin (Beghin et al., 2007; Nithianantham et al., 2015). Hence, Arl2 and tubulin binding co-factors probably regulate the centrosomal localization of D-TACC and Msps through controlling soluble tubulin heterodimer levels in the cells.

4.3 Arl2 and Msps-dependent microtubule growth is essential for asymmetric division of neural stem cells

Loss of *arl2* disrupts microtubule formation and generates ectopic neuroblasts, whereas Arl2 over-activation results in microtubule overgrowth and depletion of neuroblast in the brain (Fig. 12-14, Fig. 25). The microtubule abnormalities observed in *arl2* loss-of-function conditions resemble those reported in *msps* mutants (Fig. 17) (Cullen et al., 1999). Interestingly, neuroblast overgrowth is also observed upon *msps* loss-of-function (Fig. 33 and 34). In order to test whether Arl2 regulates asymmetric division and neuroblast self-renewal through Msps, several experiments in various genetic backgrounds have been carried out. The results show that Msps overexpression is able to suppress the microtubule defects and neuroblast

overgrowth caused by loss of *arl2* (Fig. 40). Furthermore, when Arl2 and Msps functions are both disrupted, the defective asymmetric division is dramatically enhanced (Fig. 40 and 42). These results strongly suggest that Arl2 and Msps-dependent microtubule growth is crucial for the establishment of cell polarity during neuroblast asymmetric division.

The interphase microtubule aster and astral microtubules serve as determinants for the mitotic spindle alignment (Rebollo et al. 2007; Rusan and Peifer. 2007). Here, I have also shown that microtubules are essential for establishment of cortical polarity. Both *arl2* and *msps* mutant neuroblasts display defective cortical polarity during metaphase and mis-segregation of polarized components into both daughter cells during telophase (Fig. 15 and 35). The mis-segregation of aPKC could potentially result in inheritance of self-renewal in both daughter cells (Li et al. 2014), causing formation of ectopic neuroblasts in the central brains.

Although *arl2* null neuroblasts display both centrosome defects and microtubule growth defects (Fig. 21, 23 and 24), it is speculated that cell polarity defects are caused by loss of microtubules instead of loss of centrosomes, as evidence have shown that loss of centrosome has little effect on establishment of cortical polarity in neuroblasts (Wang et al., 2011). Previous studies reported that microtubules alone are sufficient but not essential for the asymmetric localization of Pins/Gαi complex (Siegrist and Doe, 2005). Here, I have provided the first evidence showing that impairment of microtubule growth by genetic manipulation can result in defects in cell polarity and disruption of homeostasis in neural stem cells. Neuroblasts in *arl2* and *msps* mutants often fail to asymmetrically localize aPKC and Baz (Fig. 15, 16 and 35), which are two key components of the Par complex required for establishment of the cortical polarity (Rolls et al., 2003; Wodarz et

al., 1999). Several studies have indicated the requirement of microtubules for cell polarity in various cell types. For example, TBCB-dependent microtubule network formation is required for the apico-basal polarity in *Drosophila* epithelial follicle cells (Baffet et al., 2012). In *C. elegans* zygotes, microtubules nucleated from the sperm-donated centrosomes are responsible to induce self-organization of polarized PAR proteins (Motegi et al., 2011). In *Drosophila* larval brain neuroblasts, failure of asymmetric division is often linked to tumorigenesis, and microtubules play essential roles to regulate cortical polarity and in turn contribute to the balance of self-renewal and differentiation in neuroblasts.

In this thesis, I have also provided a series of experimental clues regarding how microtubules regulate asymmetric localization of aPKC. The results showed that Arl2-GDP forms a complex with Mts, which is the catalytic subunit of Protein Phosphatase 2A (PP2A) (Fig. 44). In addition, Arl2 interacts genetically with Mts to regulate aPKC localization (Fig. 44). PP2A is known to control the cortical polarity through regulating phosphorylation of Par complex components (Chabu and Doe, 2009; Krahn et al., 2009; Ogawa et al., 2009), and/or through activating the Polo/Numb pathway in neuroblasts (Wang et al., 2009a). Further studies are needed to elucidate the mechanisms underlying the microtubule pathway, especially whether the activities of Mts are compromised when microtubules are disrupted.

In $Arl2^{T30N}$-expressing neuroblasts that display milder microtubule defects, the cortical polarity remains largely unaffected (unpublished data), whereas mitotic spindles are not properly aligned along the apical-basal axis (Fig. 17). This is consistent with previous studies showing that astral microtubules are required for the correct orientation of mitotic spindles (Siegrist and Doe, 2005). The cell polarity defects are prominent in *arl2* null

neuroblasts that display severe microtubule loss (Fig. 15 and 16). In *msps* mutant neuroblasts, both cortical polarity and spindle orientation are disrupted (Fig. 35). The severe spindle mis-orientation seen in *msps* neuroblasts could be attributed to an accumulation effect of microtubule abnormalities and polarity defects, as disruption of apically localized proteins is often associated with spindle mis-orientation (Kraut et al., 1996; Wodarz et al., 2000). Together, Arl2 and Msps-dependent microtubule growth plays critical roles in neuroblast asymmetric division.

4.4 Conserved roles of Arl2 in microtubule growth and tumorigenesis

Arl2 is a highly conserved gene among eukaryote (Mori and Toda, 2013). Consistent with its reported functions in controlling microtubule formation in yeast, *C. elegans* and mammalian cells (Antoshechkin and Han, 2002; Bhamidipati et al., 2000; Mori and Toda, 2013), *Drosophila* Arl2 is a pivotal regulator of microtubule gorwth. In this thesis, I have also shown that loss of *arl2* results in overgrowth of neuroblast in the larval central brain, which resembles the phenotype of brain tumors (Fig. 12-14). Moreover, overexpression of a mammalian homologue of Arl2 is able to efficiently restore the microtubule defects and neuroblast overgrowth seen in *arl2* mutants (Fig. 45). Studies carried out in variant human breast cancer cell lines have revealed that reduced Arl2 content is associated with impaired microtubule dynamics and enhanced tumorigenesis (Beghin et al., 2009; Beghin et al., 2007). Similarly, reduced TBCC content in human breast cancer cells presents a higher sensitivity to the S-phase targeting agent Gemcitabine and enhanced tumor growth *in vivo* (Hage-Sleiman et al., 2010, 2011). The findings on *Drosophila* Arl2 may shed new light to the research on understanding the function of Arl2 in tumorigenesis and cancer progression.

Interestingly, a high level of Arl2 protein is also detected in mammalian brain samples (Shern et al., 2003). However, it remains largely unknown whether Arl2 plays any role in neural development. A recent study has shown that human Arl2 is required for the survival of neural progenitor cells, but it is unclear whether this is linked its known function in microtubule formation (Zhou et al., 2013). Several lines of evidence have indicated the involvement of tubulin binding co-factors in neural development and disease progression. Mutation in human *tbce* is associated with congenital hypoparathyroidism, mental retardation, facial dysmorphism (HRD) syndromes (Parvari et al., 2002). In a mice model of human motor neuron disease, mutation in *tbce* is also found to be the cause of progressive motor neuronopathy, suggesting a mechanistic link between TBCE-mediated tubulin formation and neurodegeneration (Bommel et al., 2002; Martin et al., 2002). In neuronal cell lines, TBCB is localized at the transition zone of the neuronal growth cone where it negatively controls axon growth (Lopez-Fanarraga et al., 2007). Hence, it remains particularly interesting to examine whether Arl2 participates in these procedures.

4.5 Conclusion

In this thesis, I have described a novel paradigm that microtubules play essential roles for the maintenance of neuroblast asymmetric division. From an un-biased RNAi screen, I have identified a previously un-characterized gene in *Drosophila*, Arl2, as a novel regulator of central brain neuroblast self-renewal. Neuroblast overgrowth is observed in various *arl2* loss-of-function conditions, including RNAi knockdown, overexpression of *arl2* dominant-negative, and *arl2* mutant MARCM clones, suggesting that Arl2 suppresses neuroblast overproliferation. Upon *arl2* loss-of-function, the asymmetric

localization of polarity proteins such as aPKC, Baz and Numb is largely disrupted, and mitotic spindles are often mis-aligned from the apico-basal axis. These results indicate that Arl2 plays an important role in controlling neuroblast asymmetric division and homeostasis.

Interestingly, loss of *arl2* results in severe defects in microtubule growth in neuroblasts. In *arl2* mutant neuroblasts, interphase microtubule aster and mitotic spindle are both disrupted. Consistently, over-activation of Arl2 induces an overgrowth of microtubules and depletion of neuroblasts in the central brain, suggesting that *Drosophila* Arl2 is an essential regulator of microtubule growth. In addition, I have carried out a series of co-immunoprecipitation experiments showing that Arl2 physically interacts with *Drosophila* TBCC, TBCD and TBCE, which are conserved chaperonins regulating tubulin biogenesis and degradation (Lewis et al., 1997; Nithianantham et al., 2015). Furthermore, I also showed that co-expression of Arl2 dominant negative with TBCD causes more severe microtubule abnormalities, aPKC polarity defects and neuroblast overgrowth. Together, these results strongly suggest that Arl2, which plays a central role for microtubule growth, functions synergistically with tubulin binding cofactors in mediating cell polarity and self-renewal in neuroblasts.

Coincidently, an *msps* mutant was isolated from an EMS-induced mutant collection. Loss of *msps* also results in defects in asymmetric division and overproliferation of neuroblasts. Msps is a well-known conserved microtubule stabilizing protein identified in different systems, and loss of *msps* disrupts spindle integrity in *Drosophila* (Brouhard et al., 2008; Cullen et al., 1999). Given that Arl2 and Msps display similar phenotype, I carried out several genetic experiments to examine whether Arl2 functions genetically with Msps to regulate neuroblast self-renewal. Surprisingly, loss of *arl2* largely disrupts

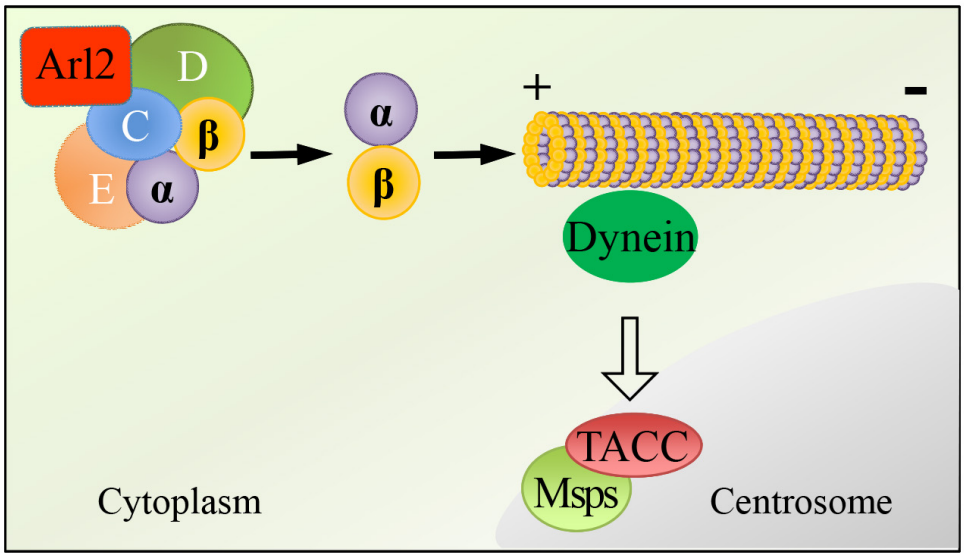

Figure 46. A working model of Arl2- and Msps-dependent microtubule growth governs asymmetric division.
Arl2 functions together with tubulin binding cofactors (TBCs) to regulate the centrosomal localization of TACC and Msps, presumably through the dynein complex. Microtubule growth, which is dependent on Arl2 and Msps, plays a critical role for the establishment of cell polarity in neuroblasts.

the centrosomal localization of Msps and D-TACC, which is a key regulator of Msps localization (Barros et al., 2005; Lee et al., 2001). Further evidence revealed that Arl2 mediates D-TACC and Msps localization through regulating dynein functions. Moreover, overexpression of an Msps transgene largely restores the microtubule defects and neuroblast overgrowth seen in *arl2* loss-of-function, while impairment of both *arl2* and *msps* results in more severe defects in cell polarity, suggesting that Arl2 functions through Msps. Therefore, Arl2- and Msps-dependent microtubule growth is an important regulator controlling neuroblast asymmetric division (Fig. 46).

In this thesis, I have also provided evidence that Arl2 forms a complex with Mts and together they are required for proper cell polarity in neuroblasts. Mts is the catalytic subunit of PP2A, a well-known cell cycle regulator and tumor suppressor (Akhmanova and Steinmetz, 2008; Chabu and Doe, 2009;

Wang et al., 2009a). Further studies can be carried out to understand the possible link between the tubulin biogenesis and the cell cycle regulator PP2A, and how they contribute to the neuroblast asymmetric division.

REFERENCE

Akhmanova, A., and Steinmetz, M.O. (2008). Tracking the ends: a dynamic protein network controls the fate of microtubule tips. Nat Rev Mol Cell Biol 9, 309-322.

Alushin, G.M., Lander, G.C., Kellogg, E.H., Zhang, R., Baker, D., and Nogales, E. (2014). High-resolution microtubule structures reveal the structural transitions in alphabeta-tubulin upon GTP hydrolysis. Cell 157, 1117-1129.

Antoshechkin, I., and Han, M. (2002). The C. elegans evl-20 gene is a homolog of the small GTPase ARL2 and regulates cytoskeleton dynamics during cytokinesis and morphogenesis. Dev Cell 2, 579-591.

Arama, E., Dickman, D., Kimchie, Z., Shearn, A., and Lev, Z. (2000). Mutations in the beta-propeller domain of the Drosophila brain tumor (brat) protein induce neoplasm in the larval brain. Oncogene 19, 3706-3716.

Artavanis-Tsakonas, S., and Simpson, P. (1991). Choosing a cell fate: a view from the Notch locus. Trends Genet 7, 403-408.

Atwood, S.X., Chabu, C., Penkert, R.R., Doe, C.Q., and Prehoda, K.E. (2007). Cdc42 acts downstream of Bazooka to regulate neuroblast polarity through Par-6 aPKC. J Cell Sci 120, 3200-3206.

Atwood, S.X., and Prehoda, K.E. (2009). aPKC phosphorylates Miranda to polarize fate determinants during neuroblast asymmetric cell division. Curr Biol 19, 723-729.

Baffet, A.D., Benoit, B., Januschke, J., Audo, J., Gourhand, V., Roth, S., and Guichet, A. (2012). Drosophila tubulin-binding cofactor B is required for microtubule network formation and for cell polarity. Mol Biol Cell 23, 3591-3601.

Bahe, S., Stierhof, Y.D., Wilkinson, C.J., Leiss, F., and Nigg, E.A. (2005). Rootletin forms centriole-associated filaments and functions in centrosome cohesion. J Cell Biol 171, 27-33.

Barros, T.P., Kinoshita, K., Hyman, A.A., and Raff, J.W. (2005). Aurora A activates D-TACC-Msps complexes exclusively at centrosomes to stabilize centrosomal microtubules. J Cell Biol 170, 1039-1046.

Basto, R., Lau, J., Vinogradova, T., Gardiol, A., Woods, C.G., Khodjakov, A., and Raff, J.W. (2006). Flies without centrioles. Cell 125, 1375-1386.

Bayraktar, O.A., and Doe, C.Q. (2013). Combinatorial temporal patterning in progenitors expands neural diversity. Nature 498, 449-455.

Beghin, A., Belin, S., Hage-Sleiman, R., Brunet Manquat, S., Goddard, S., Tabone, E., Jordheim, L.P., Treilleux, I., Poupon, M.F., Diaz, J.J., and Dumontet, C. (2009). ADP ribosylation factor like 2 (Arl2) regulates breast tumor aggressivity in immunodeficient mice. PloS one 4, e7478.

Beghin, A., Honore, S., Messana, C., Matera, E.L., Aim, J., Burlinchon, S., Braguer, D., and Dumontet, C. (2007). ADP ribosylation factor like 2 (Arl2) protein influences microtubule dynamics in breast cancer cells. Exp Cell Res 313, 473-485.

Bello, B., Reichert, H., and Hirth, F. (2006). The brain tumor gene negatively regulates neural progenitor cell proliferation in the larval central brain of Drosophila. Development 133, 2639-2648.

Bello, B.C., Izergina, N., Caussinus, E., and Reichert, H. (2008). Amplification of neural stem cell proliferation by intermediate progenitor cells in Drosophila brain development. Neural Dev 3, 5.

Berger, C., Harzer, H., Burkard, T.R., Steinmann, J., van der Horst, S., Laurenson, A.S., Novatchkova, M., Reichert, H., and Knoblich, J.A. (2012). FACS purification and transcriptome analysis of drosophila neural stem cells reveals a role for Klumpfuss in self-renewal. Cell Rep 2, 407-418.

Betschinger, J., Eisenhaber, F., and Knoblich, J.A. (2005). Phosphorylation-induced autoinhibition regulates the cytoskeletal protein Lethal (2) giant larvae. Curr Biol 15, 276-282.

Betschinger, J., Mechtler, K., and Knoblich, J.A. (2003). The Par complex directs asymmetric cell division by phosphorylating the cytoskeletal protein Lgl. Nature 422, 326-330.

Betschinger, J., Mechtler, K., and Knoblich, J.A. (2006). Asymmetric segregation of the tumor suppressor brat regulates self-renewal in Drosophila neural stem cells. Cell 124, 1241-1253.

Bhamidipati, A., Lewis, S.A., and Cowan, N.J. (2000). ADP ribosylation factor-like protein 2 (Arl2) regulates the interaction of tubulin-folding cofactor D with native tubulin. J Cell Biol 149, 1087-1096.

Bier, E., Vaessin, H., Younger-Shepherd, S., Jan, L.Y., and Jan, Y.N. (1992). deadpan, an essential pan-neural gene in Drosophila, encodes a helix-loop-helix protein similar to the hairy gene product. Gene Dev 6, 2137-2151.

Bier, E. (2005). Drosophila, the golden bug, emerges as a tool for human genetics. Nat Rev Genet 6, 9-23.

Bilen, J., and Bonini, N.M. (2005). Drosophila as a model for human neurodegenerative disease. Annu Rev Genet 39, 153-171.

Bommel, H., Xie, G., Rossoll, W., Wiese, S., Jablonka, S., Boehm, T., and Sendtner, M. (2002). Missense mutation in the tubulin-specific chaperone E (Tbce) gene in the mouse mutant progressive motor neuronopathy, a model of human motoneuron disease. J Cell Biol 159, 563-569.

Boone, J.Q., and Doe, C.Q. (2008). Identification of Drosophila type II neuroblast lineages containing transit amplifying ganglion mother cells. Dev Neurobiol 68, 1185-1195.

Bowman, S.K., Neumuller, R.A., Novatchkova, M., Du, Q., and Knoblich, J.A. (2006). The Drosophila NuMA Homolog Mud regulates spindle orientation in asymmetric cell division. Dev Cell 10, 731-742.

Bowman, S.K., Rolland, V., Betschinger, J., Kinsey, K.A., Emery, G., and Knoblich, J.A. (2008). The tumor suppressors Brat and Numb regulate transit-amplifying neuroblast lineages in Drosophila. Dev Cell 14, 535-546.

Britton, J.S., and Edgar, B.A. (1998). Environmental control of the cell cycle in Drosophila: nutrition activates mitotic and endoreplicative cells by distinct mechanisms. Development 125, 2149-2158.

Brand, M., Jarman, A.P., Jan, L.Y., and Jan, Y.N. (1993). Asense is a Drosophila neural precursor gene and is capable of initiating sense organ formation. Development 119, 1-17.

Broadus, J., Fuerstenberg, S., and Doe, C.Q. (1998). Staufen-dependent localization of prospero mRNA contributes to neuroblast daughter-cell fate. Nature 391, 792-795.

Brody, T., and Odenwald, W.F. (2000). Programmed transformations in neuroblast gene expression during Drosophila CNS lineage development. Dev Biol 226, 34-44.

Brouhard, G.J., and Rice, L.M. (2014). The contribution of alphabeta-tubulin curvature to microtubule dynamics. J Cell Biol 207, 323-334.

Brouhard, G.J., Stear, J.H., Noetzel, T.L., Al-Bassam, J., Kinoshita, K., Harrison, S.C., Howard, J., and Hyman, A.A. (2008). XMAP215 is a processive microtubule polymerase. Cell 132, 79-88.

Brownlee, C.W., Klebba, J.E., Buster, D.W., and Rogers, G.C. (2011). The Protein Phosphatase 2A regulatory subunit Twins stabilizes Plk4 to induce centriole amplification. J Cell Biol 195, 231-243.

Burd, C.G., Strochlic, T.I., and Gangi Setty, S.R. (2004). Arf-like GTPases: not so Arf-like after all. Trends Cell Biol 14, 687-694.

Cabernard, C., and Doe, C.Q. (2009). Apical/basal spindle orientation is required for neuroblast homeostasis and neuronal differentiation in Drosophila. Dev Cell 17, 134-141.

Cai, Y., Chia, W., and Yang, X. (2001). A family of snail-related zinc finger proteins regulates two distinct and parallel mechanisms that mediate Drosophila neuroblast asymmetric divisions. EMBO J 20, 1704-1714.

Cai, Y., Yu, F., Lin, S., Chia, W., and Yang, X. (2003). Apical complex genes control mitotic spindle geometry and relative size of daughter cells in Drosophila neuroblast and pI asymmetric divisions. Cell 112, 51-62.

Carmena, A., Makarova, A., and Speicher, S. (2011). The Rap1-Rgl-Ral signaling network regulates neuroblast cortical polarity and spindle orientation. J Cell Biol 195, 553-562.

Carney, T.D., Struck, A.J., and Doe, C.Q. (2013). midlife crisis encodes a conserved zinc-finger protein required to maintain neuronal differentiation in Drosophila. Development 140, 4155-4164.

Caussinus, E., and Gonzalez, C. (2005). Induction of tumor growth by altered stem-cell asymmetric division in Drosophila melanogaster. Nat Genet 37, 1125-1129.

Chabu, C., and Doe, C.Q. (2009). Twins/PP2A regulates aPKC to control neuroblast cell polarity and self-renewal. Dev Biol 330, 399-405.

Chang, K.C., Garcia-Alvarez, G., Somers, G., Sousa-Nunes, R., Rossi, F., Lee, Y.Y., Soon, S.B., Gonzalez, C., Chia, W., and Wang, H. (2010). Interplay between the transcription factor Zif and aPKC regulates neuroblast polarity and self-renewal. Dev Cell 19, 778-785.

Chell, J.M., and Brand, A.H. (2010). Nutrition-responsive glia control exit of neural stem cells from quiescence. Cell 143, 1161-1173.

Chen, K., Koe, C.T., Xing, Z.B., Tian, X., Rossi, F., Wang, C., Tang, Q., Zong, W., Hong, W.J., Taneja, R.*, et al.* (2016). Arl2- and Msps-dependent microtubule growth governs asymmetric division. J Cell Biol 212, 661-676.

Choksi, S.P., Southall, T.D., Bossing, T., Edoff, K., de Wit, E., Fischer, B.E., van Steensel, B., Micklem, G., and Brand, A.H. (2006). Prospero acts as a binary switch between self-renewal and differentiation in *Drosophila* neural stem cells. Dev Cell 11, 775-789.

Compton, D.A. (2000). Spindle assembly in animal cells. Annu Rev Biochem 69, 95-114.

Conduit, P.T., Brunk, K., Dobbelaere, J., Dix, C.I., Lucas, E.P., and Raff, J.W. (2010). Centrioles regulate centrosome size by controlling the rate of Cnn incorporation into the PCM. Curr Biol 20, 2178-2186.

Conduit, P.T., Feng, Z., Richens, J.H., Baumbach, J., Wainman, A., Bakshi, S.D., Dobbelaere, J., Johnson, S., Lea, S.M., and Raff, J.W. (2014a). The centrosome-specific phosphorylation of Cnn by Polo/Plk1 drives Cnn scaffold assembly and centrosome maturation. Dev Cell 28, 659-669.

Conduit, P.T., and Raff, J.W. (2010). Cnn dynamics drive centrosome size asymmetry to ensure daughter centriole retention in Drosophila neuroblasts. Curr Biol 20, 2187-2192.

Conduit, P.T., Richens, J.H., Wainman, A., Holder, J., Vicente, C.C., Pratt, M.B., Dix, C.I., Novak, Z.A., Dobbie, I.M., Schermelleh, L., and Raff, J.W. (2014b). A molecular mechanism of mitotic centrosome assembly in *Drosophila*. eLife 3, e03399.

Conduit, P.T., Wainman, A., and Raff, J.W. (2015). Centrosome function and assembly in animal cells. Nat Rev Mol Cell Biol 16, 611-624.

Cullen, C.F., Deak, P., Glover, D.M., and Ohkura, H. (1999). mini spindles: A gene encoding a conserved microtubule-associated protein required for the integrity of the mitotic spindle in Drosophila. J Cell Biol 146, 1005-1018.

Cunha-Ferreira, I., Rodrigues-Martins, A., Bento, I., Riparbelli, M., Zhang, W., Laue, E., Callaini, G., Glover, D.M., and Bettencourt-Dias, M. (2009). The SCF/Slimb ubiquitin ligase limits centrosome amplification through degradation of SAK/PLK4. Curr Biol 19, 43-49.

Cunningham, L.A., and Kahn, R.A. (2008). Cofactor D functions as a centrosomal protein and is required for the recruitment of the gamma-tubulin ring complex at centrosomes and organization of the mitotic spindle. J Biol Chem 283, 7155-7165.

Delgehyr, N., Rangone, H., Fu, J., Mao, G., Tom, B., Riparbelli, M.G., Callaini, G., and Glover, D.M. (2012). Klp10A, a microtubule-depolymerizing kinesin-13, cooperates with CP110 to control *Drosophila* centriole length. Curr Biol 22, 502-509.

Dho, S.E., Jacob, S., Wolting, C.D., French, M.B., Rohrschneider, L.R., and McGlade, C.J. (1998). The mammalian numb phosphotyrosine-binding domain. Characterization of binding specificity and identification of a novel PDZ domain-containing numb binding protein, LNX. J Biol Chem 273, 9179-9187.

Dick, T., Ray, K., Salz, H.K., and Chia, W. (1996). Cytoplasmic dynein (ddlc1) mutations cause morphogenetic defects and apoptotic cell death in Drosophila melanogaster. Mol Cell Biol 16, 1966-1977.

Dobbelaere, J., Josue, F., Suijkerbuijk, S., Baum, B., Tapon, N., and Raff, J. (2008). A genome-wide RNAi screen to dissect centriole duplication and centrosome maturation in Drosophila. PLoS Biol 6, e224.

Doe, C.Q., Chu-LaGraff, Q., Wright, D.M., and Scott, M.P. (1991). The prospero gene specifies cell fates in the Drosophila central nervous system. Cell 65, 451-464.

Dzhindzhev, N.S., Tzolovsky, G., Lipinszki, Z., Schneider, S., Lattao, R., Fu, J., Debski, J., Dadlez, M., and Glover, D.M. (2014). Plk4 phosphorylates Ana2 to trigger Sas6 recruitment and procentriole formation. Curr Biol 24, 2526-2532.

Dzhindzhev, N.S., Yu, Q.D., Weiskopf, K., Tzolovsky, G., Cunha-Ferreira, I., Riparbelli, M., Rodrigues-Martins, A., Bettencourt-Dias, M., Callaini, G., and Glover, D.M. (2010). Asterless is a scaffold for the onset of centriole assembly. Nature 467, 714-718.

Eroglu, E., Burkard, T.R., Jiang, Y., Saini, N., Homem, C.C., Reichert, H., and Knoblich, J.A. (2014). SWI/SNF complex prevents lineage reversion and induces temporal patterning in neural stem cells. Cell 156, 1259-1273.

Fanarraga, M.L., Bellido, J., Jaen, C., Villegas, J.C., and Zabala, J.C. (2010). TBCD links centriologenesis, spindle microtubule dynamics, and midbody abscission in human cells. PloS one 5, e8846.

Froldi, F., Szuperak, M., Weng, C.F., Shi, W., Papenfuss, A.T., and Cheng, L.Y. (2015). The transcription factor Nerfin-1 prevents reversion of neurons into neural stem cells. Gene Dev 29, 129-143.

Fry, A.M., Mayor, T., Meraldi, P., Stierhof, Y.D., Tanaka, K., and Nigg, E.A. (1998a). C-Nap1, a novel centrosomal coiled-coil protein and candidate substrate of the cell cycle-regulated protein kinase Nek2. J Cell Biol 141, 1563-1574.

Fry, A.M., Meraldi, P., and Nigg, E.A. (1998b). A centrosomal function for the human Nek2 protein kinase, a member of the NIMA family of cell cycle regulators. EMBO J 17, 470-481.

Fu, J., and Glover, D.M. (2012). Structured illumination of the interface between centriole and peri-centriolar material. Open Biol 2, 120104.

Fu, J., Hagan, I.M., and Glover, D.M. (2015). The centrosome and its duplication cycle. Cold Spring Harb Perspect Biol 7, a015800.

Fuerstenberg, S., Peng, C.Y., Alvarez-Ortiz, P., Hor, T., and Doe, C.Q. (1998). Identification of Miranda protein domains regulating asymmetric cortical localization, cargo binding, and cortical release. Mol Cell Neurosci 12, 325-339.

Fuse, N., Hisata, K., Katzen, A.L., and Matsuzaki, F. (2003). Heterotrimeric G proteins regulate daughter cell size asymmetry in *Drosophila* neuroblast divisions. Curr Biol 13, 947-954.

Gallaud, E., Caous, R., Pascal, A., Bazile, F., Gagne, J.P., Huet, S., Poirier, G.G., Chretien, D., Richard-Parpaillon, L., and Giet, R. (2014). Ensconsin/Map7 promotes microtubule growth and centrosome separation in Drosophila neural stem cells. J Cell Biol 204, 1111-1121.

Garcia-Bellido, A., and Santamaria, P. (1978). Developmental Analysis of the Achaete-Scute System of *DROSOPHILA MELANOGASTER*. Genetics 88, 469-486.

Gergely, F., Draviam, V.M., and Raff, J.W. (2003). The ch-TOG/XMAP215 protein is essential for spindle pole organization in human somatic cells. Gene Dev 17, 336-341.

Gergely, F., Kidd, D., Jeffers, K., Wakefield, J.G., and Raff, J.W. (2000). D-TACC: a novel centrosomal protein required for normal spindle function in the early Drosophila embryo. EMBO J 19, 241-252.

Giansanti, M.G., Gatti, M., and Bonaccorsi, S. (2001). The role of centrosomes and astral microtubules during asymmetric division of Drosophila neuroblasts. Development 128, 1137-1145.

Giet, R., McLean, D., Descamps, S., Lee, M.J., Raff, J.W., Prigent, C., and Glover, D.M. (2002). Drosophila Aurora A kinase is required to localize D-TACC to centrosomes and to regulate astral microtubules. J. Cell Biol 156, 437-451.

Gingras, A.C., Caballero, M., Zarske, M., Sanchez, A., Hazbun, T.R., Fields, S., Sonenberg, N., Hafen, E., Raught, B., and Aebersold, R. (2005). A novel, evolutionarily conserved protein phosphatase complex involved in cisplatin sensitivity. Mol Cell Proteomics 4, 1725-1740.

Gonzalez, C. (2007). Spindle orientation, asymmetric division and tumour suppression in Drosophila stem cells. Nat Rev Genet 8, 462-472.
Gopalakrishnan, J., Chim, Y.C., Ha, A., Basiri, M.L., Lerit, D.A., Rusan, N.M., and Avidor-Reiss, T. (2012). Tubulin nucleotide status controls Sas-4-dependent pericentriolar material recruitment. Nat Cell Biol 14, 865-873.
Grosskortenhaus, R., Pearson, B.J., Marusich, A., and Doe, C.Q. (2005). Regulation of temporal identity transitions in Drosophila neuroblasts. Dev Cell 8, 193-202.
Hage-Sleiman, R., Herveau, S., Matera, E.L., Laurier, J.F., and Dumontet, C. (2010). Tubulin binding cofactor C (TBCC) suppresses tumor growth and enhances chemosensitivity in human breast cancer cells. BMC Cancer 10, 135.
Hage-Sleiman, R., Herveau, S., Matera, E.L., Laurier, J.F., and Dumontet, C. (2011). Silencing of tubulin binding cofactor C modifies microtubule dynamics and cell cycle distribution and enhances sensitivity to gemcitabine in breast cancer cells. Mol Cancer Ther 10, 303-312.
Heitzler, P., Bourouis, M., Ruel, L., Carteret, C., and Simpson, P. (1996). Genes of the Enhancer of split and achaete-scute complexes are required for a regulatory loop between Notch and Delta during lateral signalling in Drosophila. Development 122, 161-171.
Heitzler, P., and Simpson, P. (1991). The choice of cell fate in the epidermis of Drosophila. Cell 64, 1083-1092.
Helps, N.R., Luo, X., Barker, H.M., and Cohen, P.T. (2000). NIMA-related kinase 2 (Nek2), a cell-cycle-regulated protein kinase localized to centrosomes, is complexed to protein phosphatase 1. Biochem J 349, 509-518.
Heraud-Farlow, J.E., and Kiebler, M.A. (2014). The multifunctional Staufen proteins: conserved roles from neurogenesis to synaptic plasticity. Trends Neurosci 37, 470-479.
Hirata, J., Nakagoshi, H., Nabeshima, Y., and Matsuzaki, F. (1995). Asymmetric segregation of the homeodomain protein Prospero during Drosophila development. Nature 377, 627-630.
Hoch, M., and Jackle, H. (1998). Kruppel acts as a developmental switch gene that mediates Notch signalling-dependent tip cell differentiation in the excretory organs of Drosophila. EMBO J 17, 5766-5775.
Holloway, S.L., Glotzer, M., King, R.W., and Murray, A.W. (1993). Anaphase is initiated by proteolysis rather than by the inactivation of maturation-promoting factor. Cell 73, 1393-1402.
Homem, C.C., and Knoblich, J.A. (2012). Drosophila neuroblasts: a model for stem cell biology. Development 139, 4297-4310.
Hutterer, A., Betschinger, J., Petronczki, M., and Knoblich, J.A. (2004). Sequential roles of Cdc42, Par-6, aPKC, and Lgl in the establishment of epithelial polarity during Drosophila embryogenesis. Dev Cell 6, 845-854.
Ikeshima-Kataoka, H., Skeath, J.B., Nabeshima, Y., Doe, C.Q., and Matsuzaki, F. (1997). Miranda directs Prospero to a daughter cell during Drosophila asymmetric divisions. Nature 390, 625-629.
Isshiki, T., Pearson, B., Holbrook, S., and Doe, C.Q. (2001). Drosophila neuroblasts sequentially express transcription factors which specify the temporal identity of their neuronal progeny. Cell 106, 511-521.
Ito, K., and Hotta, Y. (1992). Proliferation pattern of postembryonic neuroblasts in the brain of Drosophila melanogaster. Dev Biol 149, 134-148.

Izumi, Y., Ohta, N., Hisata, K., Raabe, T., and Matsuzaki, F. (2006). Drosophila Pins-binding protein Mud regulates spindle-polarity coupling and centrosome organization. Nat Cell Biol 8, 586-593.

Janssens, D.H., Komori, H., Grbac, D., Chen, K., Koe, C.T., Wang, H., and Lee, C.Y. (2014). Earmuff restricts progenitor cell potential by attenuating the competence to respond to self-renewal factors. Development 141, 1036-1046.

Janssens, V., and Goris, J. (2001). Protein phosphatase 2A: a highly regulated family of serine/threonine phosphatases implicated in cell growth and signalling. Biochem J 353, 417-439.

Januschke, J., and Gonzalez, C. (2010). The interphase microtubule aster is a determinant of asymmetric division orientation in Drosophila neuroblasts. J Cell Biol 188, 693-706.

Januschke, J., Llamazares, S., Reina, J., and Gonzalez, C. (2011). Drosophila neuroblasts retain the daughter centrosome. Nat Commun 2, 243.

Januschke, J., Reina, J., Llamazares, S., Bertran, T., Rossi, F., Roig, J., and Gonzalez, C. (2013). Centrobin controls mother-daughter centriole asymmetry in Drosophila neuroblasts. Nat Cell Biol 15, 241-248.

Jia, M., Shan, Z., Yang, Y., Liu, C., Li, J., Luo, Z.G., Zhang, M., Cai, Y., Wen, W., and Wang, W. (2015). The structural basis of Miranda-mediated Staufen localization during Drosophila neuroblast asymmetric division. Nat Commun 6, 8381.

Jin, S., Pan, L., Liu, Z., Wang, Q., Xu, Z., and Zhang, Y.Q. (2009). Drosophila Tubulin-specific chaperone E functions at neuromuscular synapses and is required for microtubule network formation. Development 136, 1571-1581.

Johnston, C.A., Hirono, K., Prehoda, K.E., and Doe, C.Q. (2009). Identification of an Aurora-A/PinsLINKER/Dlg spindle orientation pathway using induced cell polarity in S2 cells. Cell 138, 1150-1163.

Kahn, R.A., Volpicelli-Daley, L., Bowzard, B., Shrivastava-Ranjan, P., Li, Y., Zhou, C., and Cunningham, L. (2005). Arf family GTPases: roles in membrane traffic and microtubule dynamics. Biochem Soc T 33, 1269-1272.

Kaltschmidt, J.A., Davidson, C.M., Brown, N.H., and Brand, A.H. (2000). Rotation and asymmetry of the mitotic spindle direct asymmetric cell division in the developing central nervous system. Nat Cell Biol 2, 7-12.

Kambadur, R., Koizumi, K., Stivers, C., Nagle, J., Poole, S.J., and Odenwald, W.F. (1998). Regulation of POU genes by castor and hunchback establishes layered compartments in the Drosophila CNS. Gene Dev 12, 246-260.

Kanai, M.I., Okabe, M., and Hiromi, Y. (2005). seven-up Controls switching of transcription factors that specify temporal identities of Drosophila neuroblasts. Dev Cell 8, 203-213.

Kemphues, K.J., Wolf, N., Wood, W.B., and Hirsh, D. (1986). Two loci required for cytoplasmic organization in early embryos of Caenorhabditis elegans. Dev Biol 113, 449-460.

Klebba, J.E., Buster, D.W., Nguyen, A.L., Swatkoski, S., Gucek, M., Rusan, N.M., and Rogers, G.C. (2013). Polo-like kinase 4 autodestructs by generating its Slimb-binding phosphodegron. Curr Biol 23, 2255-2261.

Knoblich, J.A. (2010). Asymmetric cell division: recent developments and their implications for tumour biology. Nat Rev Mol Cell Biol 11, 849-860.

Knoblich, J.A., Jan, L.Y., and Jan, Y.N. (1995). Asymmetric segregation of Numb and Prospero during cell division. Nature 377, 624-627.

Koe, C.T., Li, S., Rossi, F., Wong, J.J., Wang, Y., Zhang, Z., Chen, K., Aw, S.S., Richardson, H.E., Robson, P.*, et al.* (2014). The Brm-HDAC3-Erm repressor complex suppresses dedifferentiation in Drosophila type II neuroblast lineages. eLife 3, e01906.

Komori, H., Xiao, Q., McCartney, B.M., and Lee, C.Y. (2014). Brain tumor specifies intermediate progenitor cell identity by attenuating beta-catenin/Armadillo activity. Development 141, 51-62.

Koushika, S.P., Lisbin, M.J., and White, K. (1996). ELAV, a Drosophila neuron-specific protein, mediates the generation of an alternatively spliced neural protein isoform. Curr Biol 6, 1634-1641.

Koushika, S.P., Soller, M., and White, K. (2000). The neuron-enriched splicing pattern of Drosophila erect wing is dependent on the presence of ELAV protein. Mol Cell Biol 20, 1836-1845.

Krahn, M.P., Egger-Adam, D., and Wodarz, A. (2009). PP2A antagonizes phosphorylation of Bazooka by PAR-1 to control apical-basal polarity in dividing embryonic neuroblasts. Dev Cell 16, 901-908.

Kraut, R., Chia, W., Jan, L.Y., Jan, Y.N., and Knoblich, J.A. (1996). Role of inscuteable in orienting asymmetric cell divisions in Drosophila. Nature 383, 50-55.

Kuchinke, U., Grawe, F., and Knust, E. (1998). Control of spindle orientation in Drosophila by the Par-3-related PDZ-domain protein Bazooka. Curr Biol 8, 1357-1365.

Kuh, G.F., Stockmann, M., Meyer-Ohlendorf, M., Linta, L., Proepper, C., Ludolph, A.C., Bockmann, J., Boeckers, T.M., and Liebau, S. (2012). Tubulin-binding cofactor B is a direct interaction partner of the dynactin subunit p150(Glued). Cell Tissue Res 350, 13-26.

Lai, S.L., and Doe, C.Q. (2014). Transient nuclear Prospero induces neural progenitor quiescence. eLife 3, e03363.

Lai, S.L., Miller, M.R., Robinson, K.J., and Doe, C.Q. (2012). The Snail family member Worniu is continuously required in neuroblasts to prevent Elav-induced premature differentiation. Dev Cell 23, 849-857.

Lee, C.Y., Andersen, R.O., Cabernard, C., Manning, L., Tran, K.D., Lanskey, M.J., Bashirullah, A., and Doe, C.Q. (2006a). Drosophila Aurora-A kinase inhibits neuroblast self-renewal by regulating aPKC/Numb cortical polarity and spindle orientation. Gene Dev 20, 3464-3474.

Lee, C.Y., Robinson, K.J., and Doe, C.Q. (2006b). Lgl, Pins and aPKC regulate neuroblast self-renewal versus differentiation. Nature 439, 594-598.

Lee, C.Y., Wilkinson, B.D., Siegrist, S.E., Wharton, R.P., and Doe, C.Q. (2006c). Brat is a Miranda cargo protein that promotes neuronal differentiation and inhibits neuroblast self-renewal. Dev Cell 10, 441-449.

Lee, M.J., Gergely, F., Jeffers, K., Peak-Chew, S.Y., and Raff, J.W. (2001). Msps/XMAP215 interacts with the centrosomal protein D-TACC to regulate microtubule behaviour. Nat Cell Biol 3, 643-649.

Lee, T., and Luo, L. (1999). Mosaic analysis with a repressible cell marker for studies of gene function in neuronal morphogenesis. Neuron 22, 451-461.

Lerit, D.A., and Rusan, N.M. (2013). PLP inhibits the activity of interphase centrosomes to ensure their proper segregation in stem cells. J Cell Biol 202, 1013-1022.

Lewis, S.A., Tian, G., and Cowan, N.J. (1997). The alpha- and beta-tubulin folding pathways. Trends Cell Biol 7, 479-484.

Li, H.P., Liu, Z.M., and Nirenberg, M. (1997a). Kinesin-73 in the nervous system of Drosophila embryos. Proc Natl Acad Sci USA 94, 1086-1091.

Li, L., and Vaessin, H. (2000). Pan-neural Prospero terminates cell proliferation during Drosophila neurogenesis. Gene Dev 14, 147-151.

Li, P., Yang, X., Wasser, M., Cai, Y., and Chia, W. (1997b). Inscuteable and Staufen mediate asymmetric localization and segregation of prospero RNA during Drosophila neuroblast cell divisions. Cell 90, 437-447.

Li, S., Wang, C., Sandanaraj, E., Aw, S.S., Koe, C.T., Wong, J.J., Yu, F., Ang, B.T., Tang, C., and Wang, H. (2014a). The SCFSlimb E3 ligase complex regulates asymmetric division to inhibit neuroblast overgrowth. EMBO Rep 15, 165-174.

Li, S., Wang, H., and Groth, C. (2014b). Drosophila neuroblasts as a new model for the study of stem cell self-renewal and tumour formation. Bioscience Rep 34.

Lisbin, M.J., Qiu, J., and White, K. (2001). The neuron-specific RNA-binding protein ELAV regulates neuroglian alternative splicing in neurons and binds directly to its pre-mRNA. Gene Dev 15, 2546-2561.

Llamazares, S., Moreira, A., Tavares, A., Girdham, C., Spruce, B.A., Gonzalez, C., Karess, R.E., Glover, D.M. and Sunkel, C.E. (1991). polo encodes a protein kinase homolog required for mitosis in Drosophila. Gene Dev 5, 2153-2165.

Lopez-Fanarraga, M., Carranza, G., Bellido, J., Kortazar, D., Villegas, J.C., and Zabala, J.C. (2007). Tubulin cofactor B plays a role in the neuronal growth cone. J Neurochem 100, 1680-1687.

Lu, B., Ackerman, L., Jan, L.Y., and Jan, Y.N. (1999). Modes of protein movement that lead to the asymmetric localization of partner of Numb during Drosophila neuroblast division. Mol Cell 4, 883-891.

Lu, B., Rothenberg, M., Jan, L.Y., and Jan, Y.N. (1998). Partner of Numb colocalizes with Numb during mitosis and directs Numb asymmetric localization in Drosophila neural and muscle progenitors. Cell 95, 225-235.

Lundin, V.F., Leroux, M.R., and Stirling, P.C. (2010). Quality control of cytoskeletal proteins and human disease. Trends Biochem Sci 35, 288-297.

Luo, L., Liao, Y.J., Jan, L.Y., and Jan, Y.N. (1994). Distinct morphogenetic functions of similar small GTPases: Drosophila Drac1 is involved in axonal outgrowth and myoblast fusion. Gene Dev 8, 1787-1802.

Mardin, B.R., Lange, C., Baxter, J.E., Hardy, T., Scholz, S.R., Fry, A.M., and Schiebel, E. (2010). Components of the Hippo pathway cooperate with Nek2 kinase to regulate centrosome disjunction. Nat Cell Biol 12, 1166-1176.

Martin-Bermudo, M.D., Martinez, C., Rodriguez, A., and Jimenez, F. (1991). Distribution and function of the lethal of scute gene product during early neurogenesis in Drosophila. Development 113, 445-454.

Martin, N., Jaubert, J., Gounon, P., Salido, E., Haase, G., Szatanik, M., and Guenet, J.L. (2002). A missense mutation in Tbce causes progressive motor neuronopathy in mice. Nat Genet 32, 443-447.

Matsuzaki, F., Ohshiro, T., Ikeshima-Kataoka, H., and Izumi, H. (1998). miranda localizes staufen and prospero asymmetrically in mitotic neuroblasts and epithelial cells in early Drosophila embryogenesis. Development 125, 4089-4098.

Maurange, C., Cheng, L., and Gould, A.P. (2008). Temporal transcription factors and their targets schedule the end of neural proliferation in Drosophila. Cell 133, 891-902.

Megraw, T.L., Li, K., Kao, L.R., and Kaufman, T.C. (1999). The centrosomin protein is required for centrosome assembly and function during cleavage in Drosophila. Development 126, 2829-2839.

Merkle, F.T., and Alvarez-Buylla, A. (2006). Neural stem cells in mammalian development. Curr Opin Cell Biol 18, 704-709.

Mettler, U., Vogler, G., and Urban, J. (2006). Timing of identity: spatiotemporal regulation of hunchback in neuroblast lineages of Drosophila by Seven-up and Prospero. Development 133, 429-437.

Mimori-Kiyosue, Y., Shiina, N., and Tsukita, S. (2000). The dynamic behavior of the APC-binding protein EB1 on the distal ends of microtubules. Curr Biol 10, 865-868.

Mori, R., and Toda, T. (2013). The dual role of fission yeast Tbc1/cofactor C orchestrates microtubule homeostasis in tubulin folding and acts as a GAP for GTPase Alp41/Arl2. Mol Biol Cell 24, 1713-1724, S1711-1718.

Morin, X., Daneman, R., Zavortink, M., and Chia, W. (2001). A protein trap strategy to detect GFP-tagged proteins expressed from their endogenous loci in Drosophila. Proc Natl Acad Sci USA 98, 15050-15055.

Motegi, F., Zonies, S., Hao, Y., Cuenca, A.A., Griffin, E., and Seydoux, G. (2011). Microtubules induce self-organization of polarized PAR domains in Caenorhabditis elegans zygotes. Nat Cell Biol 13, 1361-1367.

Neumuller, R.A., Richter, C., Fischer, A., Novatchkova, M., Neumuller, K.G., and Knoblich, J.A. (2011). Genome-wide analysis of self-renewal in Drosophila neural stem cells by transgenic RNAi. Cell Stem Cell 8, 580-593.

Nigg, E.A., and Stearns, T. (2011). The centrosome cycle: Centriole biogenesis, duplication and inherent asymmetries. Nat Cell Biol 13, 1154-1160.

Nipper, R.W., Siller, K.H., Smith, N.R., Doe, C.Q., and Prehoda, K.E. (2007). Galphai generates multiple Pins activation states to link cortical polarity and spindle orientation in Drosophila neuroblasts. Proc Natl Acad Sci USA 104, 14306-14311.

Nithianantham, S., Le, S., Seto, E., Jia, W., Leary, J., Corbett, K.D., Moore, J.K., and Al-Bassam, J. (2015). Tubulin cofactors and Arl2 are cage-like chaperones that regulate the soluble alphabeta-tubulin pool for microtubule dynamics. eLife 4.

Noda, Y., Kohjima, M., Izaki, T., Ota, K., Yoshinaga, S., Inagaki, F., Ito, T., and Sumimoto, H. (2003). Molecular recognition in dimerization between PB1 domains. J Biol Chem 278, 43516-43524.

Nurse, P. (1990). Universal control mechanism regulating onset of M-phase. Nature 344, 503-508.

Ogawa, H., Ohta, N., Moon, W., and Matsuzaki, F. (2009). Protein phosphatase 2A negatively regulates aPKC signaling by modulating phosphorylation of Par-6 in Drosophila neuroblast asymmetric divisions. J Cell Sci 122, 3242-3249.

Ohshiro, T., Yagami, T., Zhang, C., and Matsuzaki, F. (2000). Role of cortical tumour-suppressor proteins in asymmetric division of Drosophila neuroblast. Nature 408: 593-596.

Okumura, M., Sakuma, C., Miura, M., and Chihara, T. (2015). Linking cell surface receptors to microtubules: tubulin folding cofactor D mediates Dscam functions during neuronal morphogenesis. J Neurosci 35, 1979-1990.

Ouyang, Y., Petritsch, C., Wen, H., Jan, L., Jan, Y.N., and Lu, B. (2011). Dronc caspase exerts a non-apoptotic function to restrain phospho-Numb-induced ectopic neuroblast formation in Drosophila. Development 138, 2185-2196.

Pandey, U.B., and Nichols, C.D. (2011). Human disease models in Drosophila melanogaster and the role of the fly in therapeutic drug discovery. Pharmaco Rev 63, 411-436.

Parvari, R., Hershkovitz, E., Grossman, N., Gorodischer, R., Loeys, B., Zecic, A., Mortier, G., Gregory, S., Sharony, R., Kambouris, M.*, et al.* (2002). Mutation of TBCE causes hypoparathyroidism-retardation-dysmorphism and autosomal recessive Kenny-Caffey syndrome. Nat Genet 32, 448-452.

Pearson, B.J., and Doe, C.Q. (2003). Regulation of neuroblast competence in Drosophila. Nature 425, 624-628.

Peterson, C., Carney, G.E., Taylor, B.J., and White, K. (2002). reaper is required for neuroblast apoptosis during Drosophila development. Development 129, 1467-1476.

Petronczki, M., and Knoblich, J.A. (2001). DmPAR-6 directs epithelial polarity and asymmetric cell division of neuroblasts in Drosophila. Nat Cell Biol 3, 43-49.

Rebollo, E., Sampaio, P., Januschke, J., Llamazares, S., Varmark, H., and Gonzalez, C. (2007). Functionally unequal centrosomes drive spindle orientation in asymmetrically dividing Drosophila neural stem cells. Dev Cell 12, 467-474.

Reichert, H. (2011). Drosophila neural stem cells: cell cycle control of self-renewal, differentiation, and termination in brain development. Results and problems in cell differentiation 53, 529-546.

Richardson, H., O'Keefe, L.V., Marty, T., and Saint, R. (1995). Ectopic cyclin E expression induces premature entry into S phase and disrupts pattern formation in the Drosophila eye imaginal disc. Development 121, 3371-3379.

Riparbelli, M.G., Gottardo, M., Glover, D.M., and Callaini, G. (2014). Inhibition of Polo kinase by BI2536 affects centriole separation during Drosophila male meiosis. Cell Cycle 13, 2064-2072.

Roberts, A.J., Kon, T., Knight, P.J., Sutoh, K., and Burgess, S.A. (2013). Functions and mechanics of dynein motor proteins. Nat Rev Mol Cell Biol 14, 713-726.

Robinow, S., and White, K. (1988). The locus elav of Drosophila melanogaster is expressed in neurons at all developmental stages. Dev Biol 126, 294-303.

Rodrigues-Martins, A., Bettencourt-Dias, M., Riparbelli, M., Ferreira, C., Ferreira, I., Callaini, G., and Glover, D.M. (2007a). DSAS-6 organizes a tube-like centriole precursor, and its absence suggests modularity in centriole assembly. Curr Biol 17, 1465-1472.

Rodrigues-Martins, A., Riparbelli, M., Callaini, G., Glover, D.M., and Bettencourt-Dias, M. (2007b). Revisiting the role of the mother centriole in centriole biogenesis. Science 316, 1046-1050.

Rolls, M.M., Albertson, R., Shih, H.P., Lee, C.Y., and Doe, C.Q. (2003). Drosophila aPKC regulates cell polarity and cell proliferation in neuroblasts and epithelia. J Cell Biol 163, 1089-1098.

Rusan, N.M., and Peifer, M. (2007). A role for a novel centrosome cycle in asymmetric cell division. J Cell Biol 177, 13-20.

Schaefer, M., Petronczki, M., Dorner, D., Forte, M., and Knoblich, J.A. (2001). Heterotrimeric G proteins direct two modes of asymmetric cell division in the Drosophila nervous system. Cell 107, 183-194.

Schaefer, M., Shevchenko, A., Shevchenko, A., and Knoblich, J.A. (2000). A protein complex containing Inscuteable and the Galpha-binding protein Pins orients asymmetric cell divisions in Drosophila. Curr Biol 10, 353-362.

Schober, M., Schaefer, M., and Knoblich, J.A. (1999). Bazooka recruits Inscuteable to orient asymmetric cell divisions in Drosophila neuroblasts. Nature 402, 548-551.

Schuldt, A.J., Adams, J.H., Davidson, C.M., Micklem, D.R., Haseloff, J., St Johnston, D., and Brand, A.H. (1998). Miranda mediates asymmetric protein and RNA localization in the developing nervous system. Gene Dev 12, 1847-1857.

Sharer, J.D., Shern, J.F., Van Valkenburgh, H., Wallace, D.C., and Kahn, R.A. (2002). ARL2 and BART enter mitochondria and bind the adenine nucleotide transporter. Mol Biol Cell 13, 71-83.

Shen, C.P., Jan, L.Y., and Jan, Y.N. (1997). Miranda is required for the asymmetric localization of Prospero during mitosis in Drosophila. Cell 90, 449-458.

Shern, J.F., Sharer, J.D., Pallas, D.C., Bartolini, F., Cowan, N.J., Reed, M.S., Pohl, J., and Kahn, R.A. (2003). Cytosolic Arl2 is complexed with cofactor D and protein phosphatase 2A. J Biol Chem 278, 40829-40836.

Siegrist, S.E., and Doe, C.Q. (2005). Microtubule-induced Pins/Galphai cortical polarity in Drosophila neuroblasts. Cell 123, 1323-1335.

Siller, K.H., Cabernard, C., and Doe, C.Q. (2006). The NuMA-related Mud protein binds Pins and regulates spindle orientation in Drosophila neuroblasts. Nat Cell Biol 8, 594-600.

Siller, K.H., and Doe, C.Q. (2008). Lis1/dynactin regulates metaphase spindle orientation in Drosophila neuroblasts. Dev Biol 319, 1-9.

Singh, P., Ramdas Nair, A., and Cabernard, C. (2014). The centriolar protein Bld10/Cep135 is required to establish centrosome asymmetry in Drosophila neuroblasts. Curr Biol 24, 1548-1555.

Skeath, J.B., and Carroll, S.B. (1992). Regulation of proneural gene expression and cell fate during neuroblast segregation in the Drosophila embryo. Development 114, 939-946.

Skeath, J.B., and Doe, C.Q. (1998). Sanpodo and Notch act in opposition to Numb to distinguish sibling neuron fates in the Drosophila CNS. Development 125, 1857-1865.

Skeath, J.B., and Thor, S. (2003). Genetic control of Drosophila nerve cord development. Curr Biol Neurosci 13, 8-15.

Slack, C., Overton, P.M., Tuxworth, R.I., and Chia, W. (2007). Asymmetric localisation of Miranda and its cargo proteins during neuroblast division requires the anaphase-promoting complex/cyclosome. Development 134, 3781-3787.

Smith, C.A., Lau, K.M., Rahmani, Z., Dho, S.E., Brothers, G., She, Y.M., Berry, D.M., Bonneil, E., Thibault, P., Schweisguth, F.*, et al.* (2007). aPKC-mediated phosphorylation regulates asymmetric membrane localization of the cell fate determinant Numb. EMBO J 26, 468-480.

Song, Y., and Lu, B. (2012). Interaction of Notch signaling modulator Numb with alpha-Adaptin regulates endocytosis of Notch pathway components and cell fate determination of neural stem cells. J Biol Chem 287, 17716-17728.

Sonoda, J., and Wharton, R.P. (2001). Drosophila Brain Tumor is a translational repressor. Gene Dev 15, 762-773.

Sousa-Nunes, R., Chia, W., and Somers, W.G. (2009). Protein phosphatase 4 mediates localization of the Miranda complex during Drosophila neuroblast asymmetric divisions. Gene Dev 23, 359-372.

Sousa-Nunes, R., Yee, L.L., and Gould, A.P. (2011). Fat cells reactivate quiescent neuroblasts via TOR and glial insulin relays in Drosophila. Nature 471, 508-512.

Southall, T.D., Davidson, C.M., Miller, C., Carr, A., and Brand, A.H. (2014). Dedifferentiation of neurons precedes tumor formation in Lola mutants. Dev Cell 28, 685-696.

Spana, E.P., and Doe, C.Q. (1995). The prospero transcription factor is asymmetrically localized to the cell cortex during neuroblast mitosis in Drosophila. Development 121, 3187-3195.

Speicher, S., Fischer, A., Knoblich, J., and Carmena, A. (2008). The PDZ protein Canoe regulates the asymmetric division of Drosophila neuroblasts and muscle progenitors. Curr Biol 18, 831-837.

St Johnston, D. (2002). The art and design of genetic screens: Drosophila melanogaster. Nat Rev Genet 3, 176-188.

St Johnston, D., Beuchle, D., and Nusslein-Volhard, C. (1991). Staufen, a gene required to localize maternal RNAs in the Drosophila egg. Cell 66, 51-63.

Stevens, N.R., Dobbelaere, J., Brunk, K., Franz, A., and Raff, J.W. (2010). Drosophila Ana2 is a conserved centriole duplication factor. J Cell Biol 188, 313-323.

Suzuki, A., and Ohno, S. (2006). The PAR-aPKC system: lessons in polarity. J Cell Sci 119, 979-987.

Tian, G., Bhamidipati, A., Cowan, N.J., and Lewis, S.A. (1999). Tubulin folding cofactors as GTPase-activating proteins. GTP hydrolysis and the assembly of the alpha/beta-tubulin heterodimer. J Biol Chem 274, 24054-24058.

Tian, G., Huang, Y., Rommelaere, H., Vandekerckhove, J., Ampe, C., and Cowan, N.J. (1996). Pathway leading to correctly folded beta-tubulin. Cell 86, 287-296.

Tian, G., Lewis, S.A., Feierbach, B., Stearns, T., Rommelaere, H., Ampe, C., and Cowan, N.J. (1997). Tubulin subunits exist in an activated conformational state generated and maintained by protein cofactors. J Cell Biol 138, 821-832.

Tio, M., Udolph, G., Yang, X., and Chia, W. (2001). cdc2 links the Drosophila cell cycle and asymmetric division machineries. Nature 409, 1063-1067.

Tio, M., Zavortink, M., Yang, X., and Chia, W. (1999). A functional analysis of inscuteable and its roles during Drosophila asymmetric cell divisions. J Cell Sci 112, 1541-1551.

Truman, J.W., and Bate, M. (1988). Spatial and temporal patterns of neurogenesis in the central nervous system of Drosophila melanogaster. Dev Biol 125, 145-157.

Uemura, T., Shepherd, S., Ackerman, L., Jan, L.Y., and Jan, Y.N. (1989). numb, a gene required in determination of cell fate during sensory organ formation in Drosophila embryos. Cell 58, 349-360.

Vaessin, H., Grell, E., Wolff, E., Bier, E., Jan, L.Y., and Jan, Y.N. (1991). prospero is expressed in neuronal precursors and encodes a nuclear protein that is involved in the control of axonal outgrowth in Drosophila. Cell 67, 941-953.

Vaizel-Ohayon, D., and Schejter, E.D. (1999). Mutations in centrosomin reveal requirements for centrosomal function during early Drosophila embryo-genesis. Curr Biol 9, 889-898.

Varmark, H., Llamazares, S., Rebollo, E., Lange, B., Reina, J., Schwarz, H., and Gonzalez, C. (2007). Asterless is a centriolar protein required for centrosome function and embryo development in Drosophila. Curr Biol 17, 1735-1745.

Verdi, J.M., Schmandt, R., Bashirullah, A., Jacob, S., Salvino, R., Craig, C.G., Program, A.E., Lipshitz, H.D., and McGlade, C.J. (1996). Mammalian NUMB is an evolutionarily conserved signaling adapter protein that specifies cell fate. Curr Biol 6, 1134-1145.

Verollet, C., Colombie, N., Daubon, T., Bourbon, H.M., Wright, M., and Raynaud-Messina, B. (2006). Drosophila melanogaster gamma-TuRC is dispensable for targeting gamma-tubulin to the centrosome and microtubule nucleation. J Cell Biol 172, 517-528.

Villares, R., and Cabrera, C.V. (1987). The achaete-scute gene complex of D. melanogaster: conserved domains in a subset of genes required for neurogenesis and their homology to myc. Cell 50, 415-424.

Wang, C., Chang, K.C., Somers, G., Virshup, D., Ang, B.T., Tang, C., Yu, F., and Wang, H. (2009a). Protein phosphatase 2A regulates self-renewal of Drosophila neural stem cells. Development 136, 2287-2296.

Wang, C., Li, S., Januschke, J., Rossi, F., Izumi, Y., Garcia-Alvarez, G., Gwee, S.S., Soon, S.B., Sidhu, H.K., Yu, F.*, et al.* (2011). An ana2/ctp/mud complex regulates spindle orientation in Drosophila neuroblasts. Dev Cell 21, 520-533.

Wang, H., Ng, K.H., Qian, H., Siderovski, D.P., Chia, W., and Yu, F. (2005). Ric-8 controls Drosophila neural progenitor asymmetric division by regulating heterotrimeric G proteins. Nat Cell Biol 7, 1091-1098.

Wang, H., Ouyang, Y., Somers, W.G., Chia, W., and Lu, B. (2007). Polo inhibits progenitor self-renewal and regulates Numb asymmetry by phosphorylating Pon. Nature 449, 96-100.

Wang, H., Somers, G.W., Bashirullah, A., Heberlein, U., Yu, F., and Chia, W. (2006). Aurora-A acts as a tumor suppressor and regulates self-renewal of Drosophila neuroblasts. Gene Dev 20, 3453-3463.

Wang, X., Tsai, J.W., Imai, J.H., Lian, W.N., Vallee, R.B., and Shi, S.H. (2009b). Asymmetric centrosome inheritance maintains neural progenitors in the neocortex. Nature 461, 947-955.

Weng, M., Golden, K.L., and Lee, C.Y. (2010). dFezf/Earmuff maintains the restricted developmental potential of intermediate neural progenitors in Drosophila. Dev Cell 18, 126-135.

White, K., Grether, M.E., Abrams, J.M., Young, L., Farrell, K., and Steller, H. (1994). Genetic control of programmed cell death in Drosophila. Science 264, 677-683.

Wirtz-Peitz, F., Nishimura, T., and Knoblich, J.A. (2008). Linking cell cycle to asymmetric division: Aurora-A phosphorylates the Par complex to regulate Numb localization. Cell 135, 161-173.

Wodarz, A., Ramrath, A., Grimm, A., and Knust, E. (2000). Drosophila atypical protein kinase C associates with Bazooka and controls polarity of epithelia and neuroblasts. J Cell Biol 150, 1361-1374.

Wodarz, A., Ramrath, A., Kuchinke, U., and Knust, E. (1999). Bazooka provides an apical cue for Inscuteable localization in Drosophila neuroblasts. Nature 402, 544-547.

Xiao, Q., Komori, H., and Lee, C.Y. (2012). klumpfuss distinguishes stem cells from progenitor cells during asymmetric neuroblast division. Development 139, 2670-2680.

Xie, Y., Li, X., Zhang, X., Mei, S., Li, H., Urso, A., and Zhu, S. (2014). The Drosophila Sp8 transcription factor Buttonhead prevents premature differentiation of intermediate neural progenitors. eLife. 03596.

Yamashita, Y.M., Mahowald, A.P., Perlin, J.R., and Fuller, M.T. (2007). Asymmetric inheritance of mother versus daughter centrosome in stem cell division. Science 315, 518-521.

Yang, X., Yeo, S., Dick, T., and Chia, W. (1993). The role of a Drosophila POU homeo domain gene in the specification of neural precursor cell identity in the developing embryonic central nervous system. Gene Dev 7, 504-516.

Yu, F., Morin, X., Cai, Y., Yang, X., and Chia, W. (2000). Analysis of partner of inscuteable, a novel player of Drosophila asymmetric divisions, reveals two distinct steps in inscuteable apical localization. Cell 100, 399-409.

Yu, F., Morin, X., Kaushik, R., Bahri, S., Yang, X., and Chia, W. (2003). A mouse homologue of Drosophila pins can asymmetrically localize and substitute for pins function in Drosophila neuroblasts. J Cell Sci 116, 887-896.

Yu, F., Wang, H., Qian, H., Kaushik, R., Bownes, M., Yang, X., and Chia, W. (2005). Locomotion defects, together with Pins, regulates heterotrimeric G-protein signaling during Drosophila neuroblast asymmetric divisions. Gene Dev 19, 1341-1353.

Zhang, F., Huang, Z.X., Bao, H., Cong, F., Wang, H., Chai, P.C., Xi, Y., Ge, W., Somers, W.G., Yang, Y.*, et al.* (2016). Phosphotyrosyl phosphatase activator facilitates localization of Miranda through dephosphorylation in dividing neuroblasts. Development 143, 35-44.

Zhou, Y., Jiang, H., Gu, J., Tang, Y., Shen, N., and Jin, Y. (2013). MicroRNA-195 targets ADP-ribosylation factor-like protein 2 to induce apoptosis in human embryonic stem cell-derived neural progenitor cells. Cell Death Dis 4, e695.

Zhu, S., Barshow, S., Wildonger, J., Jan, L.Y., and Jan, Y.N. (2011). Ets transcription factor Pointed promotes the generation of intermediate neural progenitors in Drosophila larval brains. Proc Natl Acad Sci USA 108, 20615-20620.